Addis Ababa University

Addis Ababa Institute of Technology

School of Electrical and Computer Engineering

Trajectory Tracking of Fixed-Wing UAV Using Fuzzy-Based Sliding Mode Controller

---

By

Feleke Tsegaye

A Thesis Submitted to School of Graduate Studies of Addis Ababa University in Partial Fulfillment of the Requirements for the Degree of

Master of Science in Control Engineering

Thesis Advisor

Dr. Lebsework Negash (PhD)

October 2023,

Addis Ababa, Ethiopia

Addis Ababa University

Addis Ababa institute of Technology

School of Electrical and Computer Engineering

This is to certify that the thesis prepared by Feleke Tsegaye, entitled **" Trajectory Tracking of Fixed-Wing UAV Using Fuzzy-Based SMC "**, submitted in partial fulfillment of the requirements for the degree of Master of Sciences in Control Engineering, complies with the regulations of the university and meets the accepted standards with respect to originality and quality.

Approved by Board of Examiners

Name	Signature	Date
Dr. Bisrat Derebssa		
(School dean)		
Dr. Lebsework Negash		
(Chairman)		
Dr. Lebsework Negash		
(Advisor)		
Mr. Teshome Hambissa		
(Internal examiner)		
Dr. Mengesha Mamo		
(External examiner)		

Declaration

I, the undersigned, confirm that the research work entitled **"Trajectory tracking of fixed-wing UAV using fuzzy-based SMC"** is my original research work. The work has not been submitted for the award of a degree at this or any other university, to which all sources and materials used for the thesis from other sources are duly acknowledged.

Feleke Tsegaye		
Name of Student	Signature	Submission Date

This thesis has been submitted for examination with my approval as a university advisor.

Name of Advisor	Signature
Dr. Lebsework Negash	

Acknowledgment

Firstly, I would like to offer my deepest gratitude to almighty God, for his faithfulness that has brought me stability and strength in tough situations. I would like to extend my warmest thanks to my advisor Dr. Lebsework Negash and for his shared expertise, guidance, encouragement, and insightful comments offered throughout this endeavor. Without him, this endeavor wouldn't have been possible, and also it was a great opportunity for me to be under the guidance of such great teachers and scholars with whom I found inspiration and deep admiration. I am also profoundly grateful to my classmates for their moral support, fruitful discussions, and memorable history that we have had together in this master's study journey. Last but not least, I'd like to acknowledge my family as a whole. Their support and belief in me have kept my spirits and motivation high throughout this journey. I thank them for everything they have done for me, they are the reason I am where I am today.

Feleke Tsegaye

Abstract

The work in this thesis mainly focuses on trajectory tracking of fixed wing unmanned aerial vehicle (FWUAV) by using fuzzy based sliding mode controller(FSMC) for surveillance applications. Unmanned Aerial Vehicles (UAVs) are general-purpose aircraft built to fly autonomously. This technology is applied in a variety of sectors, including the military, to improve defense, surveillance, and logistics. The model of FWUAV is complex due to its high non-linearity and coupling effect. In this thesis, input decoupling is done through extracting the dominant inputs during the design of the controller and considering the remaining inputs as uncertainty. The proper and steady flight maneuvering of UAVs under uncertain and unstable circumstances is the most critical problem for researchers studying UAVs. A FSMC technique was suggested to tackle the complexity of FWUAV systems. The trajectory tracking control algorithm primarily uses the sliding-mode (SM) variable structure control method to address the system's control issue. In the SM control, a fuzzy logic control(FLC) algorithm is utilized in place of the discontinuous phase of the SM controller to reduce the chattering impact. In the reaching and sliding stages of SM control, Lyapunov theory is used to assure finite-time convergence. A comparison between the conventional SM controller and the suggested controller is done in relation to the chattering effect as well as tracking performance. It is evident that the chattering is effectively reduced, the suggested controller provides a quick response with a minimum steady-state error, and the controller is robust in the face of unknown disturbances. The designed control strategy is simulated with the nonlinear model of FWUAV using the MATLAB® / Simulink® environments. The simulation result shows the suggested controller operates effectively, maintains an aircraft's stability, and will hold the aircraft's targeted flight path despite the presence of uncertainty and disturbances.

Keywords– Fixed-wing UAVs, Sliding mode controller, Fuzzy logic controller, Chattering, Coupling effect, Surveillance, Finite-time convergence, Lyapunov theory, Flight path

Contents

List of Figures

List of Tables

List of Abbreviations

CoG	Center of Gravity
CoM	Center of Mass
DoF	Degree of Freedom
FCS	Flight Control System
FL	Fuzzy Logic
FLC	Fuzzy Logic Controller
FSMC	Fuzzy-based Sliding Mode Controller
FWUAV	Fixed Wing Unmanned Aerial Vehicle
GPS	Ground Positioning System
MF	Membership Function
MSTE	Mean Square Trajectory Error
NB	Negative Big
NDI	Nonlinear Dynamic Inversion
NED	North East Down
NM	Negative Medium
NS	Negative Small
PB	Positive Big
PID	Proportional Integral Derivative
PM	Positive Medium

PS	Positive Small
SM	Sliding Mode
SMC	Sliding Mode Controller
TIP	Tracking Improvement Percentage
UAS	Unmanned Aerial System
UAV	Unmanned Aerial Vehicle
VSCS	Variable Structure Control System
VTOL	Vertical Takeoff and Landing

Chapter 1

Introduction

1.1 Background of UAVs

Unmanned aerial vehicles, or UAVs, are sometimes known as self-propelled aircraft that fly autonomously and without the assistance of a human pilot. UAVs were first intended to be used for military objectives; their origins may be found in the 1849s, in the middle of the 19^{th} century. A new type of rotary wing aircraft called PCA-2 was designed in 1929, making it the first rotary wing aircraft to acquire flight authority [1]; unmanned balloons were formerly employed in Venice to quell public unrest [2]; The British Royal Navy developed a UAV named as in the 1930s. "Queen Bee" for anti-aircraft gunnery practice [3]. Over the past year, UAV technologies have seen enormous growth, and UAV civilian use has gained the quality of being widely admired or accepted. The market for UAVs in 2016 was approximately at $11.3bn and is forecast to increase to over $140bn in the next decade in the United States [4]. The rapid growth of the market for UAV systems has stimulated the expansion of their application in different sectors, among them military and surveillance, search and rescue operations, and infrastructure, which are of significant importance [5].

Surveillance techniques are highly desirable in sectors where territory control is essential. At this time, UAVs are applied to many surveillance applications like aerial image acquisition, aerial video recording, etc., with prevailing success due to their high maneuverability and low cost, making them convenient for the techniques of surveillance.

Unmanned aircraft system (UAS) refers to both the aircraft and all of the supporting components utilized in the systems, such as the motors, sensors, micro-controllers, software, ground

station computers, and user interface [6]. But this thesis mainly focuses on the aircraft's guidance, navigation, and control system.

UAVs can be classified based on various criteria; based on the type of wing, they can be classified as fixed-wing and rotary-wing (multirotor) UAVs, as shown in figure 1.1. Fixed-wing UAVs are renowned for their exceptional benefits, including increased flight safety, faster coverage of bigger regions, and longer flying autonomy [7]. However, due to the complexity of the dynamics and system interactions, designing a fixed-wing UAV control system is incredibly difficult. More UAV models have been created to resemble the real system, as a result of which it is advantageous to apply strong control algorithms to address the aforementioned issues [8]. Since fixed-wing UAVs have a long flight range, a large cargo capacity, and a rapid flight speed, they are frequently utilized to do jobs demanding high altitude and high speed. Fixed-wing UAVs are powered by aerodynamic forces acting on a fixed surface. While there are numerous benefits to fixed-wing UAVs, it can be challenging to build control systems that guarantee optimal performance. This is due to the fact that precise models are required for the design of controllers, but because fixed-wing UAVs have many state and control input values coupled together, uncertainty, and non-linearity, their models are highly complicated. Numerous studies on the modeling process of fixed-wing UAVs have been carried out [8], [9]; nevertheless, they are limited to developing approximate mathematical and dynamic models.Many presumptions must be made while analyzing a fixed-wing UAV, such as treating the vehicle as a rigid body with constant ground acceleration. This is the primary cause of the uncertainty in system parameters and what separates the real model from the ideal model.

To overcome the coupling effect of the system (FWUAV), this thesis decouple the control input of the system based on the decoupling principle of the multi-variable system. FWUAVs are both state variables and control input coupled, but SMC tolerates state coupling, and then the control input decoupling is held in this thesis work, the decoupling process mainly depends on extracting the dominant control quantity in the design of the controller and treating the remaining quantity as uncertainty [10] [11].

Regarding the control strategy, fuzzy-based sliding mode controller (FSMC) is chosen for this thesis so that the system complexity may not be an issue due to the proposed control strategy having a tendency to tolerate state variable coupling and system complexity.

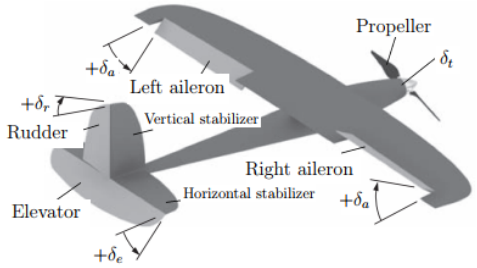

(a) Fixed wing UAV example

(b) Rotary wing UAV example

Figure 1.1: Illustrations for the types of UAVs based on wing type

1.2 Statement of The Problem

Regarding monitoring, it should be noted that our nation is still developing and has a number of criminal difficulties. Video surveillance using security UAVs can perform useful and essential tasks. A drone can fly quickly, locate hazards, and offer aerial images and live video. This makes it possible for security officers to assess the risk and choose the best course of action. Therefore, developing a trajectory tracking controller for fixed-wing UAVs is crucial for creating effective surveillance. For a variety of reasons, fixed-wing aircraft trajectory tracking during surveillance is crucial [12]:-

Real-time monitoring: Surveillance agencies can closely watch the aircraft's movement and obtain real-time data about its location, speed, altitude, and direction by correctly following its trajectory. This real-time monitoring guarantees that the aircraft does not depart from its planned trajectory and remains within the designated surveillance region.

Target identification and classification: Targets can be precisely identified and classified using trajectory tracking. Surveillance agencies can evaluate whether a target is a possible threat or a risk to national security by analysing the feed from the UAV.

Data analysis and intelligence gathering: Data obtained during surveillance missions is useful for further data analysis and intelligence gathering. Surveillance agencies can gather useful insights and identify potential dangers or trends by monitoring the patterns and behavior of targets over time. This data can be used to improve national security measures and decision-making processes.

Safety and avoids conflicts: Accurate trajectory tracking ensures the fixed-wing aircraft's safety during surveillance operations. It aids in the avoidance of possible collisions with other aircraft, obstructions, or entry into the airspace. Surveillance agencies can warn the pilot to any potential conflicts or risks that may develop throughout the flight by preserving up-to-date trajectory data.

It is critical to keep in mind that when controllers attempt to use fixed-wing UAV surveillance for criminal situations or other tasks which need trajectory tracking problem, many of the physical characteristics depend on specific physical circumstances. For outdoor operations, these effects are significant because of temperature, many other unclear environmental scenarios, and variations in process dynamics. In these cases, conventional feedback controllers fail to ensure stability and follow designated trajectories with acceptable performance. Hence, trajectory tracking SM control techniques integrated with fuzzy-logic (FL) controls are designed so that the drawback of SM controllers, which is a chattering effect on the control effort, is reduced.

1.3 Objectives

1.3.1 General Objective

Designing a trajectory-tracking fuzzy-based SMC for FWUAV that can handle system complexity and has the ability to reject disturbances is the overall goal of this research.

1.3.2 Specific Objectives

- Derive a mathematical model of FWUAV using the Newton-Euler approach.
- Validate the dynamic model of FWUAVs. (Model verification).
- Decouple the system in terms of the control input (control input decoupling).
- Design a conventional sliding mode controller.
- Design a fuzzy logic controller to replace the discontinuous phase of SMC in order to reduce the chattering effect.
- Designing a proper trajectory for each stage of the aircraft's flight path.
- Use simulation in MATLAB®/Simulink® environment to simulate the mathematical models of the FWUAV with the suggested controller.

1.4 Scope of The Thesis

The scope of this thesis is a derivation of a mathematical model of the FWUAV (fixed-wing UAV) by using a Newton-Euler method, a control input decoupling, and designing trajectory

tracking fuzzy-based sliding mode controller that will be tuned for efficient stabilization of attitude, altitude, and position control of FWUAVs for the plant's dynamic model in the presence of external perturbation. The system and controller designs will be put into practise in the MATLAB®/Simulink® environment.

1.5 Significance of The Research Work

The significance of this research work is mentioned as follows:

- **Surveillance:** UAVs are increasingly used for surveillance and security purposes. Trajectory tracking allows them to monitor specific areas, follow targets, or conduct patrols. In surveillance applications, trajectory tracking helps UAVs maintain a desired altitude and position, enabling them to capture clear and steady footage. By following predefined trajectories, UAVs can ensure comprehensive coverage of an area of interest, improving situational awareness and enhancing security measures.

- **Emergency response:** Trajectory tracking is essential for UAVs involved in emergency response operations. UAVs equipped with trajectory tracking can be deployed to assess disaster-affected areas, search for missing persons, and provide situational awareness to emergency response teams. By following specific trajectories, UAVs can systematically search large areas, cover regions that is difficult for humans to access, and relay information in real-time. This aids in quick decision-making, efficient resource allocation, and timely rescue and relief efforts.

- **Agriculture:** UAVs equipped with trajectory tracking capabilities can be used in precision agriculture. They can fly over farmlands, collecting data and monitoring crop health, soil conditions, and water usage. By following specific trajectories, UAVs can cover the entire field efficiently, capturing high-resolution images and providing valuable insights to optimize crop management. The trajectory tracking helps ensure complete coverage and avoids missing any areas, leading to improved crop yields and reduced resource wastage.

- **Autonomous delivery:** Trajectory tracking is crucial for UAVs involved in autonomous delivery systems. These UAVs follow pre-defined paths to transport goods from one location to another. By accurately tracking the trajectory, they can navigate through obstacles, maintain a safe distance from buildings or people, and deliver

packages to their destinations. The trajectory tracking algorithms ensure smooth and reliable delivery operations, enhancing the efficiency and safety of autonomous delivery systems.

1.6 Contribution of The Research Work

- **The UAV dynamics is modelled using a more general aerodynamic model**. Previous researches [13], [14], [15], [16] used simplified models obtained in specific flying conditions without regard for uncertainty during decoupling. To address this issue, a more generic model that takes into account the cross-dependencies between the coefficients, aerodynamic angles, and control surfaces in a nonlinear form is examined in the controller design phase.

- **For trajectory-tracking of fixed-wing UAVs, a cascade or nested loop control technique is examined, in which the outer loop sets the desired thrust and attitude angles for the inner loop**. This approach helps to control the full degree of freedom of the aircraft.

- **Improve the tracking performance of the traditional SMC by using intelligent control (fuzzy logic controller for this thesis), as well as reduce chattering.**

1.7 Outline of The Research Work

This chapter, which serves as the introduction, is one of the 6 that make up the entire thesis. Additional information about the upcoming chapter is given as; A review of earlier work is given in **"Chapter 2"** (literature review). This chapter reviews various research publications that serve as the foundation for this thesis. The mathematical model of the aeroplane will be covered in **"Chapter 3"** and the model will be validated using the Simulink environment. The controller's architecture in **"Chapter 4"** ensures that the fixed-wing UAV takes the necessary course. The specific design of the attitude and position controllers is detailed along with their properties for reliable performance and convergence. **"Chapter 5"** shows the simulation results of the planned controller's performance and explain how the proposed controller decreases chattering and is robust to unidentified disturbances. The findings and suggestions for additional research are presented in **"Chapter 6"**.

Chapter 2

Literature Reviews

2.1 Motivation For The Literature Survey

UAVs can currently support an indisputable list of capabilities and improve a variety of crucial activities for both military and civilian purposes. Among the type of UAVs fixed-wing UAVs can usually carry heavier payloads for longer distances and flight time than both VTOL(vertical take-off and landing) and rotary-wing UAVs while they use lesser power [17]. As a result, fixed-wing UAVs are best suited for tasks that need extended flight times, such as mapping, surveillance, and combat. Regarding controllers, there are numerous manufactured and commercially available flight controller products. Although these controllers enable the user to carry out a variety of duties, including autonomous flight control, guiding, and way-point navigation, they also rapidly make certain tasks easier for the internal control system. They are useful for higher-level control activities as a result, the low-level flight path control law is constructed and evaluated for various trajectories in this thesis to offer greater flexibility in control law formulation and execution.

2.2 Overview of The Past Works

For fixed-wing propeller-driven UAVs, the author in [18] presents the synthesis of a flight path PID (proportional-integral-derivative) control system that gives UAVs autonomy to respond independently to the desired aircraft state and accessibility by a higher-level control layer so they can be used in a versatile, resilient, and decentralized system. However, this paper's limitation was that it did not use the entire model when simulating fixed-wing UAVs because the PID controller that was suggested could not tolerate state variable coupling,

system complexity, or from the six degrees of freedom; only three of them were controlled.

An adaptive PID flight controller based on parameter optimization with fuzzy inference was developed by the author in [19] to manage the height dynamics of the Aerosonde UAV. Using an online fuzzy inference technique, the PID parameters are modified self-adaptively. In comparison to the recommended adaptive PID flight controller, two alternative controllers are presented. The first controller is a PID that has been genetically modified, and the second is a fuzzy logic controller. The simulation results demonstrate that the proposed adaptive PID controller possesses good performance characteristics and strong stability. However, this study only regulates one of the six degrees of freedom for the fixed-wing UAV, which is altitude.

An innovative adaptive back-stepping control strategy for unmanned aerial vehicles is discussed in [20], which is based on invariant manifolds and functions with considerable uncertainty in the aerodynamic coefficients. This system is used to control and track the pitch, yaw, and bank (roll) angles of the aircraft. The modular structure of the control law includes a control module and a recently developed non-linear estimator. The estimation error can be given predetermined dynamics because the estimator is based on invariant manifolds. Since they do not require accurate aerodynamic models, the estimator and adaptive back-stepping control law cover the whole flight envelope. The stability of the entire closed-loop system is investigated using the Lyapunov stability theory The practicality of the suggested control law is illustrated using a small unmanned aerial vehicle's full six-degree-of-freedom non-linear model. The outcomes of the numerical simulation demonstrate that, in spite of several unidentified aerodynamic coefficients, this method can produce satisfying command tracking. Only the three rotating motions of the airplane are regulated in this study; the translational motion of the aircraft is not addressed.

The design of attitude and airspeed controllers for a fixed-wing unmanned aerial vehicle is covered by the author in [21]. A suggested adaptive second-order sliding mode control that is robust in the presence of external disturbances and improves performance under numerous operating circumstances Furthermore, this control resists overestimating control gains and does not call for knowledge of disturbance bounds. Additionally, an extended observer is created to estimate immeasurable states and outside disturbances in order to execute this controller. Additionally, appropriate circumstances are provided to ensure the

observer-based control's closed-loop stability. The performance of the suggested method is evaluated for active disturbance rejection based on sliding mode control in simulation results using a full six-degree of freedom model. The author in this paper also does not address the altitude, the position along the x-axis, and the position along the y-axis of the aircraft.

The author in reference [22] proposes the design of a controller for a fixed-wing aircraft to control the altitude, yaw angle, and roll angle based on the backstepping and sliding mode controllers. This paper conducted a comparative analysis of such methodologies (back-stepping, sliding mode, and back-stepping-based sliding mode controllers) to determine which controller has better performance when it is used for the autonomous flight control of the fixed-wing UAV. The integrated form of the backstepping and sliding mode controller performs satisfactorily in the simulation of this work. However, backstepping produces a lot of torque, and the sliding mode controller's control signal has the dreaded undesired chattering.

The author in [23] proposes a higher-order sliding mode controller to stabilize the lateral dynamics of the fixed-wing UAV. In this work, the guidance and control system is based on inner and outer loop design procedures; the outer guidance loop gives command for the inner guidance loop to generate the desired roll angle. The author of this paper also uses the nonlinear sliding manifold for guidance logic design. But the author considers only the lateral dynamics of the UAV system, and the proposed controller is mathematically intensive, making it difficult to prove the stability of the system [24].

In [25] a control technique was designed to address the complexity of the coupled nonlinear model of a fixed-wing UAV system and the uncertainty caused by a large number of interference sources. It combines sliding mode variable structure control with fuzzy adaptive control. The controller algorithm significantly relies on the sliding mode variable structure control approach to address the control problem of the closely coupled complicated nonlinear system. To mitigate the chattering issue of the conventional sliding mode controller, a fuzzy adaptive strategy based on sliding mode control is developed, which approximates the unknown functions and uncertain parameters caused by external disturbances. Based on the fuzzy object ranges in this work, two kinds of fuzzy adaptive sliding mode controllers were developed. However, no examination of the robustness of the developed controller is performed in this paper, and the simulation results are based on an approximation of the

model recovered during decoupling rather than the whole dynamics of the FWUAV model.

The authors in [26] discuss the design of four controllers for a fixed-wing unmanned aerial vehicle (UAV) based on a back-stepping and sliding mode controller. They are interested in doing a comparison analysis of such approaches to determine which controller performs best when utilized for autonomous flight (altitude, yaw, and roll) of a fixed-wing UAV. Back-stepping, sliding mode control (SMC), back-stepping with sliding mode control, and back-stepping with two sliding mode controls are the designed controllers. The simulation results are used to analyze the controllers. Finally, they offer an open-loop experimental result to validate the magnitude of the control signals produced in simulations. The shortcoming of this paper is that the controllers have chattering for SMC, and the control efforts for the back-stepping sliding mode controller are extremely large.

Chapter 3

Modeling of Fixed-Wing UAVs

This chapter assesses a mathematical modeling of a fixed-wing aircraft. To properly model aerial vehicles, it is necessary to comprehend several coordinate frames. As mentioned in Section 3.1, the results show how rotational formations and coordinate systems may be applied to clarify the location with respect to xy-plane, the altitude and orientation of the aircraft using sensor data. A wind triangle description is next discussed, which is important because it clarifies how aerodynamics and wind disturbances impact rigid-body motion (Section 3.2). The UAV's equations of motion may be determined from this point on (Section 3.3), and expressions for external forces and moments are presented in Section 3.4. (Section 3.5) contains a verification of the constructed model.

In order to uphold the universality of the kinematics and dynamics model for fixed-wing UAVs, it is necessary to establish the following assumptions for subsequent analysis [27].

1. Assume that the Earth does not undergo rotation or revolution, and its curvature is negligible.
2. The fixed-wing UAVs' structure remains rigid and does not undergo deformation or vibration when exposed to external forces.
3. The fixed-wing UAV's fuselage exhibits perfect symmetry with respect to the central axis plane.

3.1 Coordinate Frames

Understanding how various bodies are oriented in relation to one another is crucial for comprehending the mathematical model of the UAV system. Most obviously, we require

knowledge of the FWUAV's orientation with respect to the reference frame of the planet. Various coordinate frames are included in this chapter. Utilizing diverse coordinate systems are crucial because of [6] [28]:

- A fixed, inertial frame of reference is used to calculate Newton's equations of motion. On the other hand, motion is expressed a body-fixed framework.
- Aerodynamic forces and torques acting on the aircraft body can best be described in a body-fixed frame of reference.
- The inertial frame contains almost all mission requirements, including loiter spots and flying paths. Additionally, map data is also provided in an Earth frame of reference.
- Accelerometers and rate gyros are examples of on-board sensors that collect data about the body frame. As an alternative, GPS measures location, velocity, and course with respect to inertial frame.

3.1.1 Inertial Frame (Earth Frame) (F^i)

The defined home location serves as the origin of the inertial coordinates, which is a terrestrial frame. As seen in the left figure 3.1 the unit vector i^i points north, j^i points east, and k^i points to the earth's center or beneath. The NED (Northeast Down) reference frame is the name given to this.

3.1.2 Vehicle Frame (F^v)

The inertial frame is simply transformed into the center of mass (CoM) of the vehicle, which is the vehicle frame. In the figure 3.1, the axes of F^v are assigned in the same direction as F^i. In order to understand the body frame, it is necessary to include rotations about the

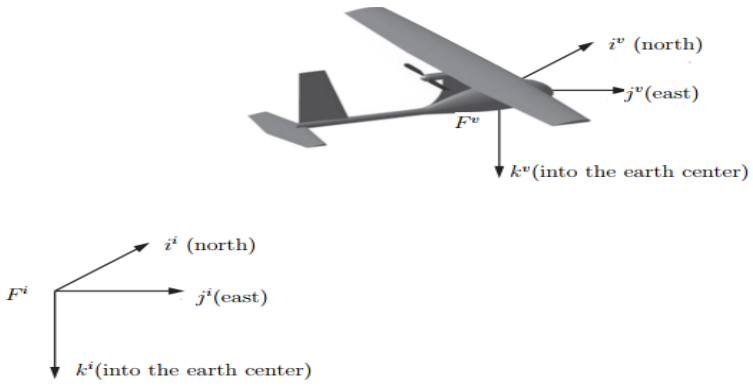

Figure 3.1: The inertial frame F^i and the vehicle frame F^v [6] [28].

k-axis, the new j-axis, and the newer i-axis, respectively. These rotations are represented by the angles ϕ, θ, and ψ, as will be discussed. These are the Euler angles, and the usual NASA notation is used for their names.

3.1.3 Body Frame (F^b)

The frame F^{v1} must first be defined as follows in order to move the vehicle frame to body frame:

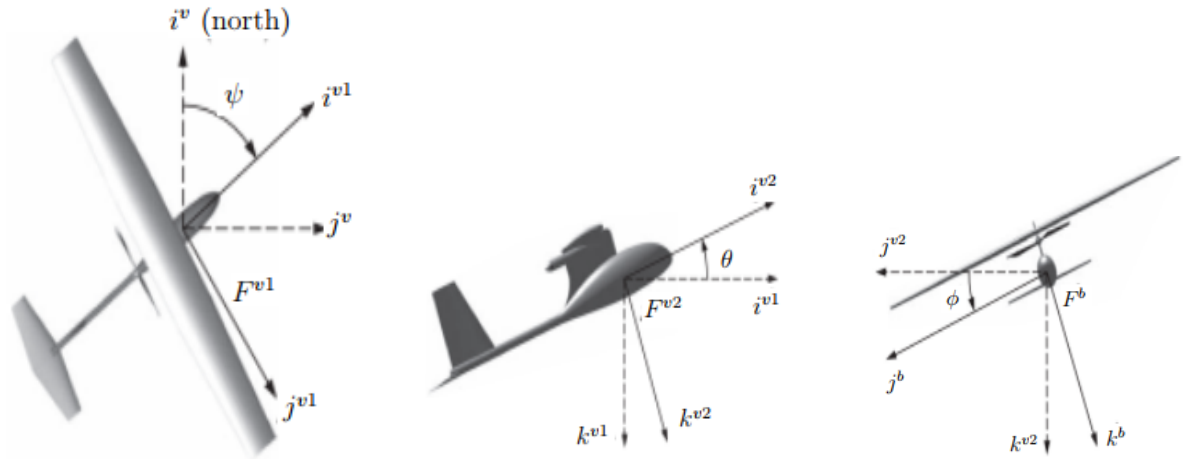

(a) From the vehicle frame, given by F^v, to the subsequent frame given as F^{v1}.

(b) From subsequent frame represented as F^{v1} to subsequent frame given as F^{v2}

(c) From subsequent frame represented as F^{v2} to the body frame given as F^b

Figure 3.2: Definition of a frame through three rotations: ϕ, θ, and ψ [6] [28].

$$P^{v1} = R_v^{v1}(\psi) * P^v \tag{3.1}$$

where a right-hand rotation matrix around the k^v-axis through the angular measurement corresponding to yaw is $R_v^{v1}(\psi)$. In Figure 3.2a, the i^{v1}-axis of F^{v1} is shown pointing in the direction of the airframe's nose. Then, another rotation is carried out about j^{v1} around the pitch angle θ. Subsequently, introduce the newly established intermediate coordinate system F^{v2}, in which P^{v1} is expressed equivalently as:

$$P^{v2} = R_{v1}^{v2}(\theta) * P^{v1} \tag{3.2}$$

Similarly to earlier, i^{v2} now points to the UAV's nose, whereas k^{v1} now points to the abdomen (Figure 3.2b). The body frame F^b is obtained at the conclusion after the last revolution around the axis i^{v2} by the roll angle ϕ. i^b in this instance denotes the airframe's nose, j^b the

right wing, and k^b the belly (Figure 3.2c). The following is the conversion of F^{v2} to F^b:

$$P^b = R^b_{v2}(\phi) * P^{v2} \tag{3.3}$$

The equivalent rotation matrix from the vehicle frame to the body frame is given by [6]:

$$R^b_v(\phi,\theta,\psi) = R^b_{v2}(\phi)R^{v2}_{v1}(\theta)R^{v1}_v(\psi) = \begin{bmatrix} C_\theta C_\psi & C_\theta S_\psi & -S_\theta \\ S_\psi S_\theta C_\psi - C_\phi S_\psi & S_\psi S_\theta S_\phi + C_\phi C_\psi & S_\phi C_\theta \\ C_\phi S_\theta C_\psi + S_\phi S_\psi & C_\psi S_\theta S_\psi - S_\psi C_\psi & C_\phi C_\theta \end{bmatrix} \tag{3.4}$$

When C represents the cosine function and S represents the sin function. And ϕ, θ, and ψ are the Euler angles (yaw, pitch, and roll), which provide a natural tendency to take the place of the orientation of the body with respect to the earth's fixed frame in a three-dimensional context. The sequence of rotations ψ-θ-ϕ is commonly employed for aircraft and represents one of the various Euler angle systems in use [29].

3.1.4 The Stability and Wind Frames F^s, F^w

Wind and stability coordinate systems must be introduced to provide the necessary framework definitions and to create the appropriate context for dealing with aerodynamic forces. Airspeed is represented by the symbol V_a and refers to the speed of the aircraft relative to

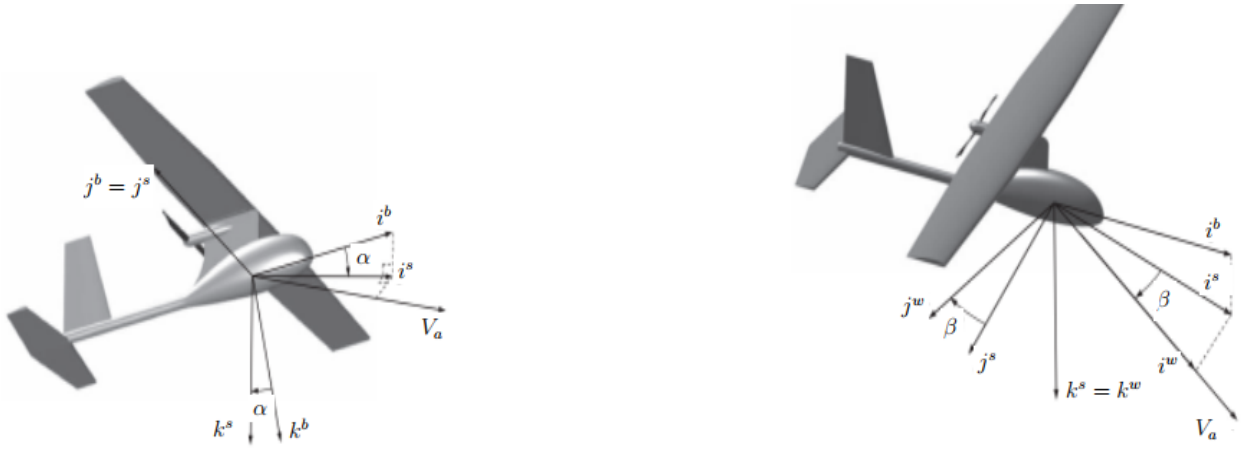

(a) From the body frame given by F^b to the subsequent stability frame given by F^s

(b) From the stability frame represented by F^s to the subsequent wind frame F^w

Figure 3.3: Representation of stability and wind frame [6] [28]

the air around it. To generate the necessary lift for flight, the wings must operate at an angle relative to the positive velocity vector, denoted as the angle of attack (α). To establish

the stability frame, j^b needs to be rotated left by an angle of α from F^b. Given the critical role of the angle of attack, which needs to be conducive during the right rotation from the stable frame to the body frame, a leftward rotation becomes essential. Figure 3.3a visually depicts this phenomenon. The F^b to F^sconversion map is [6] [28]:

$$P^s = R_b^s(\alpha) * P^b \tag{3.5}$$

When the rotation matrix for left-handed rotation, denoted as $R_b^s(\alpha)$, is provided:

$$R_b^s(\alpha) = \begin{bmatrix} cos\alpha & 0 & sin\alpha \\ 0 & 1 & 0 \\ -sin\alpha & 0 & cos\alpha \end{bmatrix} \tag{3.6}$$

A different angle, known as the horizontal slip (or side slip) angle β, must be found when the velocity vector $(i^b; k^b)$ is not in the plane. A fresh coordinate system, referred to as the wind frame F^w, is defined by performing a rightward rotation of the stability frame by an angle β around the k^s axis (as depicted in Figure 3.3b). Subsequently, the airspeed direction V_a is aligned with the unit vector i^w. The transformation comes from [6] [28]:

$$P^w = R_s^w(\beta) * P^s \tag{3.7}$$

Where

$$R_b^w(\alpha) = \begin{bmatrix} cos\beta & sin\beta & 0 \\ -sin\beta & cos\beta & 0 \\ 0 & 0 & 1 \end{bmatrix} \tag{3.8}$$

Lastly, the following is the general transformation from the body frame to the wind frame [6] [28]:

$$R_b^w(\alpha, \beta) = R_s^w(\beta) * R_b^s(\alpha) = \begin{bmatrix} C_\beta C_\alpha & S_\beta & C_\beta S_\alpha \\ -S_\beta C_\alpha & C_\beta & -S_\beta S_\alpha \\ -S_\alpha & 0 & C_\alpha \end{bmatrix} \tag{3.9}$$

3.2 Air, Wind, and Ground Speed

Talking about UAV, a wind has an important influence on the flight mechanism. Furthermore, aerodynamic forces are based on the relative speed of the surrounding air. As a result,

during modeling, wind must be properly taken into account. The following calculations are done in an effort to determine the fundamental formulations for the UAV's equations of motion. V_w stands for the wind speed relative to the earth frame. In a similar manner, V_a is used to describe speed in relation to the same frame. We define the ground speed as V_g and the drone's speed in relation to the inertial frame of reference as an example to show how to account for the wind. Equation (3.10) represents the vectors of airspeed, ground speed, and wind-speed. [6] [28]:

$$V_a = V_g - V_w \tag{3.10}$$

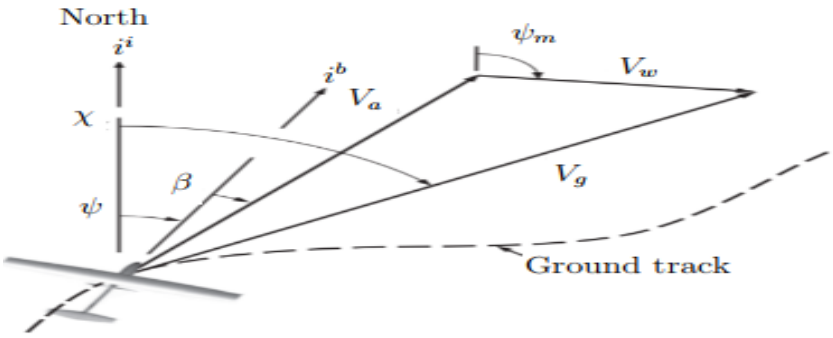

Figure 3.4: The wind triangle [6].

$$V_g^b = \begin{bmatrix} u \\ v \\ w \end{bmatrix} \tag{3.11}$$

The components along the axes (i^b; j^b; k^b) can be used to represent ground speed in the frame [6] [28]: The components of the wind as illustrated in the body frame, are similarly derived from [6] [28]:

$$V_w^b = \begin{bmatrix} u_w \\ v_w \\ w_w \end{bmatrix} = R_v^b(\phi, \theta, \psi) \begin{bmatrix} w_n \\ w_e \\ w_d \end{bmatrix} \tag{3.12}$$

when

$$V_w = \begin{bmatrix} w_n \\ w_e \\ w_d \end{bmatrix} \tag{3.13}$$

when

$$V_a^w = \begin{bmatrix} V_a \\ 0 \\ 0 \end{bmatrix} \tag{3.14}$$

Remember that air speed, denoted by the symbol V_a, indicates the drone's speed in the wind, as shown in equation 3.14 [6] [28].

$$V_a^b = \begin{bmatrix} u - u_w \\ v - v_w \\ w - w_w \end{bmatrix} = \begin{bmatrix} u_r \\ v_r \\ w_r \end{bmatrix} = R_w^b \begin{bmatrix} V_a \\ 0 \\ 0 \end{bmatrix} = V_a \begin{bmatrix} cos\alpha cos\beta \\ sin\beta \\ sin\alpha cos\beta \end{bmatrix} \tag{3.15}$$

From this equation, solve for V_a, α, and β as follows:

$$V_a = \sqrt{u_r^2 + v_r^2 + w_r^2} \tag{3.16}$$

$$\alpha = tan^{-1}(w_r/v_r) \tag{3.17}$$

$$\beta = sin^{-1}(v_r/\sqrt{u_r^2 + v_r^2 + w_r^2}) \tag{3.18}$$

These equations (3.16, 3.17, and 3.18) are the foundation for the dynamic and kinetic development of the FWUAV. The wind triangle is taken into consideration in figure 3.4 in order to have all the required components of the picture. An angle formed between the wind vector and i^i is denoted as ψ_w. The angle between true north and the projection of V_g on the horizontal plane $(i^b; j^b)$ is defined by the addition of the angle χ. If the effect of wind is not taken into account, there will be significant simplification results. As an instance, when $V_w = 0$, the conditions are such that $V_a = V_g, u = u_r, v = v_r$, $w = w_r, \psi = \chi$ (assuming $\beta = 0$ as well) [6] [28]

3.3 Kinematics and Flight Dynamics

When creating the equations of motion for a Fixed-Wing Unmanned Aerial Vehicle (FWUAV), translational motion is related with three positional states and three velocity states. There are three velocity states and three angular locations associated with rotational motion as well, for a total of twelve state variables. The state variables are summarized in Table 3.1, and Figure 3.5 explains the axis of motion [6] [28].

3.3.1 Kinematics

In the description of the states presented in Table 3.1, a body frame velocities u, v, and w are utilized to elucidate the components of speed within the inertial frame. Consequently, the process involves deriving and rotating for the coordination of translational speed and position [6] [28]:

$$\begin{bmatrix} \dot{p_n} \\ \dot{p_e} \\ \dot{p_d} \end{bmatrix} = R_b^v(\phi, \theta, \psi) \begin{bmatrix} u \\ v \\ w \end{bmatrix} \tag{3.19}$$

The complex derivative derived from the angular positions and velocities explains the rolling, pitch, and tilt angles with respect to the relevant mid-frames. If the correct rotational transformations are executed as follows, the angular rate of the body frame can be represented as a derivative of the Euler angle [6] [28]:

$$\begin{bmatrix} p \\ q \\ r \end{bmatrix} = \begin{bmatrix} \dot{\phi} \\ 0 \\ 0 \end{bmatrix} + R_{v2}^b(\phi) \begin{bmatrix} 0 \\ \dot{\theta} \\ 0 \end{bmatrix} + R_{v2}^b(\phi) R_{v1}^{v2}(\theta) \begin{bmatrix} 0 \\ 0 \\ \dot{\psi} \end{bmatrix} \tag{3.20}$$

Which is equal to:

$$\begin{bmatrix} p \\ q \\ r \end{bmatrix} = \begin{bmatrix} 1 & 0 & -sin\theta \\ 0 & cos\phi & sin\phi cos\theta \\ 0 & -sin\phi & cos\phi cos\theta \end{bmatrix} \begin{bmatrix} \dot{\phi} \\ \dot{\theta} \\ \dot{\psi} \end{bmatrix} \tag{3.21}$$

By rearranging the expression above we can find:

$$\begin{bmatrix} \dot{\phi} \\ \dot{\theta} \\ \dot{\psi} \end{bmatrix} = \begin{bmatrix} 1 & tan\theta sin\phi & cos\phi tan\theta \\ 0 & cos\phi & -sin\phi \\ 0 & sin\phi/cos\theta & cos\psi/cos\theta \end{bmatrix} \begin{bmatrix} p \\ q \\ r \end{bmatrix} \tag{3.22}$$

Equation (3.22) above demonstrates that the singularity in the Euler angle representation of the attitude occurs at $\theta = 90°$, for this reason, the angle of deviation is unknown. This phenomenon is often referred to as gimbal locking. But fortunately, for fixed-wing drones, this is not the case because, in normal flight, the pitch angle is always less than 90° [6] [28].

Table 3.1: The variables representing the state of the drone in the equations of motion.

Name	Description
P_n	Drone's north inertia position along $i^i in F^i$
P_e	The drone's east inertia position along $j^i in F^i$
P_d	The drone's down inertia position along $k^i in F^i$
u	Actual body frame speed along $i^b in F^b$
v	Actual body frame speed along j^b in F^b
w	Actual body frame speed along k^b in F^b
ϕ	Roll angle determined relative to F^{v2}
θ	Pitch angle established in relation to F^{v1}.
ψ	Yaw angle determined relative to F^v
p	The measured roll rate along i^b in the body frame F^b.
q	The measured pitch rate along i^b in the body frame F^b.
r	The measured yaw rate along i^b in the body frame F^b.

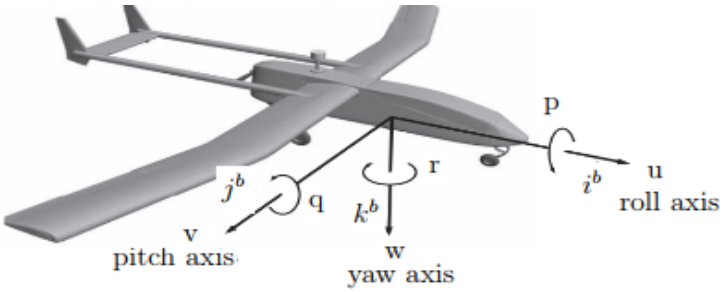

Figure 3.5: Definition of axes of motion [6] [28].

3.3.2 Dynamics of a Rigid Body

To derive the kinetic equation of motion, Newton's second law is employed. The forces and moments are computed within an inertial frame of reference, but it is also possible to express these quantities in terms of components related to alternative frames, such as the body frame. For the analysis, let's consider a simplified, flat Earth model suitable for small drones.

3.3.3 Motion Involving The Change of Position.

The application of Newton's second law to a body undergoing translational motion can be elucidated as follows:

$$m\frac{\mathrm{d}}{\mathrm{d}t_i}V_g = F \tag{3.23}$$

In this context, where m represents the mass of the UAV, $\frac{d}{t_i}$ denotes the time derivative in the inertial frame (with the subscript i indicating the derivative is taken in the inertial frame), and F signifies the sum of all external forces acting on the UAV. These external forces encompass gravitational, aerodynamic, and propulsive forces [6]. The derivative of

the velocity in the inertial frame can be expressed in terms of the derivative in the body frame and the angular velocity, following the vector derivative rule:

$$\frac{\mathrm{d}}{\mathrm{d}t_i}V_g = \frac{\mathrm{d}}{\mathrm{d}t_b}V_g + w_{b/i} \times V_g \tag{3.24}$$

Here, $w_{b/i}$ represents the angular speed of the drone with respect to the Earth's frame of reference. By utilizing equations (3.23) and (3.24), an alternative expression of Newton's second law can be derived, incorporating differentiation in the body frame:

$$m(\frac{\mathrm{d}}{\mathrm{d}t_b}V_g^b + w_{b/i}^b \times V_g^b) = F^b \tag{3.25}$$

When $V_g^b = \begin{bmatrix} u & v & w \end{bmatrix}^T$, $w_{b/i}^b = \begin{bmatrix} p & q & r \end{bmatrix}^T$, $F^b = \begin{bmatrix} F_x & F_y & F_z \end{bmatrix}^T$, $\frac{\mathrm{d}}{\mathrm{d}t_b}V_g^b = \begin{bmatrix} \dot{u} & \dot{v} & \dot{w} \end{bmatrix}^T$. By computing the cross product in equation (3.25), we can obtain the following expressions:

$$\begin{bmatrix} \dot{u} \\ \dot{v} \\ \dot{w} \end{bmatrix} = \begin{bmatrix} rv - qw \\ pw - ru \\ qu - pu \end{bmatrix} + \frac{1}{m}\begin{bmatrix} F_x \\ F_y \\ F_z \end{bmatrix} \tag{3.26}$$

3.3.4 Motion Relative to Rotation

For motion relative to the rotation, Newton's equation is stated as:

$$(\frac{\mathrm{d}}{\mathrm{d}t_b}h)^i = M \tag{3.27}$$

When M is the total of all externally exerted moments and h is the vector form of the angular momentum. Moments that are added around the UAV's center of mass are given by the equation above. Using the vector derivative technique, it is possible to expand the angular momentum derivative obtained in the inertial frame, as seen below [6].

$$(\frac{\mathrm{d}}{\mathrm{d}t_b}h)^i = (\frac{\mathrm{d}}{\mathrm{d}t_b}h)^b + w_{b/i} \times h = M^b \tag{3.28}$$

In the context of a rigid body, angular momentum is defined as the multiplication of the inertia matrix J and the angular velocity vector, denoted as $h^b = J * w_{b/i}^b$,Here, J represents the inertia tensor. In simpler terms, the angular momentum of the rigid body is determined

by multiplying its inertia matrix with the angular velocity vector.

$$J = \begin{bmatrix} J_{xx} & -J_{xy} & -Jxz \\ -J_{xy} & J_{yy} & -Jyz \\ -J_{xz} & -J_{yz} & Jzz \end{bmatrix} \tag{3.29}$$

When: $J_{xx} = \int (x^2 + y^2)\, dm$, $J_{yy} = \int (x^2 + z^2)\, dm$, $J_{zz} = \int (x^2 + z^2)\, dm$, $J_{xy} = \int (xy)\, dm$, $J_{xz} = \int (xz)\, dm$, $J_{yz} = \int (yz)\, dm$. Since the drones are often symmetric to the plane made by i^b and k^b, we set $J_{xy} = J_{yz}$ to be equal to 0. Since J has been identified in a content frame of reference, it follows that its derivative in an analog frame is $(\frac{\mathrm{d}}{\mathrm{d}t}J)^b = 0$ [6]. Equation (3.28) then becomes:

$$J(\frac{\mathrm{d}}{\mathrm{d}t}w_{b/i})^b + (w_{b/i})^b \times J(w_{b/i})^b = M^b \tag{3.30}$$

By rearranging the above equation we obtain :

$$\dot{w}^b_{b/i} = J^{-1}(-w^b_{b/i} \times (Jw^b_{b/i}) + M^b) \tag{3.31}$$

Under the assumption of the rigid body is symmetric about the plane spanned by i^b and k^b i.e $(J_{xy} = J_{yx} = 0)$ the inverse of the inertia matrix is determined as follows:

$$J^{-1} = \begin{bmatrix} J_{zz}/\Gamma & 0 & J_{xz}/\Gamma \\ 0 & 1/J_{yy} & 0 \\ J_{xz}/\Gamma & 0 & J_{xx}/\Gamma \end{bmatrix} \tag{3.32}$$

when $\Gamma = J_{xx}J_{zz} - J^2_{xz}$. By letting (p,q,r) be the angular rates and the summation of the moment be (L, M, N) then the rotational dynamic equation can be written as:

$$\dot{w}^b_{b/i} = \begin{bmatrix} \dot{p} \\ \dot{q} \\ \dot{r} \end{bmatrix} = \begin{bmatrix} \Gamma_1 pq - \Gamma_2 pr \\ \Gamma_5 pr - \Gamma_6(p^2 - r^2) \\ \Gamma_7 pq - \Gamma_1 qr \end{bmatrix} + \begin{bmatrix} \Gamma_3 L + \Gamma_4 N \\ 1/J_{yy} M \\ \Gamma_4 L + \Gamma_8 N \end{bmatrix} \tag{3.33}$$

When

$$\Gamma_1 = \frac{J_{xz}(J_{xx} - Jyy + J_{zz})}{\Gamma}$$
$$\Gamma_2 = \frac{J_{zz}(J_{zz} - J_{yy}) + J_{xz}^2}{\Gamma}$$
$$\Gamma_3 = \frac{J_{zz}}{\Gamma}$$
$$\Gamma_4 = \frac{J_{xz}}{\Gamma}$$
$$\Gamma_5 = \frac{J_{zz} - J_{xx}}{J_{yy}}$$
$$\Gamma_6 = \frac{J_{xz}}{J_{yy}}$$
$$\Gamma_7 = \frac{(J_{xx} - J_{yy})J_{xx} + J_{xz}^2}{\Gamma}$$
$$\Gamma_8 = \frac{J_{xx}}{\Gamma}$$

The six-degree of freedom, twelve-state model for the dynamics and kinematics of the FWUAV is enlisted below and is based on the aforementioned computations of mathematical methods (p_n, p_e, and p_d represent position along x, y, z respectively) [6] [28].

$$\begin{aligned}
\begin{bmatrix} \dot{p_n} \\ \dot{p_e} \\ \dot{p_d} \end{bmatrix} &= \begin{bmatrix} C_\theta C_\psi & S_\phi S_\theta C_\psi - C_\phi S_\psi & C_\phi S_\theta C_\psi + S_\phi S_\psi \\ C_\theta S_\psi & S_\phi S_\theta S_\psi + C_\phi C_\psi & C_\phi S_\theta S_\psi - S_\phi C_\psi \\ -S_\theta & S_\phi C_\theta & C_\phi C_\theta \end{bmatrix} \begin{bmatrix} u \\ v \\ w \end{bmatrix} \\
\begin{bmatrix} \dot{u} \\ \dot{v} \\ \dot{w} \end{bmatrix} &= \begin{bmatrix} rv - qw \\ pw - ru \\ qu - pu \end{bmatrix} + 1/m \begin{bmatrix} F_x \\ F_y \\ F_z \end{bmatrix} \\
\begin{bmatrix} \dot{\phi} \\ \dot{\theta} \\ \dot{\psi} \end{bmatrix} &= \begin{bmatrix} 1 & tan\theta sin\phi & cos\phi tan\theta \\ 0 & cos\phi & -sin\phi \\ 0 & sin\phi/cos\theta & cos\psi/cos\theta \end{bmatrix} \begin{bmatrix} p \\ q \\ r \end{bmatrix} \\
\begin{bmatrix} \dot{p} \\ \dot{q} \\ \dot{r} \end{bmatrix} &= \begin{bmatrix} \Gamma_1 pq - \Gamma_2 pr \\ \Gamma_5 pr - \Gamma_6(p^2 - r^2) \\ \Gamma_7 pq - \Gamma_1 qr \end{bmatrix} + \begin{bmatrix} \Gamma_3 L + \Gamma_4 N \\ 1/J_{yy} M \\ \Gamma_4 L + \Gamma_8 N \end{bmatrix}
\end{aligned} \tag{3.34}$$

Equations (3.31)–(3.34) outline the dynamics of the UAV, but they are incomplete as they do not account for the externally applied forces and moments. The following section will address this gap by developing models that consider the effects of gravity, aerodynamics, and propulsion on the system.

3.4 External Forces and Moments

The primary objective of this section is to delineate the forces and moments generated by a UAV. Gravity, aerodynamics, and propulsion are the principal causes of the forces and moments, respectively. The total of all applied forces and moments is [6] [28] [30]:

$$F = F_g + F_a + F_p \tag{3.35}$$

$$M = M_a + M_p \tag{3.36}$$

When the subscript "g" indicates gravity effect, "a" indicates aerodynamic effect, and "p" indicates propulsion effect,

3.4.1 Gravitational Forces

The gravitational field's influence on a UAV can be described as a force proportionate to the mass applied to the CoM, acting in the direction k^i. The gravitational force in the vehicle frame F^v is given by [6] [28]:

$$F_g^v = \begin{bmatrix} 0 \\ 0 \\ mg \end{bmatrix}$$

Newton's second rule of motion, however, assumes that forces are on the axis of the body frame. The gravitational force must then be converted into its body reference frame as follows:

$$F_g^b = R_v^b \begin{bmatrix} 0 \\ 0 \\ mg \end{bmatrix} = \begin{bmatrix} -mgsin\theta \\ mgcos\theta sin\phi \\ mgcos\theta cos\phi \end{bmatrix} \tag{3.37}$$

Because gravitational force is at the UAV's center of mass, zero moments are generated by gravity.

3.4.2 Aerodynamics Force and Moments

The control surface is listed before we are going to drive the equation of force and moment exerted on the body. The typical configuration is depicted in Figure 3.6, with δ_a denoting the aileron deflection, δ_e representing the elevator deflection, δ_r indicating the rudder deflection,

and δ_t signifying the throttle. One method of expressing the aileron deflection is as follows:

$$\delta_a = \frac{1}{2}(\delta_{al} - \delta_{ar}) \tag{3.38}$$

when δ_{al} and δ_{ar} are the left and right deflections of the aileron, respectively. Each deflection's dimension is radians, but the throttle is %. The indication of the direction of surface deflection is specified by applying a right-hand rule at the control surface junction. A positive direction is shown in the figure below. A positive δ_a may produce a rolling moment along a positive i^b(the x-axis of the body frame) with respect to convention.

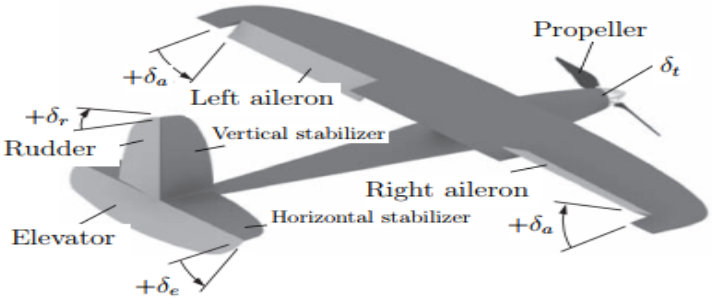

Figure 3.6: Fixed wing UAV's control surfaces and propeller [6] [28].

The total movement of a FWUAV can be categorized into two complementary motion modes. This categorization facilitates a more straightforward representation suitable for the application of control techniques. The two modes include lateral-directional motion and longitudinal motion [6].

3.4.2.1 Aerodynamics of Longitudinal Motion

Lift, drag, and pitching moments, these forces and moments are responsible for the motion of the body within the plane. $(i^b; k^b)$. Lift and drag forces, as well as tilting moments, are strongly influenced by angle of attack, tilt speed q and lift deflection δ_e as follows [6] [28].

$$F_{lift} = \frac{1}{2}\rho {V_a}^2 S C_L(\alpha, q, \delta_e) \tag{3.39}$$

$$F_{drag} = \frac{1}{2}\rho {V_a}^2 S C_D(\alpha, q, \delta_e) \tag{3.40}$$

$$M = \frac{1}{2}\rho {V_a}^2 S c C_M(\alpha, q, \delta_e) \tag{3.41}$$

When "S" is the planform area of a single wing, "c" is the primary chord of the wing, and "ρ" is the air density and airspeed of "V_a", non-dimensional coefficients C_L, C_D, and C_M are

impacted by α, q, and δ_e. A first-order Taylor series can be used to determine the connection between two coefficients [6]:

$$C_L(\alpha, q, \delta_e) = C_{L0} + \frac{\partial C_L}{\partial \alpha}\alpha + \frac{\partial C_L}{\partial q}q + \frac{\partial C_L}{\partial \delta_e}\delta_e \tag{3.42}$$

The C_{L0} represents C_L during $\alpha = q = \delta_e = 0$. It is evident that the partial derivatives of this dimensionless linear approximation can be readily computed. As C_L, as well as the angles α and δ_e (given in radians), are dimensionless, the only component requiring non-dimensionalization is $\frac{\partial C_L}{\partial q}$. Considering that the dimension of q is in rad/s, a standard factor to apply is c/(2Va). Consequently, equation (3.42) can be reformulated as follows: [6] [28]:

$$C_L(\alpha, q, \delta_e) = C_{lo} + C_{L_\alpha}\alpha + C_{l_q}\frac{c}{2V_a}q + C_{l\delta_e}\delta_e \tag{3.43}$$

When $C_{l_\alpha} = \frac{\partial C_L}{\partial \alpha}$, $C_{l_q} = \frac{\partial C_L}{\frac{\partial qc}{2V_a}}$, $C_{l\delta_e} = \frac{\partial C_L}{\partial \delta_e}$. Similarly, we establish linear approximations for the aerodynamic drag force and pitching moment as follows:

$$C_D(\alpha, q, \delta_e) = C_{do} + C_{d\alpha}\alpha + C_{dq}\frac{c}{2V_a}q + C_{d\delta_e}\delta_e \tag{3.44}$$

$$C_M(\alpha, q, \delta_e) = C_{mo} + C_{m\alpha}\alpha + C_{mq}\frac{c}{2V_a}q + C_{m\delta_e}\delta_e \tag{3.45}$$

The elevating(lifting) force and drag(retarding) force are described in the frame of stability Figure 3.7. To be described onto the F^b, the following equation is true [6] [28]:

$$\begin{bmatrix} f_x \\ 0 \\ f_z \end{bmatrix} = R_s^b(\alpha) \begin{bmatrix} -F_{drag} \\ 0 \\ -F_{lift} \end{bmatrix} \tag{3.46}$$

Where

$$R_s^b(\alpha) = \begin{bmatrix} cos\alpha & 0 & -sin\alpha \\ 0 & 1 & 0 \\ sin\alpha & 0 & cos\alpha \end{bmatrix}$$

The negative sign indicates the NED convention of the F^b.

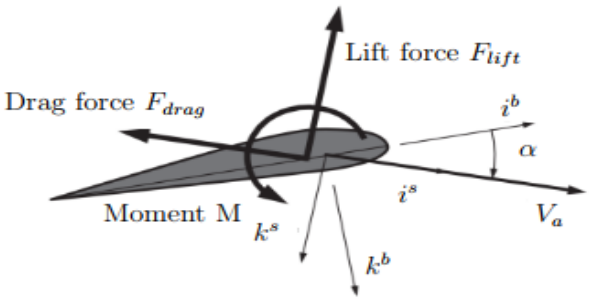

Figure 3.7: Elevating and retarding forces at the positive axes of the angle of attack [6] [28].

3.4.2.2 Aerodynamics of Lateral Motion

The aerodynamics of lateral force and moment directly affect the lateral axes of j^b, and also the moment of roll and yaw, which affected by β as shown in the next expression [6] [28]: When C_L, C_Y, and C_N are a function of $(\beta, p, r, \delta_a, \delta_r)$

$$f_y = \frac{1}{2}\rho V_a^2 S C_Y \tag{3.47}$$

$$L = \frac{1}{2}\rho V_a^2 S b C_L \tag{3.48}$$

$$N = \frac{1}{2}\rho V_a^2 S b C_N \tag{3.49}$$

When b represents the wing span. By following a similar way to longitudinal aerodynamics, the coefficient of lateral aerodynamics's first-order Taylor serious expansion will be expressed as follow [6] [28]:

$$\begin{aligned} C_Y &= C_{yo} + C_{y\beta}\beta + C_{yp}\frac{b}{2V_a}p + C_{yr}\frac{b}{2V_a}r + C_{Y\delta_a}\delta_a + C_{Y\delta_r}\delta_r \\ C_L &= C_{lo} + C_{l\beta}\beta + C_{lp}\frac{b}{2V_a}p + C_{lr}\frac{b}{2V_a}r + C_{l\delta_a}\delta_a + C_{l\delta_r}\delta_r \\ C_N &= C_{no} + C_{n\beta}\beta + C_{np}\frac{b}{2V_a}p + C_{nr}\frac{b}{2V_a}r + C_{n\delta_a}\delta_a + C_{n\delta_r}\delta_r \end{aligned} \tag{3.50}$$

Two generalisations are made in this section: the first is that for UAVs symmetric about $(i^b; k^b)$, C_{Y0}, C_{l0}, and C_{n0} are zero. The second claim is that the coefficients linked to α, β, p, q, and r are known as stability variables, whereas the coefficients linked to δ_a, δ_e, and δ_r are known as control variables.

3.4.3 Force and Moments of Propulsion

Many diverse propeller models can be found in many works of literature. The Bernoulli principle can be used to compute the propeller's thrust and yield a simple model that is useful for UAV modeling. It is expressed as [6]:

$$F_p = S_p \Delta P \tag{3.51}$$

When "S_p" is the area covered by the propeller and $\Delta P = P_{out} - P_{in}$ where "P''_{in} is pressure before the propeller and "P_{out}" is pressure after the propeller. By the principle of Bernoulli, input and output pressure can be expressed as [6] [28]:

$$P_{in} = P_o + \frac{1}{2}\rho V_a^2 \tag{3.52}$$

$$P_{out} = P_o + \frac{1}{2}\rho V_{out}^2 \tag{3.53}$$

When V_{out} is the air velocity at the way out of the propeller. The angular velocity of the propeller and the pulse-width-modulation command δ_t have a linear connection without taking into account the motor's transients. In turn, the propeller produces a way-out air speed of [6] [28]: When k_{mot} is the motor constant.

$$V_{out} = k_{mot}\delta_t$$

Given S_{pr} as the propeller's coverage area, the thrust produced by the motor is:

$$F_{xp} = S_{pr}C_{pr}(P_{out}) - P_{in}$$

$$= \frac{1}{2}\rho S_{pr}C_{pr}[(k_{mot}\delta_t)^2 - V_a^2]$$

Then

$$f_p = \frac{1}{2}\rho S_{pr}C_{pr}\begin{bmatrix}(k_{mot}\delta_t)^2 - V_a^2\\ 0\\ 0\end{bmatrix} \tag{3.54}$$

The thrust exerted directly along the i^b body-axis of the aircraft is typically taken into consideration while developing UAVs. Then, no moments are produced by the thrust regarding the CoM of the UAV [6] [28].

The UAV propeller revolves, applying force to the air that flows through it and advancing the air speed at the same time to provide thrust force on the UAV. The air pulls on the propeller with equal and opposing forces. Overall, these forces cause the UAV to experience torque about its rotational axis. The motor on the UAV generates torque. Torque is a measure of the rotational force applied to an object. In this case, it's the force applied to the propeller. When the torque generated by the motor is applied to the propeller, it induces the propeller to rotate. The torque applied to the propeller is proportional to the square of the propeller's rotational velocity. This means that if you double the rotational velocity of the propeller, the torque will be four times greater (2 squared). The torque generated by the motor is pointed in the opposite direction to the rotation of the propeller. This is a consequence of Newton's third law of motion, which states that for every action, there is an equal and opposite reaction. In this case, the action is the torque applied to the propeller, and the reaction is the equal and opposite torque exerted on the motor. [6] [28]

$$T_p = -k_{Tp}(k_\Omega \delta_t)^2 \tag{3.55}$$

Given the propeller's speed $\Omega = k_\Omega \delta_t$ and the experimentally measured constant k_{Tp}. The moment of propulsion is given by [6] [28]:

$$m_p = \begin{bmatrix} -k_{Tp}(k_\Omega \delta_t)^2 \\ 0 \\ 0 \end{bmatrix} \tag{3.56}$$

The impact of propeller torque is typically subtle and may go unnoticed. However, neglecting the torque effect can lead to a continuous rolling motion opposite to the propeller's rotation. To counteract this, a slight adjustment of the aileron, creating a rolling moment, can effectively offset the propeller torque [6] [28]. Figure 3.8 further illustrates the control allocation and flight dynamics as created in Simulink.

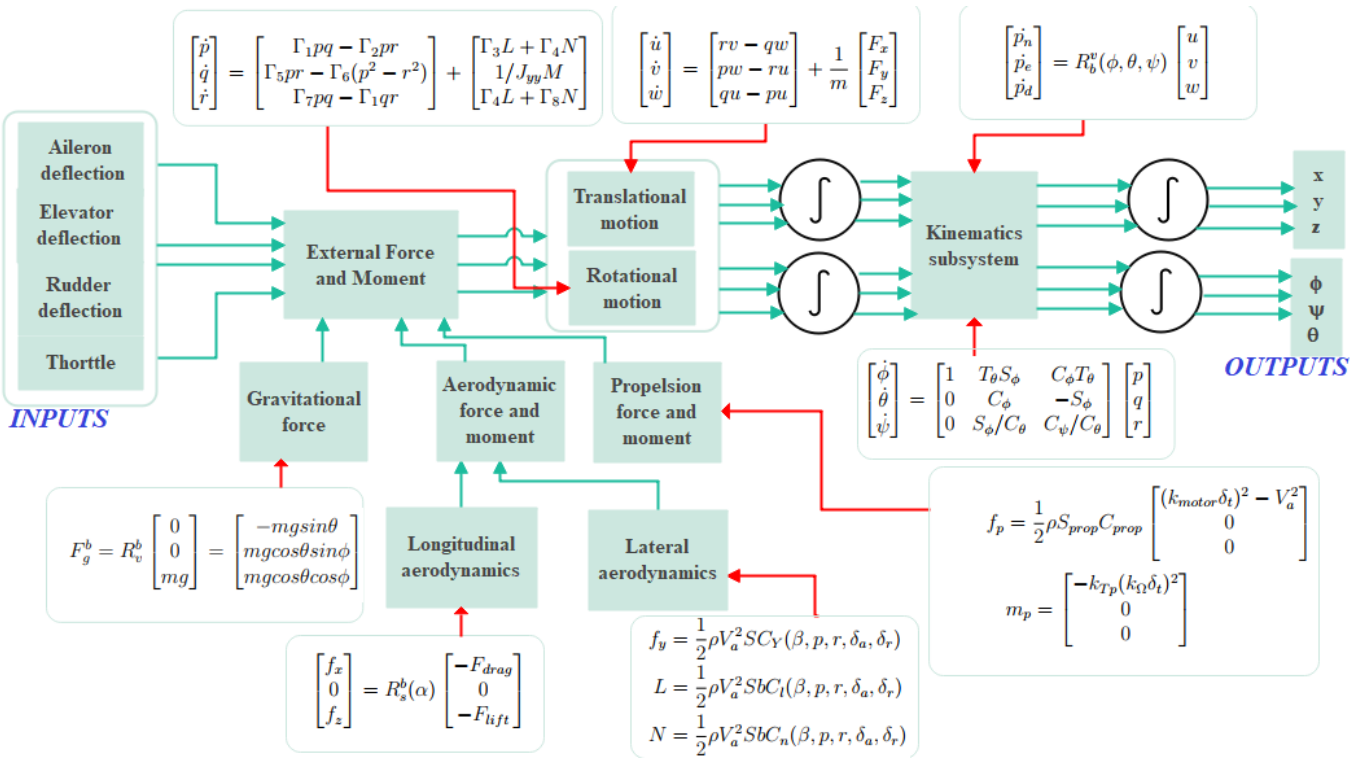

Figure 3.8: Description of the overall nonlinear model of FWUAV

3.5 Model Verification of FWUAV

The FWUAV is modeled as a nonlinear system in the Simulink environment and adheres to physical constraints. Simply apply a control input from the plant (the elevator, rudder, aileron, and throttle deflections) with the parameters of the fixed-wing UAV model shown in the table 3.2 to evaluate the model. Additionally, the general condition of the FWUAV is tested to verify the model. Figure 3.9 represents the open loop model of the fixed-wing UAV, which is built in the Simulink environment. The change of state along with the navigation behavior of the aircraft is tasted with the property of the four control efforts, which is explained in the open-loop simulation result. The model verification of the fixed-wing UAV

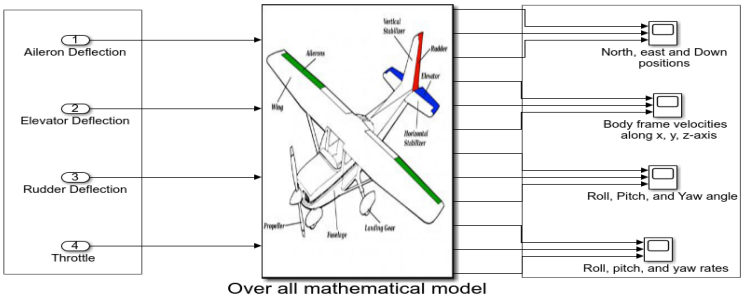

Figure 3.9: Over all flight dynamics of fixed-wing UAV

is held in two different scenarios by applying the arbitrary input command as follows:

Table 3.2: Aerodynamic coefficients and characteristics pertaining to the Aerosonde Unmanned Aerial Vehicle (UAV) [6] [28].

parameter	value	Long.coff	value	Lat.coff	value
m	$13.5Kg$	C_{L_0}	0.28	C_{Y_0}	0
J_x	$0.8244kg\text{-}m^2$	C_{D_0}	0.03	C_{l_0}	0
J_y	$1.135kg\text{-}m^2$	C_{m_0}	-0.02338	C_{n_0}	0
J_z	$1.759kg\text{-}m^2$	C_{L_α}	3.45	C_{Y_β}	-0.98
J_{xz}	$0.1204kg\text{-}m^2$	C_{D_α}	0.3	C_{l_β}	-0.12
S	$0.55m^2$	C_{m_α}	-0.38	C_{n_β}	0.25
b	$2.8956m$	C_{L_q}	0	C_{Y_p}	0
c	$0.18994m$	C_{D_q}	0	C_{l_p}	-0.26
S_{pr}	$0.2027m^2$	C_{m_q}	-3.6	C_{n_p}	0.022
ρ	$1.2682kg/m^3$	$C_{L_\delta e}$	-0.36	C_{Y_r}	0
K_{mot}	80	$C_{D_{\delta e}}$	0	C_{l_r}	0.14
K_{T_p}	0	$C_{m_{\delta e}}$	-0.50	C_{n_r}	-0.35
K_ω	0	C_{pr}	1	$C_{Y_{\delta a}}$	0
		C_{D_p}	0.0437	$C_{l_{\delta r}}$	0.105
				$C_{l_{\delta a}}$	0.08
				$C_{n_{\delta a}}$	0.06
				$C_{Y_{\delta r}}$	-0.17
		$C_{n_{\delta r}}$	-0.032		

Scenario one (applying the elevator deflection)

The aircraft's nose position and wing's angle of attack are both controlled by the elevator. The amount of lift produced by the wing changes as the local flight path's inclination changes. The result is that the airplane climbs or dives. Thus, when the elevator kick shown in figure 3.10 is applied for the open loop system of the fixed wing UAV in figure 3.9 with no rudder and aileron deflections while keeping the throttle of (0.08), then the longitudinal dynamic state(u, w, q, θ)(the translational velocity along the x-axis and z-axis, pitch rate, and pitch angle, respectively) makes a change at the moment of the elevator kick, as shown in figure 3.11 to 3.13. The open loop simulation result shows the elevator command performs as expected.

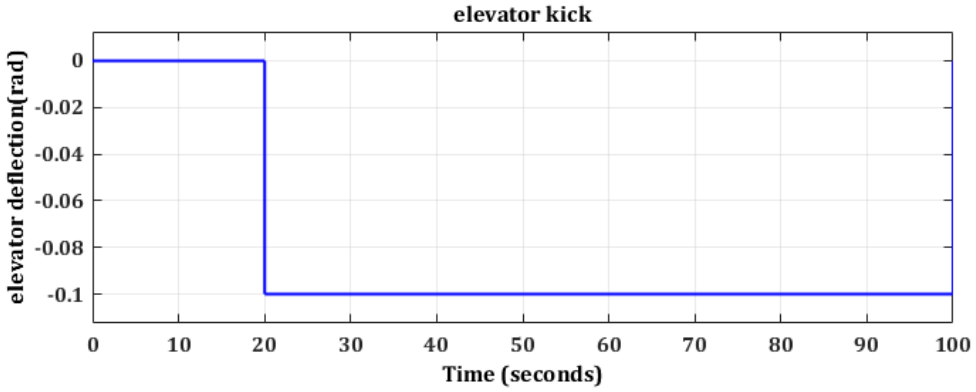

Figure 3.10: Elevator and aileron deflection input signal.

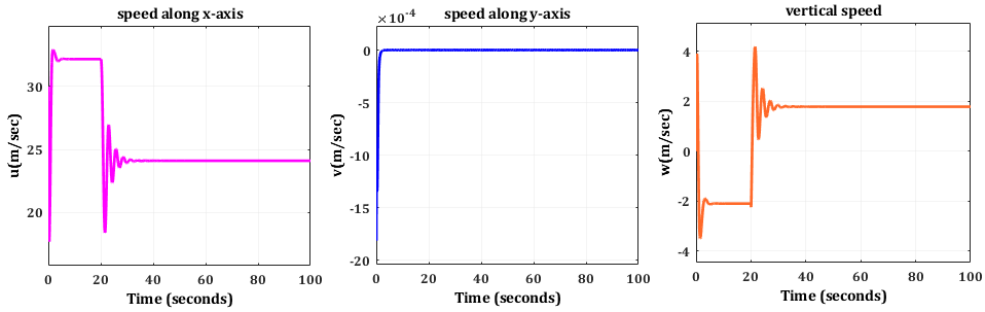

Figure 3.11: The effect of elevator deflection on translational velocities.

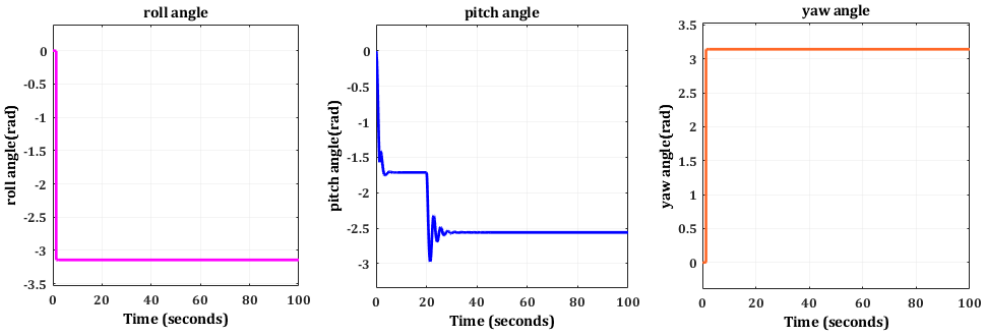

Figure 3.12: The effect of elevator deflection on the orientation of the aircraft.

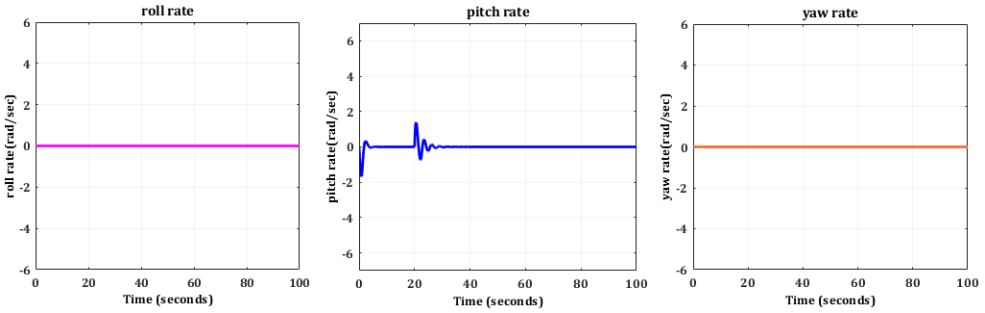

Figure 3.13: The effect of elevator deflection on the roll, pitch, and yaw rate of the aircraft.

Scenario two (applying the aileron deflection)

At the back of the wing, on either side, are two control surfaces known as ailerons. When one is raised, the other is lowered, since they operate in opposition to one another. Their

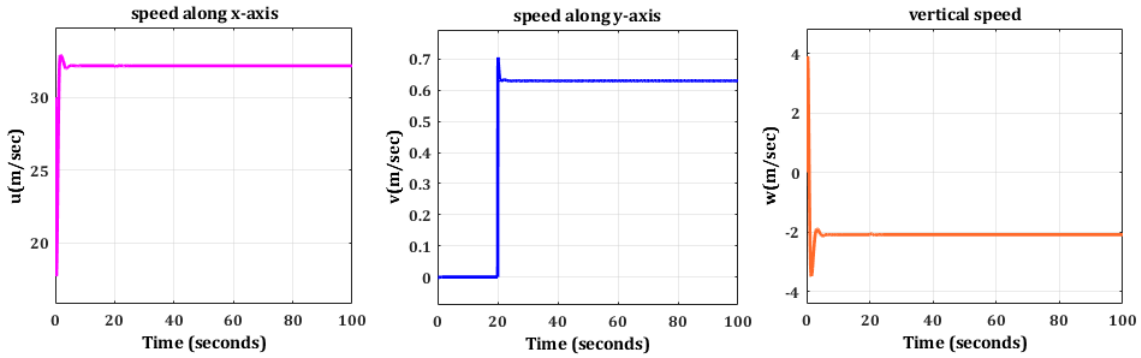

Figure 3.14: The effect of aileron deflection on translational velocities.

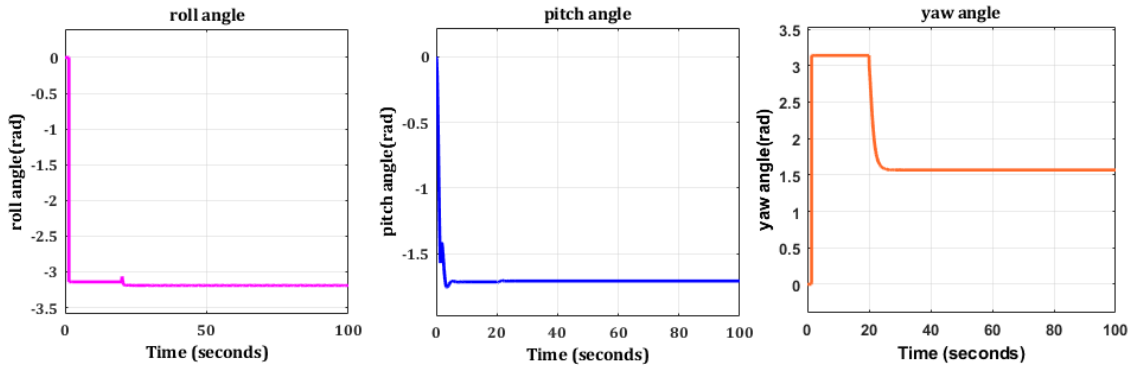

Figure 3.15: The effect of aileron deflection on the orientation of the aircraft

purpose is to make one wing lift more while the other lifts less. They turn the airplane sideways by doing this, which enables the aircraft to turn. Thus, when the aileron deflection in figure 3.10 is applied to the open loop of the fixed wing UAV in figure 3.9 with no rudder and elevator deflection while keeping the throttle of (0.08), the lateral state of the fixed wing UAV(v, p, r, ψ, ϕ)(body frame velocity along the y-axis, roll and, yaw rates as well as roll, and yaw angle, respectively) are making a change as shown in figures 3.14, 3.15 and 3.16 at the time of the aileron deflection is applied to the system as input. From these results, it can be concluded that the mathematical model works correctly.

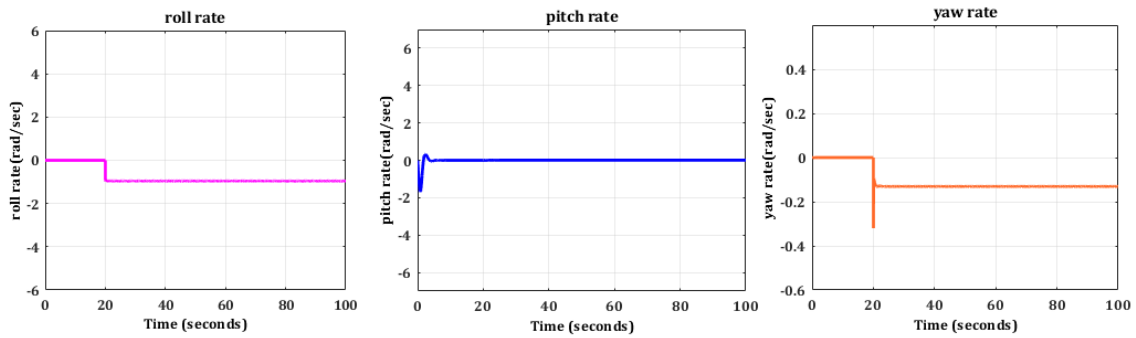

Figure 3.16: The effect of aileron deflection on the roll, pitch, and yaw rate of the aircraft

Chapter 4

Decoupling, State Space Representation, And Controller Design

This chapter describes the decoupling, state space representation, and controller design for FWUAV based on the mathematical models described in Chapter 3.

4.1 Decoupling of The Mathematical Model

The FWUAV (Fixed-Wing Unmanned Aerial Vehicle) model represents a complex and nonlinear system with multiple inputs, multiple outputs, significant coupling, and under-actuation. The decoupling process involves identifying the primary state variable in the control procedure and treating the remaining control variables as uncertainties [10]. It is known that the three control surfaces are used for controlling the rotational position of the aircraft; now it is going to be considered that each control surface controls a single rotation, i.e., the aileron deflection is for roll angle control, the elevator deflection is for pitch angle control, and the rudder deflection is for yaw (heading) motion control.

Roll angle

Since the pitch angle (θ) during rolling motion will often be comparatively small throughout flight, then the roll rate p will primarily impacts $\dot{\phi}$. Then, from equation (3.34),

$$\dot{\phi} = p + q \sin\phi \tan\theta + r \cos\phi \tan\theta$$

let's define

$$d_{\phi_1} = q\sin\phi\tan\theta + r\cos\phi\tan\theta$$

then

$$\dot{\phi} = p + d_{\phi_1}$$

let take first derivative of both sides yields:

$$\ddot{\phi} = \dot{p} + \dot{d}_{\phi_1}$$

And from equation(3.34) substitute for $\dot{p}$ in to the above equation as:

$\ddot{\phi} = \Gamma_1 pq - \Gamma_2 qr + \frac{1}{2}\rho V_a^2 Sb$

$$\times(Cp_o + C_{p_\beta}\beta + C_{p_p}\frac{b}{2V_a}p + Cp_r\frac{b}{2V_a}r + Cp_{\delta_a}\delta_a + Cp_{\delta_r}\delta_r) + \dot{d}_{\phi_1}$$

$$= \Gamma_1 pq - \Gamma_2 qr + \tfrac{1}{2}\rho V_a^2 Sb$$

$$\times(Cp_o + C_{p_\beta}\beta + C_{p_p}\frac{b}{2V_a}(\dot{\phi} - d_{\phi_1}) + Cp_r\frac{b}{2V_a}r + Cp_{\delta_a}\delta_a + Cp_{\delta_r}\delta_r) + \dot{d}_{\phi_1}$$

$$\ddot{\phi} = g_{\phi_1}\dot{\phi} + g_{\phi_2}\delta_a + d_{\phi_2} \tag{4.1}$$

When

$$d_{\phi_2} = \Gamma_1 pq - \Gamma_2 qr + \frac{1}{2}\rho V_a^2 Sb(Cp_o + C_{p_\beta}\beta - C_{p_p}\frac{b}{2V_a}d_{\phi_1} + Cp_r\frac{b}{2V_a}r + Cp_{\delta_r}\delta_r) + \dot{d}_{\phi_1} \tag{4.2}$$

$$g_{\phi_1} = \frac{1}{4}\rho V_a Sb^2 C_{p_p}$$

$$g_{\phi_2} = \frac{1}{2}\rho V_a^2 SbC_{p_{\delta_a}}$$

Pitch angle

In a similar way to roll angle, the primary variable that affects pitch angle θ is pitch rate q. From equation (3.34), we have:

$$\dot{\theta} = q\cos\phi - r\sin\theta$$

by adding q on both sides, we get:

$$\dot{\theta} = q + q(\cos\phi - 1) - r\sin\phi$$

then let's define

$$d_{\theta_1} = q(\cos\phi - 1) - r\sin\phi$$

$$\dot{\theta} = q + d_{\theta_1}$$

take a derivative for both sides, then we get:

$$\ddot{\theta} = \dot{q} + \dot{d}_{\theta_1}$$

From (3.34) substitute for $\dot{q}$ then:

$$\ddot{\theta} = \Gamma_6(r^2 - p^2) + \Gamma_5 pr + \frac{\rho V_a^2 cS}{2J_y}(Cm_o + C_{m_\alpha}(\theta - \gamma) + \frac{c}{2V_a}C_{m_q}(\dot{\theta} - d_{\theta_1}) + C_{\delta_e}\delta_e) + \dot{d}_{\theta_1}$$

Let's define:

$$d_{\theta_2} = \Gamma_6(r^2 - p^2) + \Gamma_5 pr + \frac{\rho V_a^2 cS}{2J_y}(Cm_o - C_{m_\alpha}\gamma - \frac{c}{2V_a}C_{m_q}d_{\theta_1}) + \dot{d}_{\theta_1} \tag{4.3}$$

$$g_{\theta_1} = \frac{1}{4J_y}\rho V_a c^2 S C_{m_q}$$

$$g_{\theta_2} = \frac{1}{2J_y}\rho V_a^2 cS C_{m_\alpha}$$

$$g_{\theta_3} = \frac{1}{4J_y}\rho V_a^2 cS C_{m_{\delta_a}}$$

Then

$$\ddot{\theta} = g_{\theta_1}\dot{\theta} + g_{\theta_2}\theta + g_{\theta_3}\delta_e + d_{\theta_2} \tag{4.4}$$

Yaw angle

Here, the primary variable that influences rotational motion in the y direction is the yaw rate r. Then

$$\dot{\psi} = q\sin\phi\sec\theta + r\cos\phi\sec\theta$$

Adding r on both sides yields:

$$\dot{\psi} = r + q\sin\phi\sec\theta + r(\cos\phi\sec\theta - 1)$$

Let's define

$$d_{\psi_1} = q\sin\phi\sec\theta + r(\cos\phi\sec\theta - 1)$$

$$\dot{\psi} = r + d_{\psi_1}$$

differentiate both sides to gate the second derivatives of the yaw angle as follow:

$$\ddot{\psi} = \dot{r} + \dot{d}_{\psi_1} \tag{4.5}$$

Then substitute for $\dot{r}$ from equation(3.34):

$$\ddot{\psi} = \Gamma_7 pq - \Gamma_1 qr + \frac{1}{2}\rho V_a^2 Sb(C_{ro} + C_{r_\beta}\beta + C_{r_p}\frac{bp}{2V_a} + C_{r_r}\frac{br}{2V_a} + C_{r_{\delta_a}}\delta_a + C_{r_{\delta_r}}\delta_r) + \dot{d}_{\psi_1}$$

$$= \Gamma_7 pq - \Gamma_1 qr + \frac{1}{2}\rho V_a^2 Sb(C_{ro} + C_{r_\beta}\beta + C_{r_p}\frac{bp}{2V_a} + C_{r_r}\frac{b}{2V_a}(\dot{\psi} - d_{\psi_1}) + C_{r_{\delta_a}}\delta_a + C_{r_{\delta_r}}\delta_r) + \dot{d}_{\psi_1}$$

Let define

$$g_{\psi_1} = \frac{1}{4}\rho V_a Sb^2 C_{r_r}$$

$$g_{\psi_2} = \frac{1}{2}\rho V_a^2 SbC_{r_{\delta_r}}$$

$$d_{\psi_2} = \Gamma_7 pq - \Gamma_1 qr + \frac{1}{2}\rho V_a^2 Sb(C_{ro} + C_{r_\beta}\beta + C_{r_p}\frac{bp}{2V_a} - C_{r_r}\frac{b}{2V_a}(d_{\psi_1}) + C_{r_{\delta_a}}\delta_a) + \dot{d}_{\psi_1} \tag{4.6}$$

$$\ddot{\psi} = g_{\psi_1}\dot{\psi} + g_{\psi_2}\delta_r + d_{\psi_2} \tag{4.7}$$

when

$$\begin{bmatrix} C_{po} & C_{ro} \\ C_{p\beta} & C_{r\beta} \\ C_{pp} & C_{rr} \\ C_{p\delta a} & C_{p\delta a} \end{bmatrix} = \begin{bmatrix} \Gamma_3 C_{lo} + \Gamma_4 C_{no} & \Gamma_4 C_{lo} + \Gamma_8 C_{no} \\ \Gamma_3 C_{l\beta} + \Gamma_4 C_{n\beta} & \Gamma_4 C_{l\beta} + \Gamma_8 C_{n\beta} \\ \Gamma_3 C_{lp} + \Gamma_4 C_{np} & \Gamma_4 C_{lr} + \Gamma_8 C_{nr} \\ \Gamma_3 C_{l\delta a} + \Gamma_4 C_{n\delta a} & \Gamma_4 C_{l\delta a} + \Gamma_8 C_{n\delta r} \end{bmatrix}$$

$C_{pr} = \Gamma_3 C_{lr} + \Gamma_4 C_{nr}$, $C_{p\delta r} = \Gamma_3 C_{l\delta r} + \Gamma_4 C_{n\delta r}$, $C_{r\delta a} = \Gamma_4 C_{l\delta a} + \Gamma_8 C_{n\delta a}$, $C_{rp} = \Gamma_4 C_{lp} + \Gamma_8 C_{np}$.

For translational motion, the force is exerted on the body frame, and the positions (x,y,z) are in the inertial frame so that the translational speeds (u,v,w) are transferred to the inertial frame by multiplying a transformation matrix from the body frame to the inertial frame in equation (3.4). This is because FWUAV is an under-actuated system that has four inputs to control six degrees of freedom. It is then needed to make the system fully actuated by assigning a virtual controller. Similar to this, all applied forces are stated in a body frame, which must then be transformed into an inertial frame by multiplying the transformation matrix. The process is demonstrated below: The following is the matrix of transformations from the body frame to the inertial frame:

$$R_b^i = \begin{bmatrix} C_\theta C_\psi & S_\phi S_\theta C_\psi - C_\phi S_\psi & C_\phi S_\theta C_\psi + S_\phi S_\psi \\ C_\theta S_\psi & S_\phi S_\theta S_\psi + C_\phi C_\psi & C_\phi S_\theta S_\psi - S_\phi C_\psi \\ -S_\theta & S_\phi C_\theta & C_\phi C_\theta \end{bmatrix}$$

The body frame velocity transformed to the inertial frame as

$$\begin{bmatrix} u \\ v \\ w \end{bmatrix} = (R_b^i)^T \begin{bmatrix} \dot{p_n} \\ \dot{p_e} \\ \dot{p_d} \end{bmatrix} = (R_b^i)^T \begin{bmatrix} \dot{x} \\ \dot{y} \\ \dot{z} \end{bmatrix} \tag{4.8}$$

Then, as we know, the air speed is the vector sum of translational velocity; thus, thus V_a can be obtained by:

$$V_a = \sqrt{u^2 + v^2 + w^2}$$

In the inertial frame, the sum of all forces exerted is equal to the product of a body's mass and the body's acceleration (Newton's second law). i.e

$$m\ddot{X} = (R_b^i)(F_a^B + F_p^B) + F_g \tag{4.9}$$

When X is $\begin{bmatrix} x & y & z \end{bmatrix}^T$ then from this we can obtain the translational equation as follows: C_α is for $\cos\alpha$ and S_α is for $\sin\alpha$ when

$$C_D(\alpha, q, \delta_e) = C_{Do} + C_{D\alpha}\alpha + C_{Dq}\frac{c}{2V_a}q + C_{D\delta_e}\delta_e$$

$$C_L(\alpha, q, \delta_e) = C_{Lo} + C_{L_\alpha}\alpha + C_{L_q}\frac{c}{2V_a}q + C_{L\delta_e}\delta_e$$

$$C_Y(\beta, p, r, \delta_a, \delta_r) = C_{Yo} + C_{Y\beta}\beta + C_{Yp}\frac{b}{2V_a}p + C_{Yr}\frac{b}{2V_a}r + C_{Y\delta_a}\delta_a + C_{Y\delta_r}\delta_r$$

$$\begin{bmatrix} m\ddot{x} \\ m\ddot{y} \\ m\ddot{z} \end{bmatrix} = \begin{bmatrix} 0 \\ 0 \\ mg \end{bmatrix} + \frac{1}{2}\rho V a^2 S(R_b^i) \begin{bmatrix} -C_\alpha C_D - C_\alpha C_L \\ C_Y \\ S_\alpha C_D - C_\alpha C_L \end{bmatrix} + \frac{1}{2}\rho S_P C_p(R_b^i) \begin{bmatrix} (K_{mot}\delta_t)^2 - Va^2 \\ 0 \\ 0 \end{bmatrix} \tag{4.10}$$

Then, from this:

$$\ddot{x} = \frac{1}{m} cos\theta cos\psi U_1 + \frac{1}{m} d_x \tag{4.11}$$

$$\ddot{y} = \frac{1}{m} cos\theta sin\psi U_1 + \frac{1}{m} d_y \tag{4.12}$$

$$\ddot{z} = -\frac{1}{m} sin\theta U_1 + g + \frac{1}{m} d_z \tag{4.13}$$

When

$$U_1 = \frac{1}{2}\rho S_p C_p((K_{mot}\delta_t)^2 - V_a^2)$$

$$\begin{bmatrix} d_x \\ d_y \\ d_z \end{bmatrix} = \frac{1}{2}\rho V_a^2 S \begin{bmatrix} C_\theta C_\psi & S_\phi S_\theta C_\psi - C_\phi S_\psi & C_\phi S_\theta C_\psi + S_\phi S_\psi \\ C_\theta S_\psi & S_\phi S_\theta S_\psi + C_\phi C_\psi & C_\phi S_\theta S_\psi - S_\phi C_\psi \\ -S_\theta & S_\phi C_\theta & C_\phi C_\theta \end{bmatrix} \begin{bmatrix} -cos\alpha C_D - sin\alpha C_L \\ C_Y \\ sin\alpha C_D - cos\alpha C_L \end{bmatrix} \tag{4.14}$$

Then the over all decoupled mathematical model which governs the dynamics of the FWUAV is:

$$\begin{cases} \ddot{x} = \cos\psi\cos\theta\dfrac{U_1}{m} + \dfrac{1}{m}d_x \\ \ddot{y} = \sin\psi\cos\theta\dfrac{U_1}{m} + \dfrac{1}{m}d_x \\ \ddot{z} = -\sin\theta\dfrac{U_1}{m} + g + \dfrac{1}{m}d_x \\ \ddot{\phi} = g_{\phi_1}\dot{\phi} + g_{\phi_2}\delta_a + d_{\phi_2} \\ \ddot{\theta} = g_{\theta_1}\dot{\theta} + g_{\theta_2}\theta + g_{\theta_3}\delta_e + d_{\theta_2} \\ \ddot{\psi} = g_{\psi_1}\dot{\psi} + g_{\psi_2}\delta_r + d_{\psi_2} \end{cases} \tag{4.15}$$

4.2 State Space Representation of The Model

A state space representation is a mathematical representation of a physical system in which first-order differential equations are used to link input, output, and state variables. The

concept of "state space" refers to a space whose axes are state variables. Within that space, the system's state can be represented as a vector [31]. Let's denote the twelve FWUAV dynamics states as:

$$[x, \dot{x}, y, \dot{y}, z, \dot{z}, \phi, \dot{\phi}, \theta, \dot{\theta}, \psi, \dot{\psi}] = [x_1, x_2, x_3, x_4, x_5, x_6, x_7, x_8, x_9, x_{10}, x_{11}, x_{12}]$$

and the outputs are represented by $Y = [x_1, x_3, x_5, x_7, x_9, x_{11}] = [x, y, z, \phi, \theta, \psi]$ then the overall first-order differential equation of the system can be written as follows: From equations (4.11), (4.12), and (4.13), let $x_1 = x, \dot{x} = x_2$ then $\ddot{x} = \dot{x}_2$ in a similar way for the y and z and for rotational motion dynamics, then the state space representation of the dynamics is written as follows: When

$$\begin{aligned} U_x &= cos\theta cos\psi U_1 \\ U_y &= cos\theta sin\psi U_1 \\ U_z &= -sin\theta U_1 + mg \end{aligned} \tag{4.16}$$

are virtual position control inputs which are responsible for adjusting the actual trajectory with respect to the desired trajectory. This approach of controlling a nonlinear system as if it is linear is known as nonlinear dynamic inversion(NDI) [32] which is a very known method selected in aircraft automatic flight control systems (FCS). And g for gravity (U_1, U_2, U_3, U_4) are the propulsion force, the Aileron, the elevator, and the rudder definitions, respectively.

$$\begin{cases} \dot{x}_1 = x_2 \\ \dot{x}_2 = \frac{1}{m}U_x + \frac{1}{m}d_x \\ \dot{x}_3 = x_4 \\ \dot{x}_4 = \frac{1}{m}U_y + \frac{1}{m}d_y \\ \dot{x}_5 = x_6 \\ \dot{x}_6 = \frac{1}{m}U_z + \frac{1}{m}d_z \\ \dot{x}_7 = x_8 \\ \dot{x}_8 = g_{\phi_1}x_8 + g_{\phi_2}U_2 + d_{\phi_2} \\ \dot{x}_9 = x_{10} \\ \dot{x}_{10} = g_{\theta_1}x_{10} + g_{\theta_2}x_9 + g_{\theta_3}U_3 + d_{\theta_2} \\ \dot{x}_{11} = x_{12} \\ \dot{x}_{12} = g_{\psi_1}x_{12} + g_{\psi_2}U_4 + d_{\psi_2} \end{cases} \tag{4.17}$$

And also $d_{\phi_2}, d_{\psi_2}, d_{\theta_2}$ are explained in equation(4.2), (4.3), (4.6) respectively.

4.3 Controller Design

4.3.1 Sliding Mode Controller Design

4.3.1.1 Overview of SMC

The variable structure control system (VSCS) was created from the pioneering work in Russia of Emelyanow and Barbashin in the early 1960s [33]. The idea did not appear outside Russia until the mid-1970s, when a book by Itkis (1976) and a survey paper by Utkin (1977) were published in England [33]. As the name suggests, a variable structure control mechanism is a type of control mechanism where a control law is purposefully changed during the control process based on some clearly stated principles that depend on the state of the system. Sliding-mode controllers are robust and efficient for systems with substantial uncertainties, including parameter variations, unmodeled dynamics, and external disturbances [34].

The most important aspect of SMC is that it secures the state's sliding motion on the sliding surface, enabling the controlled system to distinguish between the reaching phase and the sliding phase of its state motion. [33].

Reaching-phase:-

- Is characterised as the process by which the controlled system's states are moved from its initial state (x_0) to its final state, the sliding surface as shown in figure 4.1.
- Is a non-robust phase and the system dynamics are highly sensitive to external disturbances.
- The sliding surface here is different from zero, and the discontinued control law is responsible for this phase.

Sliding-phase:-

- At this point, the system states are unaffected by uncertainty and are dependent on the sliding surface.
- Is a robust phase, and an equivalent control strategy will compel the dynamics of the system to remain on the sliding surface.

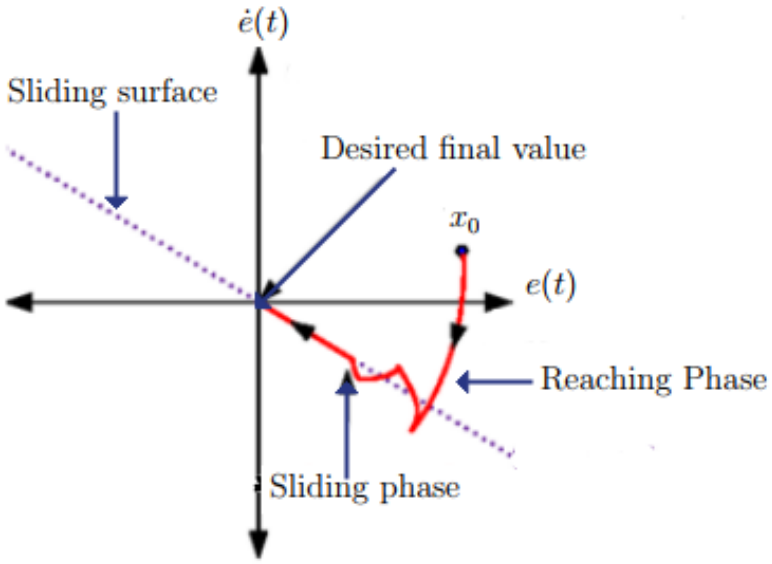

Figure 4.1: SMC tracking dynamics [35]

In order to accomplish the sliding condition in the reaching phase, a discontinuous type of control law (U_{dis}) is used, and in the sliding phase, the equivalent control law (U_{eq}) is responsible for the system dynamics to stay in the sliding surface [33]. Then the resulting control law becomes:

$$U(t) = U_{eq}(t) + U_{dis}(t) \tag{4.18}$$

4.3.1.2 Control Architecture

Because of the under-actuation of the FWUAV translational dynamics, the translational motion of the plant is controlled indirectly. As a result, the nested control approach as shown in figure 4.2, is used, and the reference attitude signals are obtained by the outer position control loop based on the position's reference target response. And the inside loop controls the FWUAV's attitude depending on the generated signals. To assure that every FWUAV output follows specified trajectories, virtual controllers are introduced to the plant. The physical meaning of this control strategy is the control of the translation motion of the FWUAV based on desired Euler angles and the overall thrust force which are indicated in equations 4.16 and 4.19.

$$\begin{cases} \psi_d = \arctan(\dfrac{U_y}{U_x}) \\ \theta_d = \arcsin[\dfrac{mg - U_z}{U_1}] \\ U_1 = \sqrt{U_x^2 + U_y^2 + U_z^2} \end{cases} \tag{4.19}$$

Outer loop controller design

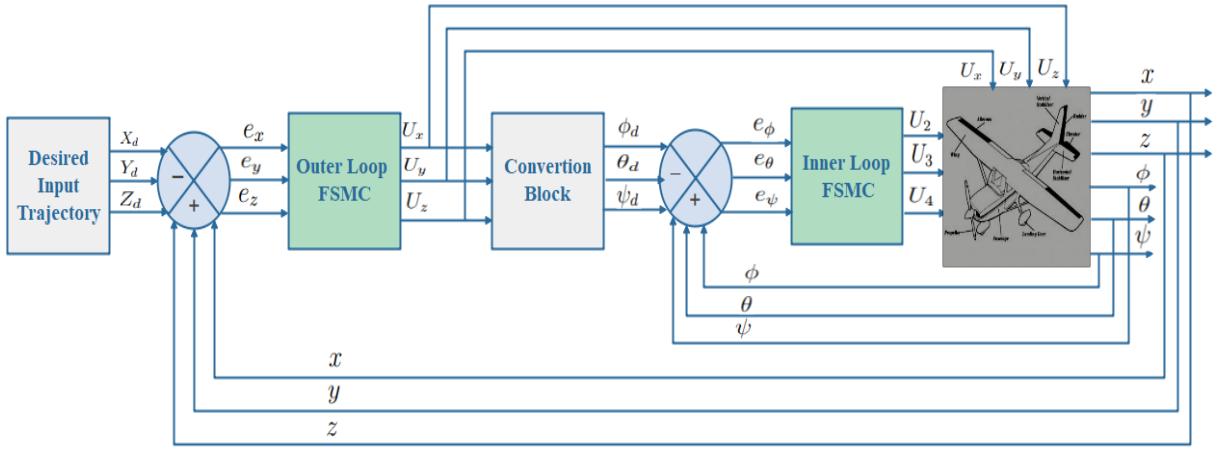

Figure 4.2: Control architecture scheme block diagram

The outer loop is used to indirectly control the three inertial positions (x, y, and z). So the virtual control concept is used to perform this task. The outer control loop controller outputs (U_x, U_y, and U_z) are used to determine the desired yaw and pitch angles, as shown in equations 4.16 and 4.19:

Designing a sliding mode controller consists of two steps: the first step is designing a sliding surface, which is a function of the error dynamics during tracking problems, and then designing a control law. The sliding surface $s(X,t) = 0$ with initial conditions $e(0) = 0$ can be defined as, when X is a column vector in 3D [36]:

$$s(X,t) = (\frac{d}{dt} + c)^{n-1} e(t) \tag{4.20}$$

where c is a strictly positive real constant, which indicates the slope of the sliding manifolds, and e is the tracking error. For n = 2 (second-order system), the sliding surface becomes:

$$s = \dot{e} + ce \tag{4.21}$$

Let us define the position error which is the difference between the actual value and the desired value and its derivatives:-

$$\begin{bmatrix} e_x \\ e_y \\ e_z \end{bmatrix} = \begin{bmatrix} x - x_d \\ y - y_d \\ z - z_d \end{bmatrix}, \begin{bmatrix} \dot{e}_x \\ \dot{e}_y \\ \dot{e}_z \end{bmatrix} = \begin{bmatrix} \dot{x} - \dot{x}_d \\ \dot{y} - \dot{y}_d \\ \dot{z} - \dot{z}_d \end{bmatrix}, \begin{bmatrix} \ddot{e}_x \\ \ddot{e}_y \\ \ddot{e}_z \end{bmatrix} = \begin{bmatrix} \ddot{x} - \ddot{x}_d \\ \ddot{y} - \ddot{y}_d \\ \ddot{z} - \ddot{z}_d \end{bmatrix} \tag{4.22}$$

Then the sliding surface for the position becomes:-

$$\begin{bmatrix} s_x \\ s_y \\ s_z \end{bmatrix} = \begin{bmatrix} \dot{e}_x \\ \dot{e}_y \\ \dot{e}_z \end{bmatrix} + c \begin{bmatrix} e_x \\ e_y \\ e_z \end{bmatrix} \tag{4.23}$$

From the state space representation of the system in equation 4.17, the dynamic equation that governs the forward motion is:

$$\dot{x}_1 = x_2 \tag{4.24}$$

$$\dot{x}_2 = \frac{1}{m}U_x + \frac{1}{m}d_x \tag{4.25}$$

When $\dot{x} = x_2$ and $x = x_1$ then the controller design is shown below: from equation (4.21), the sliding manifold is given by

$$s_x = \dot{e}_x + c_x e_x$$

Making the derivative of the sliding manifold is equal to zero will therefore yield an equivalent control approach. i.e

$$\dot{s}_x = 0 \Rightarrow c_x \dot{e}_x + \ddot{e}_x = c_x[x_2 - x_d] + \dot{x}_2 - \ddot{x}_d = c_x[x_2 - x_d] + \frac{1}{m}U_x + \frac{1}{m}d_x - \ddot{x}_d = 0$$

Then, by rearranging the above equation, the equivalent control law can be:

$$U_{xeq} = m[\ddot{x}_d - \frac{1}{m}d_x - c_x[x_2 - \dot{x}_d]] \tag{4.26}$$

Let's choose the discontinuous controller:

$$U_{xdis} = -k_x sgn(s_x) \tag{4.27}$$

As previously stated, the overall control law is made up of two terms: the equivalent and the discontinuous controller. Then

$$U_x = U_{xeq} + U_{xdis} = m[\ddot{x}_d - \frac{1}{m}d_x - c_x[x_2 - \dot{x}_d]] - k_x sgn(s_x) \tag{4.28}$$

Condition on the switching gain(k_i)

The control rule must satisfy the gradient of the Lyapunov candidate decreasing as time

grows in the Lyapunov function, which is selected to be a positive definite function i.e., $\dot{V}_i(.) < 0$ in order to assure the reach-ability condition [37]. As the Lyapunov candidate, let's pick a positive definite function [37]:

$$V_x = \frac{1}{2}s_x^2 \tag{4.29}$$

The goal is to create a gain for a discontinuous control strategy that causes the gradient of the selected Lyapunov candidate to decrease as time goes on.

$$\begin{aligned}
\dot{V}_x &= s_x\dot{s}_x < 0 \\
&= s_x[c_x(x_2 - \dot{x}_d + \dot{x}_2 - \ddot{x}_d] < 0 \\
&= s_x[c_x(x_2 - \dot{x}_d) + \frac{1}{m}d_x + \ddot{x}_d - \frac{1}{m}d_x - c_x(x_2 - \dot{x}_d) - k_x sgn(s_x) - \ddot{x}_d] < 0 \\
&= s_x[-k_x sgn(s_x)] < 0
\end{aligned}$$

In order to satisfy this condition, the gain must be positive, i.e $k_x > 0$.

Following a similar procedure for the vertical motion controller (U_z) and the lateral motion controller (U_y), it can be written as follows: From equation (4.17), the lateral motion dynamics is

$$\begin{cases} \dot{x}_3 = x_4 \\ \dot{x}_4 = \frac{1}{m}U_y + \frac{1}{m}d_y \end{cases} \tag{4.30}$$

$$\begin{cases} U_{yeq} = m[\ddot{y}_d - c_y(x_4 - \dot{y}_d - \frac{1}{m}d_y)] \\ U_{ydis} = -k_y sgn(s_y) \\ U_y = m[\ddot{y}_d - c_y(x_4 - \dot{y}_d) - \frac{1}{m}d_y] - k_y sgn(s_y) \end{cases} \tag{4.31}$$

$$\begin{cases} \dot{x}_5 = x_6 \\ \dot{x}_6 = \frac{1}{m}U_z + \frac{1}{m}d_z \end{cases} \tag{4.32}$$

$$\begin{cases} U_{zeq} = m[\ddot{z}_d - c_z(x_6 - \dot{z}_d - \frac{1}{m}d_z)] \\ U_{zdis} = -k_y sgn(s_y) \\ U_z = m[\ddot{z}_d - c_y(x_6 - \dot{z}_d) - \frac{1}{m}d_z] - k_z sgn(s_z) \end{cases} \tag{4.33}$$

In the reach-ability condition, by following the same approach as the horizontal control strategy, the gain along the y-axis and z-axis is positive. i.e $k_{y,z} > 0$

The outer loop control effort (U_x, U_y, and U_z) are responsible for adjusting the actual trajectory based on the desired trajectory by reducing the tracking error to zero. In order to compensate for under-actuation of the FWUAV, θ, ψ, and U_1 are employed to generate three virtual controls that are utilized to control the position independently. In other words, those virtual control inputs imply that the three inputs (θ, ψ, and U_1) indirectly govern the motion along x, y, and z. The relationship between the desired pitch angle, yaw angle, and U_1 is explained in equation 4.19. Finally, the three virtual control inputs are:

$$\begin{cases} U_x = m[\ddot{x}_d - \frac{1}{m}d_x - c_x[x_2 - \dot{x}_d]] - k_x sgn(s_x) \\ U_y = m[\ddot{y}_d - c_y(x_4 - \dot{y}_d) - \frac{1}{m}d_y] - k_y sgn(s_y) \\ U_z = m[\ddot{z}_d - c_y(x_6 - \dot{z}_d) - \frac{1}{m}d_z] - k_z sgn(s_z) \end{cases} \tag{4.34}$$

Inner loop controller design

This loop controls FWUAV's attitude. The roll desired angle (ϕ_d) is given on the basis of task that the fixed-wing UAV needs to accomplish, and the desired pitch (θ_d) and yaw (ψ_d) angles are obtained from the outer control loop as shown in equation (4.19). Then let's define the sliding surface and error dynamics for the attitude of the system as follows:

$$\begin{bmatrix} e_\phi \\ e_\theta \\ e_\psi \end{bmatrix} = \begin{bmatrix} x_7 - \phi_d \\ x_9 - \theta_d \\ x_{11} - \psi_d \end{bmatrix} \tag{4.35}$$

$$\begin{bmatrix} s_\phi \\ s_\theta \\ s_\psi \end{bmatrix} = \begin{bmatrix} c_\phi e_\phi + \dot{e}_\phi \\ c_\theta e_\theta + \dot{e}_\theta \\ c_\psi e_\psi + \dot{e}_\psi \end{bmatrix} \tag{4.36}$$

When (x_7, x_9, x_{11}) represents the roll, pitch, and yaw angle respectively and c_i $(i = \phi, \theta, \psi)$ is a positive real constant which indicates the slope of the sliding manifold and determined by the designer based on Hurwitz stability criterion.

Roll angle controller design

From the state space model in equation(4.17), the dynamic equation which governs the roll motion is:-

$$\begin{cases} \dot{x}_7 = x_8 \\ \dot{x}_8 = g_{\phi_1} x_8 + g_{\phi_2} U_2 + d_{\phi_2} \end{cases} \tag{4.37}$$

$$\begin{aligned} s_\phi &= c_\phi e_\phi + \dot{e}_\phi \\ &= c_\phi [x_7 - \phi_d] + x_8 - \dot{\phi}_d \\ \dot{s}_\phi &= c_\phi \dot{e}_\phi + \ddot{e}_\phi \\ &= c_\phi [x_8 - \dot{\phi}_d] + \dot{x}_8 - \ddot{\phi}_d \\ &= c_\phi [x_8 - \dot{\phi}_d] + g_{\phi_1} x_8 + g_{\phi_2} U_2 + d_{\phi_2} - \ddot{\phi}_d \\ \dot{s}_\phi &= 0 \\ &= c_\phi [x_8 - \dot{\phi}_d] + g_{\phi_1} x_8 + g_{\phi_2} U_2 + d_{\phi_2} - \ddot{\phi}_d = 0 \end{aligned}$$

Then, by rearranging the above equation, the equivalent control law for the roll motion controller is given by:

$$U_{2eq} = \frac{1}{g_{\phi_2}} [-c_\phi (x_8 - \dot{\phi}_d) - g_{\phi_1} x_8 - d_{\phi_2} + \ddot{\phi}_d] \tag{4.38}$$

Let's choose the discontinuous control law:

$$U_{2dis} = -k_\phi sgn(s_\phi) \tag{4.39}$$

Then the overall control law for the rolling motion input is:

$$U_2 = U_{2eq} + U_{2dis} = \frac{1}{g_{\phi_2}} [-c_\phi (x_8 - \dot{\phi}_d) - g_{\phi_1} x_8 - d_{\phi_2} + \ddot{\phi}_d] - k_\phi sgn(s_\phi) \tag{4.40}$$

The switching gain can be determined by choosing a positive definite Lyapunov function, as we do during position controller design. Then let's define the Lyapunov candidate:

$$\begin{aligned} V_\phi &= \frac{1}{2} s_\phi^2 \\ \dot{V}_\phi &= s_\phi \dot{s}_\phi < 0 \\ &= s_\phi [c_\phi [x_8 - \dot{\phi}_d] + g_{\phi_1} x_8 + g_{\phi_2} U_2 + d_{\phi_2} - \ddot{\phi}_d] < 0 \end{aligned}$$

$$= s_\phi[c_\phi[x_8 - \dot{\phi}_d] + g_{\phi_1}x_8 + g_{\phi_2}[\frac{1}{g_{\phi_2}}[-c_\phi(x_8 - \dot{\phi}_d) - g_{\phi_1}x_8 - d_{\phi_2} + \ddot{\phi}_d]$$

$$-k_\phi sgn(s_\phi)] + d_{\phi_2} - \ddot{\phi}_d] < 0$$

$$= s_\phi[g_{\phi_2}(-k_\phi sgn(s_\phi)] < 0$$

$$= -g_{\phi_2}k_\phi|s_\phi| < 0$$

$$\Rightarrow k_\phi < 0$$

g_{ϕ_2} is already a negative constant, then the domain of switching gain(k_ϕ) must be less than zero to satisfy the reachability condition.

Pitch angle controller design

The dynamic equation that governs the pitch motion is given in(4.17) as:

$$\begin{cases} \dot{x}_9 = x_{10} \\ \dot{x}_{10} = g_{\theta_1}x_{10} + g_{\theta_2}x_9 + g_{\theta_3}U_3 + d_{\theta_2} \end{cases} \tag{4.41}$$

$$s_\theta = c_\theta e_\theta + \dot{e}_\theta$$

$$= c_\theta[x_9 - \theta_d] + x_{10} - \dot{\theta}_d$$

$$\dot{s}_\theta = c_\theta \dot{e}_\theta + \ddot{e}_\theta$$

$$= c_\theta[x_{10} - \dot{\theta}_d] + \dot{x}_{10} - \ddot{\theta}_d$$

$$= c_\theta[x_{10} - \dot{\theta}_d] + g_{\theta_1}x_{10} + g_{\theta_2}x_9 + g_{\theta_3}U_3 + d_{\theta_2} - \ddot{\theta}_d$$

$$\dot{s}_\theta = 0$$

$$= c_\theta[x_{10} - \dot{\theta}_d] + g_{\theta_1}x_{10} + g_{\theta_2}x_9 + g_{\theta_3}U_3 + d_{\theta_2} - \ddot{\theta}_d = 0$$

Then by rearranging the above equation the equivalent control law will be:

$$U_{3eq} = \frac{1}{g_{\theta_3}}[-c_\theta(x_{10} - \dot{\theta}_d) - g_{\theta_1}x_{10} - g_{\theta_2}x_9 - d_{\theta_2} + \ddot{\theta}_d] \tag{4.42}$$

Let's choose the discontinuous control law:

$$U_{3dis} = -k_\theta sgn(s_\theta) \tag{4.43}$$

Then the overall control effort for the pitching motion will be:

$$U_3 = U_{3eq} + U_{3dis} = \frac{1}{g_{\theta_3}}[-c_\theta(x_{10} - \dot{\theta}_d) - g_{\theta_1}x_{10} - g_{\theta_2}x_9 - d_{\theta_2} + \ddot{\theta}_d] - k_\theta sgn(s_\theta) \tag{4.44}$$

The switching gain can be determined by choosing the Lyapunov candidate in which the gradient of the Lyapunov function must decrease as time go up.

$$\begin{aligned}
V_\theta &= \frac{1}{2}s_\theta^2 \\
\dot{V}_\theta &= s_\theta \dot{s}_\theta < 0 \\
&= s_\theta[c_\theta[x_{10} - \dot{\theta}_d] + g_{\theta_1}x_{10} + g_{\theta_2}x_9 + g_{\theta_3}U_3 + d_{\theta_2} - \ddot{\theta}_d] < 0 \\
&= s_\theta[c_\theta(x_{10} - \dot{\theta}_d) + g_{\theta_1}x_{10} + g_{\theta_2}x_9 + g_{\theta_3}[\frac{1}{g_{\theta_3}}[-c_\theta(x_{10} - \dot{\theta}_d) - g_{\theta_1}x_{10} - g_{\theta_2}x_9 - d_{\theta_2} + \ddot{\theta}_d] \\
&- k_\theta sgn(s_\theta)] + d_{\theta_2} - \ddot{\theta}_d] < 0 \\
&= s_\theta[g_{\theta_3}(-k_\theta sgn(s_\theta)] < 0 \\
&= -g_{\theta_3}k_\theta|s_\theta| < 0, g_{\theta_3} < 0 \\
&\Rightarrow k_\theta < 0
\end{aligned}$$

g_{θ_3} is already a negative constant then the domain of switching gain(k_θ) must be less than zero to satisfy the reach-ability condition.

Yaw angle controller design

From the state space model in equation(4.17), the dynamic equation which governs the yaw motion is:-

$$\begin{cases} \dot{x}_{11} = x_{12} \\ \dot{x}_{12} = g_{\psi_1}x_{12} + g_{\psi_2}U_4 + d_{\psi_2} \end{cases} \tag{4.45}$$

$$
\begin{aligned}
s_\psi &= c_\psi e_\psi + \dot{e}_\psi \\
&= c_\psi[x_{11} - \psi_d] + x_{12} - \dot{\psi}_d \\
\dot{s}_\psi &= c_\psi \dot{e}_\psi + \ddot{e}_\psi \\
&= c_\psi[x_{12} - \dot{\psi}_d] + \dot{x}_{12} - \ddot{\psi}_d \\
&= c_\psi[x_{12} - \dot{\psi}_d] + g_{\psi_1} x_{12} + g_{\psi_2} U_4 + d_{\psi_2} - \ddot{\psi}_d \\
\dot{s}_\psi &= 0 \\
&= c_\psi[x_{12} - \dot{\psi}_d] + g_{\psi_1} x_{12} + g_{\psi_2} U_4 + d_{\psi_2} - \ddot{\psi}_d = 0
\end{aligned}
$$

The equivalent yaw control input is:

$$U_{4eq} = \frac{1}{g_{\psi_2}}[-c_\psi(x_{12} - \dot{\psi}_d) - g_{\psi_1} x_{12} - d_{\psi_2} + \ddot{\psi}_d] \tag{4.46}$$

Let's choose the discontinuous control effort be:

$$U_{4dis} = -k_\psi sgn(s_\psi) \tag{4.47}$$

Then the overall control law for the yawing motion control input is:

$$U_4 = \frac{1}{g_{\psi_2}}[-c_\psi(x_{12} - \dot{\psi}_d) - g_{\psi_1} x_{12} - d_{\psi_2} + \ddot{\psi}_d] - k_\psi sgn(s_\psi) \tag{4.48}$$

The switching gain can be determined by choosing a positive definite Lyapunov function as we do before. Then let's define the Lyapunov candidate:

$$
\begin{aligned}
V_\psi &= \frac{1}{2} s_\psi^2 \\
\dot{V}_\psi &= s_\psi \dot{s}_\psi < 0 \\
&= s_\psi[c_\psi(x_{12} - \dot{\psi}_d) + g_{\psi_1} x_{12} + g_{\psi_2} U_4 + d_{\psi_2} - \ddot{\psi}_d] < 0 \\
&= s_\psi[c_\psi[x_{12} - \dot{\psi}_d] + g_{\psi_1} x_{12} + g_{\psi_2}[\frac{1}{g_{\psi_2}}[-c_\psi(x_{12} - \dot{\psi}_d) - g_{\psi_1} x_{12} - d_{\psi_2} + \ddot{\psi}_d] \\
&- k_\psi sgn(s_\psi)] + d_{\psi_2} - \ddot{\psi}_d] < 0 \\
&= s_\psi[g_{\psi_2}(-k_\psi sgn(s_\psi)] < 0 \\
&= -g_{\psi_2} k_\psi |s_\psi| < 0 \\
&\Rightarrow k_\psi < 0
\end{aligned}
$$

In order to reduce chattering, an approximate (smoothed) implementation of sliding mode

control method is applied in place of the discontinuous signum function being replaced by the quasi function, or tanh function [38].

$$U_{idis} = -k_i \tanh(s_i/\epsilon) \tag{4.49}$$

When "i" represents (x, y, z, ϕ, θ, ψ) $\epsilon > 0$ and $\epsilon \approx 0$. Then the overall control effort for both translational and rotational motion is:

$$\begin{cases} U_x = m[\ddot{x}_d - \frac{1}{m}d_x - c_x[x_2 - \dot{x}_d]] - k_x \tanh(\frac{s_x}{\epsilon}) \\ U_y = m[\ddot{y}_d - c_y(x_4 - \dot{y}_d) - \frac{1}{m}d_y] - k_y \tanh(\frac{s_y}{\epsilon}) \\ U_z = m[\ddot{z}_d - c_y(x_6 - \dot{z}_d) - \frac{1}{m}d_z] - k_z \tanh(\frac{s_z}{\epsilon}) \\ U_2 = \frac{1}{g_{\phi_2}}[-c_\phi(x_8 - \dot{\phi}_d) - g_{\phi_1}x_8 - d_{\phi_2} + \ddot{\phi}_d] - k_\phi \tanh(\frac{s_\phi}{\epsilon}) \\ U_3 = \frac{1}{g_{\theta_3}}[-c_\theta(x_{10} - \dot{\theta}_d) - g_{\theta_1}x_{10} - g_{\theta_2}x_9 - d_{\theta_2} + \ddot{\theta}_d] - k_\theta \tanh(\frac{s_\theta}{\epsilon}) \\ U_4 = \frac{1}{g_{\psi_2}}[-c_\psi(x_{12} - \dot{\psi}_d) - g_{\psi_1}x_{12} - d_{\psi_2} + \ddot{\psi}_d] - k_\psi \tanh(\frac{s_\psi}{\epsilon}) \end{cases} \tag{4.50}$$

But by using this smoothed approximate implementation of SMC, we can reduce chattering for a simple system (i.e., a system with little uncertainty and little external disturbance). Then we have to use another mechanism for further reduction of the chattering problem. To overcome this issue, fuzzy-based SMC (FSMC) will be implemented for this thesis.

4.3.2 Fuzzy-Based SM Controller Design

Even though the sliding mode controller has many preferable properties like disturbance rejection, tolerating parameter variation, and uncertainties, the chattering effect followed by the discontinuity in the control effort has a negative impact on the actuators and is often mentioned as a main drawback for real-time implementations. Chattering has to be reduced for the controller to properly carry out the desired task. The smoothed implementation of SMC does not completely remove the chattering of the discontinuous function; hence, it needs the integration of an advanced intelligent controller like the FSMC for this thesis. The integration is accomplished by replacing the discontinuous phase of SMC with a fuzzy logic controller. A fuzzy control system denotes the control of processes through the fuzzy linguistic rule of inference. To explain fuzzy control more, it is a mathematical system that

analyzes analog input values based on logical variables [39]. And it is a way of representing, manipulating, and executing a human's heuristic understanding of how to control a system [40].

Fuzzy logic controllers(FLCs) are control systems that are characterized by a knowledge base consisting of the so-called fuzzy IF-THEN rules. In the fuzzy IF-THEN rule, a word can be characterized by a continuous membership function, which takes values from 0 to 1, representing the degree of truth of the statements [41]. Therefore, the fuzzy logic controller consists of four main components to interact with the real system or plant. These components are fuzzification, inference system, knowledge base, and defuzzification, which are explained below [42]:

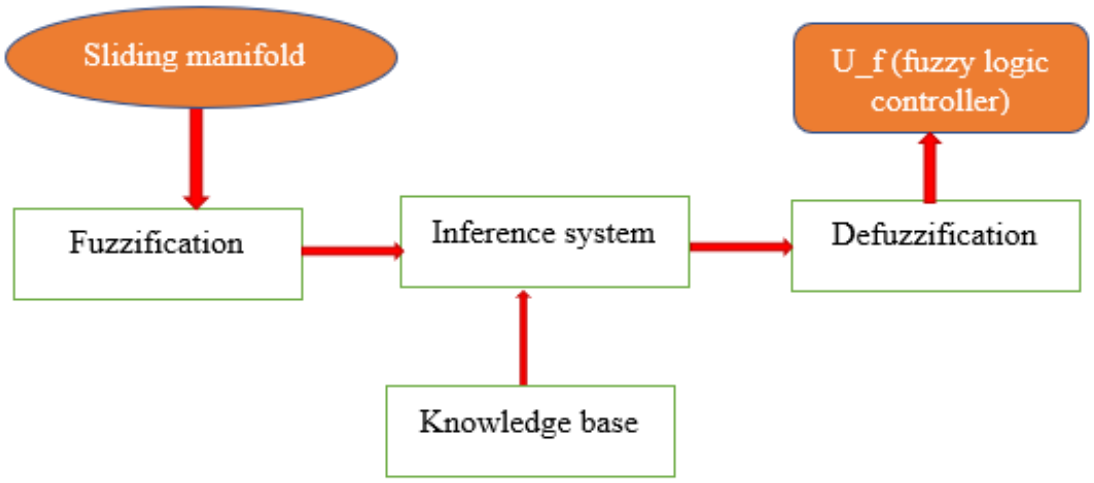

Figure 4.3: Structure and components of fuzzy logic control system

4.3.2.1 Fuzzification

Fuzzification converts crisp inputs into a fuzzy set and assigns a degree of membership function between 0 and 1 to each fuzzy input value. The fuzzified output is interpreted and correlated to the rule in the rule base. In this step, the decision that needs to be made is relays on the total number of inputs, the scope of the discourse inverse, and the number and shape of fuzzy set [42].

4.3.2.2 Rule Base or Knowledge Base

The rule base grasps knowledge in the form of IF-THEN rules which are given by an expert based on how to manage the system effectively. The rule base is the most vital part of FLCs

so that the remaining components are going to implement the defined rule in a sensible and effective way [43].

4.3.2.3 Fuzzy Inference Mechanism

The two primary approaches of the inference mechanisms are composition-based inference and individual rule-based inference systems [44]. In this method, the combination of the fuzzifier's output and the rule base is employed to construct the output fuzzy set. This set is then applied by the defuzzifier, which calculates the controller output based on the established fuzzy set [44].

In composition-based inference approaches, the entire set of rules in the rule base is consolidated into a single fuzzy relation. The inference is then conducted between the fuzzified input and this comprehensive fuzzy relation, defining the complete set of rules. Ultimately, a fuzzy set is derived to depict the fuzzy value of the overall control output. Conversely, in individual rule-based mechanisms, each rule in the rule base defines a distinct output fuzzy set. The overall output of the fuzzy inference mechanism is determined by aggregating these individual output fuzzy sets. Generally, the individual rule-based inference mechanism is preferred over the composition rule-based approach due to its computational efficiency and memory-saving characteristics [44].

There are three primary types of operations employed in the inference mechanism. The initial type involves operations among the terms found in the premises of rules within the rule base. Typically, the premises' terms are linked by AND, OR, and NOT operators. Nevertheless, in the majority of control applications, the AND operator is the one predominantly utilized [44]. These operators perform computations on the membership degrees of input values, producing a singular outcome that represents the certainty of each rule in the rule base. The next type of operation is implication, involving the interaction between the certainty of a rule and the output fuzzy set associated with that rule. Following implication, each rule in the rule base generates an inferred output represented as a fuzzy set. Aggregation, the third operation type, consolidates all the inferred output fuzzy sets to derive a comprehensive output fuzzy set.

4.3.2.4 Defuzzification

In this process, the output from the inference mechanism is defuzzified in order to get a numerical or crisp controller output. The most known defuzzification mechanism is the center of gravity(CoG) method [44], which specifies the numerical controller output as the center of the area covered by the membership function $\mu_{out}(u)$ which is expressed as:

$$k = \frac{\int u\mu_{out}(u)du}{\int \mu_{out}(u)du} \tag{4.51}$$

But, the integral calculation in the center of gravity mechanism is computationally difficult, it is because $\mu_{out}(u)$ is not regular [44]. Since the resultant output fuzzy set is the union of the implied output fuzzy set, a good approximation of (4.35) is a center of average defuzzification mechanism which is expressed mathematically in (4.36), so it is computationally not difficult, and it is widely implemented in defuzzification mechanism for practical implementation of fuzzy logic control application [45].

$$k = \frac{\Sigma_{i=1}^{N} c_i u_i}{\Sigma_{i=1}^{N} u_i} \tag{4.52}$$

Where k is a crisp controller output, N is the total number of rules, c_i is the center of gravity for the implied fuzzy set for rule i, and u represents the area under the implied fuzzy set.

4.3.2.5 Membership Function

The MF helps us to express the linguistic terms in the form of numerical value and represents the fuzzy set graphically. For example, a fuzzy set A in the universe of discourse X is expressed as $\mu_A : X \rightarrow [0\ 1]$, i.e. every component of X represented by a value between 0 and 1, and it is referred to as a degree of membership. The x and y axis of a membership function denotes the universe of discourse and the degree of membership in the interval of [0 1] [45]. Based on the shape, the membership function can be categorized as triangular, trapezoidal, Gaussian, bell-shaped and etc. Some of them are illustrated in the figure below. the selection of the shape of the membership function is relays on the interest of the designer since there is no unique rule about selecting. For this thesis, a triangular membership function is chosen due to ease of calculation [34].

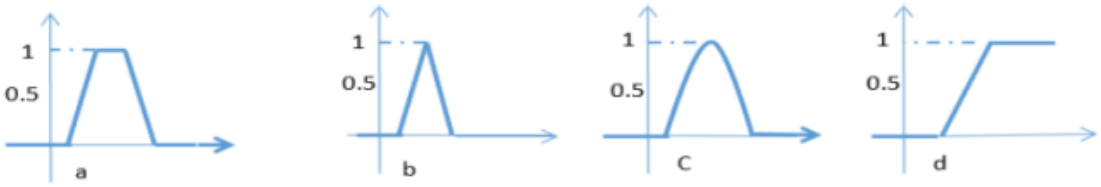

Figure 4.4: Illustration of membership function (a) Trapezoidal (b) triangular (C) Gaussian and (d) monotonic

There are three procedures to follow during the design of a fuzzy logic controller;

- Determine the fuzzy logic input and output; sliding manifold(s) as input and discontinuous controller as output in this thesis.
- Determine the processing that is suitable for the controller input and possibly post-processing for the output.
- Design every component of the fuzzy components explained above.

4.3.2.6 Fuzzy Logic Gain Tuning for The Discontinuous Control Effort

The goal of this section is to replace the discontinuous phase of a sliding mode controller with a fuzzy logic controller to control the reaching phase dynamics and reduce the chattering effect. During the conventional sliding mode controller, the control effort results in oscillating at a high frequency (ideally infinite frequency), which causes a problem known as chattering. It is unwanted because it can excite the high-frequency dynamics of the system. To reduce chattering, a continuous fuzzy logic control(u_f) is used to approximate the (u_{dis}) [46].

The design of the fuzzy controller starts with defining the crisp sliding surface $s = 0$ to the fuzzy sliding surface explained as linguistic expression; (s is ZERO). The following fuzzy set is defined to segment the domain of discourse of s:

$$E(s) = [NB, NM, NS, ZERO, PS, PM, PB] = [F_s^1, ..., F_s^7] \tag{4.53}$$

Where [NB, NM, NS, ZERO, PS, PM, PB] are labels of the fuzzy set denoting negative large, negative medium, negative small, zero, positive small, positive medium, and accordingly positive large, and E(s) is the term set of (s). The term and label of the fuzzy set are

indicated for the output (u_f) as follows:

$$E(u_f) = [NB, NM, NS, ZERO, PS, PM, PB] = [F_{u_f}^1, ..., F_{u_f}^7] \tag{4.54}$$

The fuzzy logic controller is designed using the MATLAB fuzzy logic toolbox and has one input linguistic variable and one output linguistic variable as shown in the figure below. These linguistic variables have seven linguistic values explained above with a triangular shape membership function(MF). For each(six) state of the plant(FWUAV) the fuzzy logic control

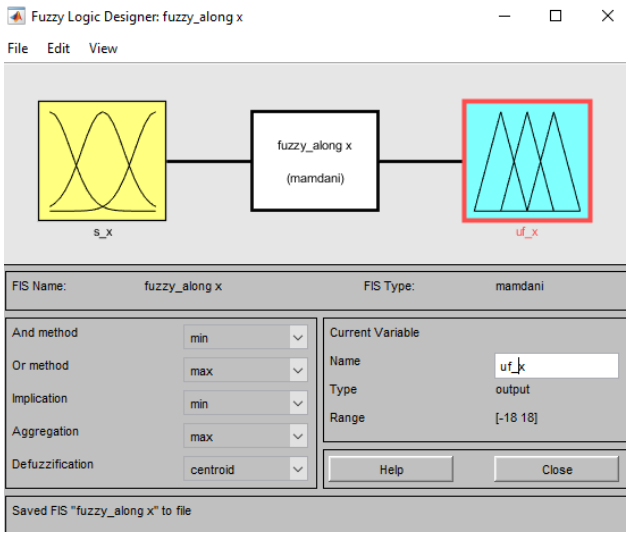

Figure 4.5: Fuzzy logic designer

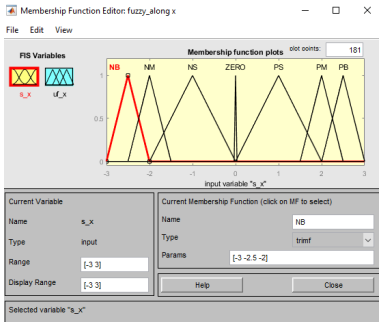

(a) MF of input(Sliding surface)

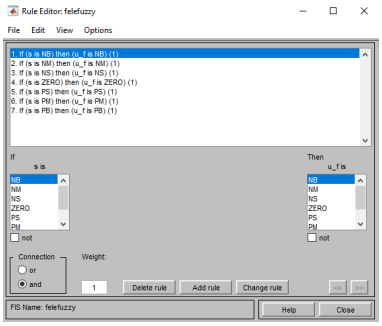

(b) Rule editor for input and output membership function

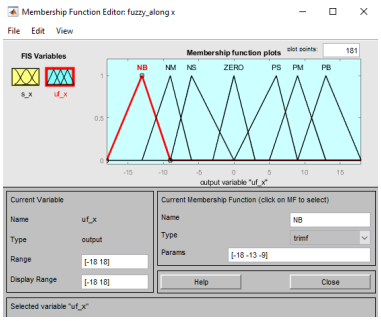

(c) MF of output(gain tuner for discontinuous controller)

Figure 4.6: Fuzzy logic designer and MF editor for input and output of fuzzy logic controller

system decides the gain based on the sliding variable(s_i). The input and the output of the fuzzy logic system are divided into seven linguistic values as noted in equation (4.54)and(4.55) and the rule base is given as follows: 'i' represents for (x,y,z,ϕ,θ,ψ)

- IF S_i is NB THEN U_{fi} is NB
- IF S_i is NM THEN U_{fi} is NM
- IF S_i is NS THEN U_{fi} is NS
- IF S_i is ZERO THEN U_{fi} is ZERO
- IF S_i is PS THEN U_{fi} is PS
- IF S_i is PM THEN U_{fi} is PM
- IF S_i is PB THEN U_{fi} is PB

Input(S_i)	NB	NM	NS	ZERO	PS	PM	PB
Output(U_{fi})	NB	NM	NS	ZERO	PS	PM	PB

Table 4.1: Fuzzy logic controller rule base for input and output membership function

Then, after designing the fuzzy logic controller, the overall control effort becomes the sum of the equivalent controller and the fuzzy logic controller (the discontinuous part of SMC is being replaced by the fuzzy controller), when $U_{fi}(t)$ is the output of a fuzzy system.

$$U_i(t) = U_{equ}(t) + U_{fi}(t) \tag{4.55}$$

4.4 Constraints Imposed on Control Inputs

There are many reasons to constrain the control surface of the aircraft, among which are [47]:

- **Safety**: Limiting control surface deflection ensures that the aircraft operates within safe operating limits. Excessive deflection can result in structural damage, control loss, or structural failure.
- **Structural integrity**: Control surfaces are built to withstand specific loads and forces. Constrained deflections keep control surfaces, pivots, and other associated components from becoming overly stressed, guaranteeing their structural integrity.
- **Stability and Control**: The deflection of control surfaces impacts the aircraft's stability and control. The aircraft's response to control inputs can be carefully handled by regulating their deflection, making it easier for the pilot to maintain control and stability during flight.

And the Thrust force is calculated based on the thrust-to-weight ratio, which is usually a maximum ratio of 2:1. The constraint values are shown in the following table:

Controllers	Thrust	Aileron deflection	Elevator deflection	Rudder deflection
Values	$<= 270N$	$\pm 0.92rad$	$\pm 0.92rad$	$\pm 0.92rad$

Table 4.2: Maximum and minimum boundary for the control input

Chapter 5

Simulation Results and Discussion

The primary focus of discussion will revolve around the effectiveness of the proposed control law. This is because the central objective of this thesis is to develop an effective trajectory-tracking controller for the fixed-wing UAV using fuzzy logic-based sliding mode control.

5.1 Introduction

This chapter will illustrate the simulation outcomes of the closed-loop system, incorporating the proposed plant model and the designed controller, implemented using MATLAB®/Simulink®. The comprehensive Simulink model, displaying the integration of the designed controller with the fixed-wing UAV model, is presented in Figure 5.1,

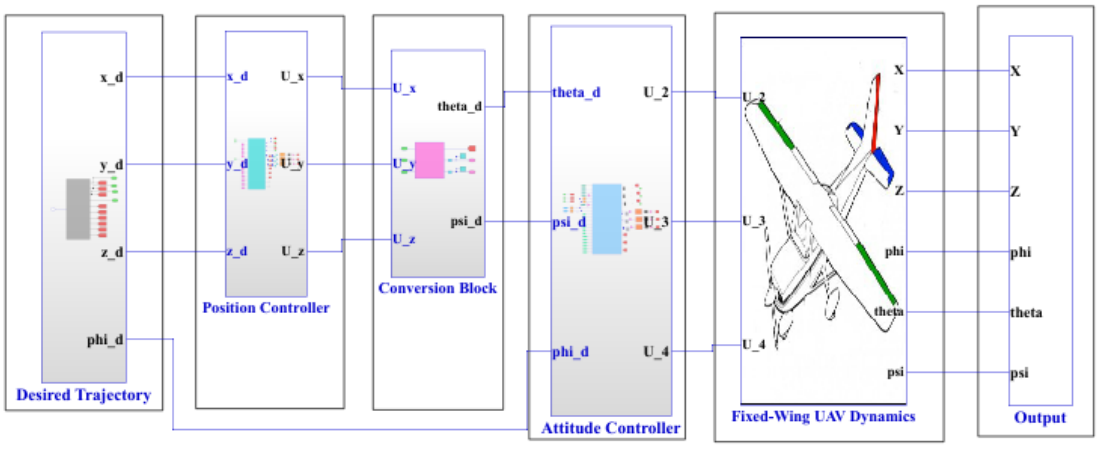

Figure 5.1: Overall developed Simulink model

The overall model includes the following:

- Trajectory planning: Which involves the generation of a feasible reference trajectory, in which the trajectory must fulfill the slope continuity and path continuity constraints

because of the natural appearance of the proposed plant.

- The conversion block: Involves the generation of the desired input for the rotational motion (the inner loop) from the virtual control outputs.
- Controller block: There are two control blocks for this system: the outer control block for the position motion control and the inner control block for the rotational motion control.
- The actual plant model: Is the modeling of FWUAV.
- The last block is the output block, which involves performance analysis by comparing the desired and the actual or measured trajectories.

5.2 Simulation Result For Different Reference Trajectories

5.2.1 Helical Trajectory Tracking For SMC

The helical reference trajectory is obtained by $x_d = 10\cos t$, $y_d = 10\sin t$, and $z_d = t$. As seen from the dynamic model of the system, some parameters are considered as uncertainty during the decoupling procedure. Then the tracking performance of the control effort is seen for both cases: without the considered disturbance and with disturbance.

5.2.1.1 Case One Pure Scenario

The resulting helical 3D trajectory tracking response of the position of the FWUAV and the resulting rotational motion tracking for a pure scenario, i.e., $(d_x, d_y, d_z, d_{\phi_2}, d_{\theta_2}, d_{\psi_2})$ are assumed to be zero, as shown in the figures 5.2, 5.3, and 5.4.

5.2.1.2 Case Two With Uncertainty

The resulting helical 3D trajectory tracking response of the position of the FWUAV and the resulting rotational motion tracking with the considered uncertainties during the decoupling process, i.e., $(d_x, d_y, d_z, d_{\phi_2}, d_{\theta_2}, d_{\psi_2})$ are added into the dynamics of the system as shown in the figures 5.5, 5.6, and 5.7. For both cases, the control effort meets the constraint imposed in Chapter 4 at Table 4.2. From these two cases, we can observe that the sliding mode controller can tolerate uncertainty, and the resulting control efforts are affected by chattering.

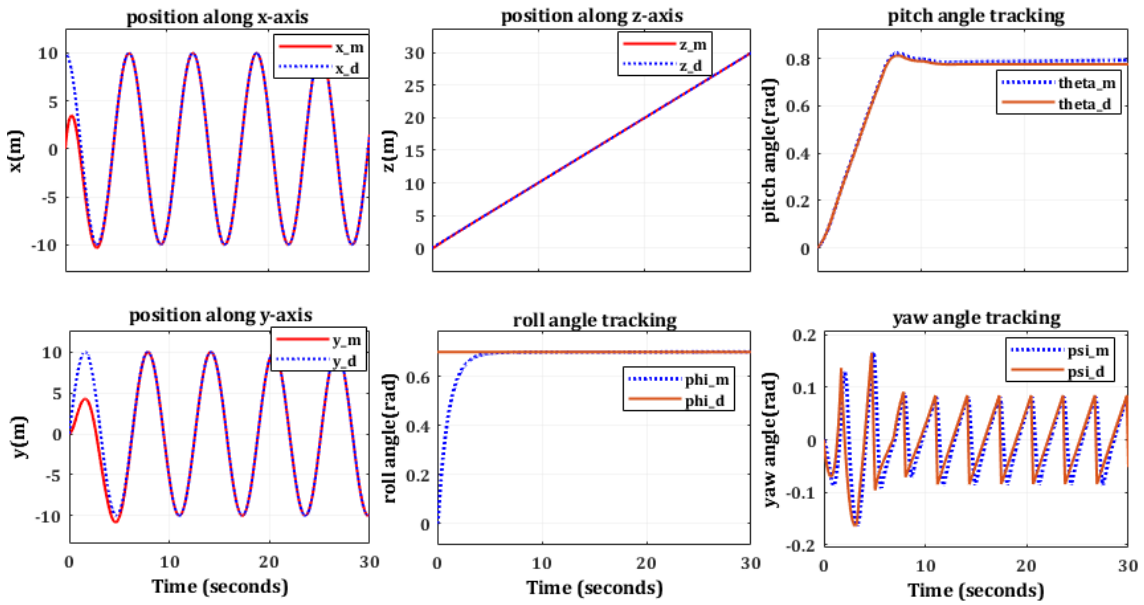

Figure 5.2: Helical trajectory position and attitude controller tracking performance for case one

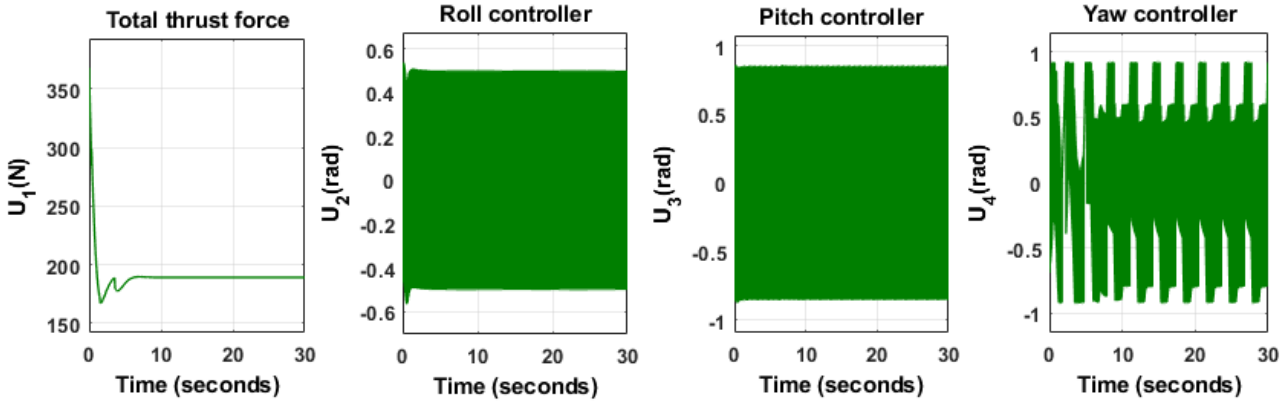

Figure 5.3: Total thrust force and deflection commands for pure scenario

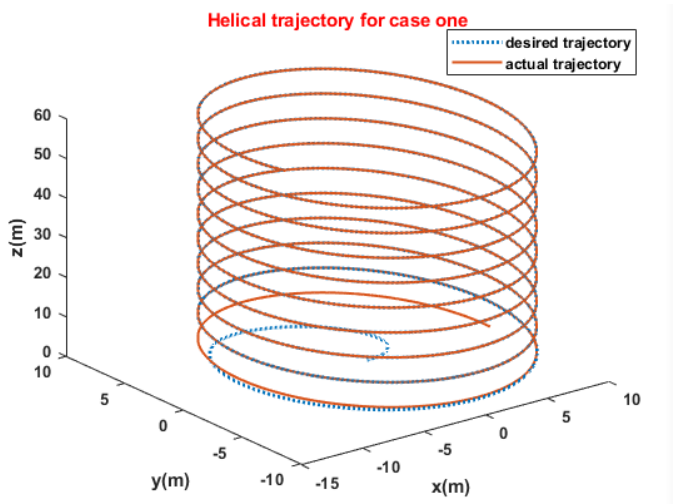

Figure 5.4: 3D helical trajectory SMC tracking plot for pure scenario

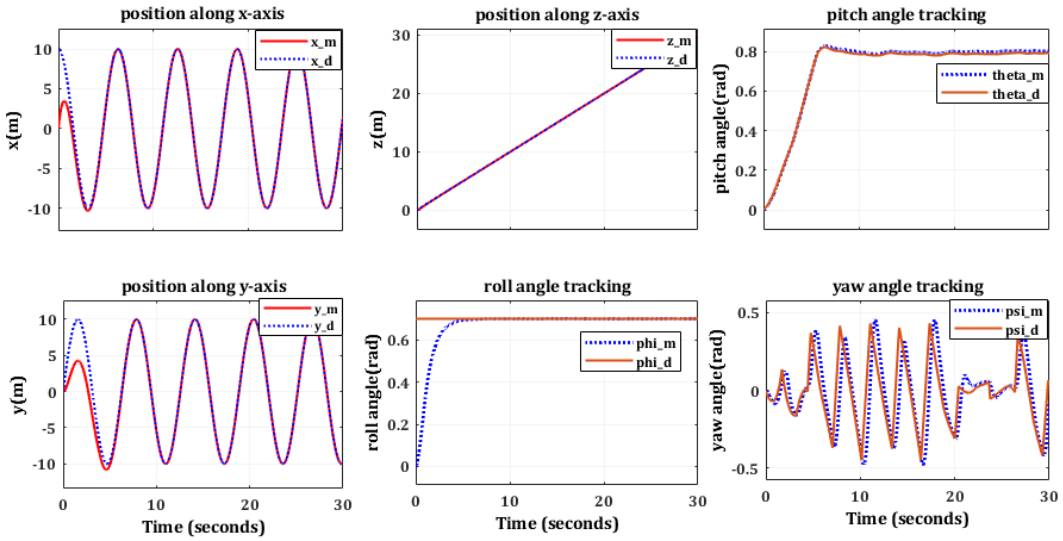

Figure 5.5: Helical trajectory position and attitude sliding mode controller tracking performance for case two

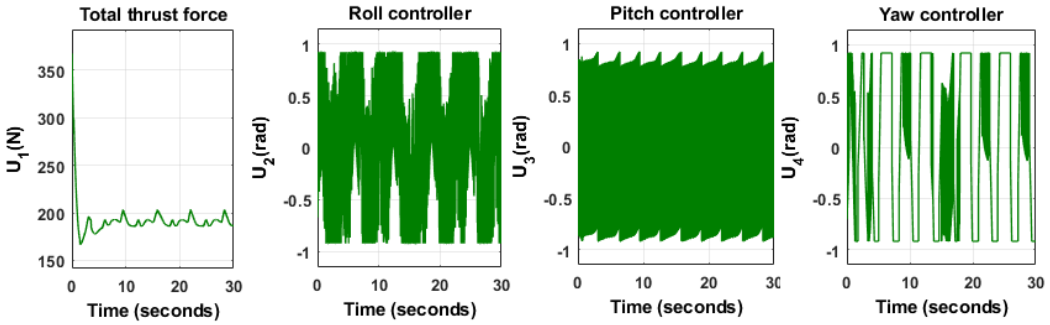

Figure 5.6: Control efforts for the second scenario

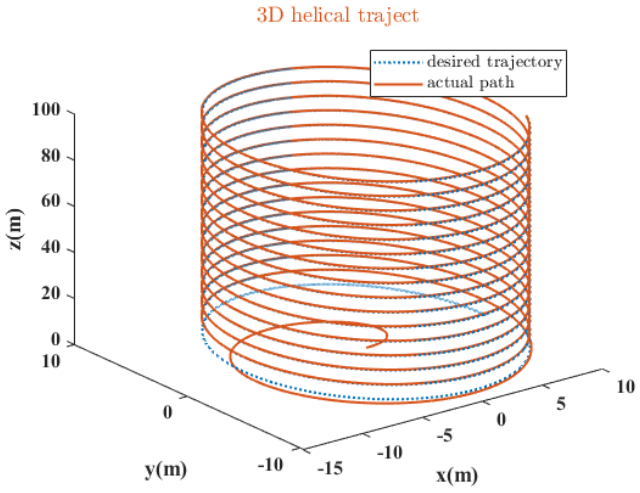

Figure 5.7: Helical trajectory SMC tracking 3D plot for case two

5.2.2 Helical Trajectory Tracking For FSMC

This section depicts the performance of the FSMC and the chattering effect compared with the classical SMC. Then it is clear that the chattering effect is reduced, as we expected,

during FSMC compared with SMC. As well, the control efforts are in between the maximum and minimum values, as explained in Table 4.2.

5.2.2.1 Tracking Performance During Pure Scenario

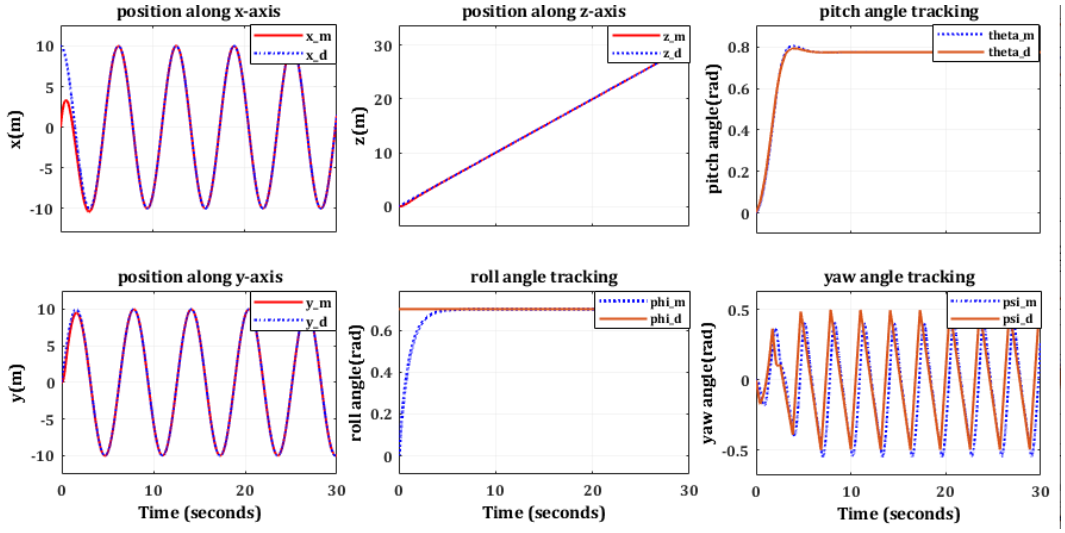

Figure 5.8: Helical trajectory tracking performance of FSMC for pure scenario

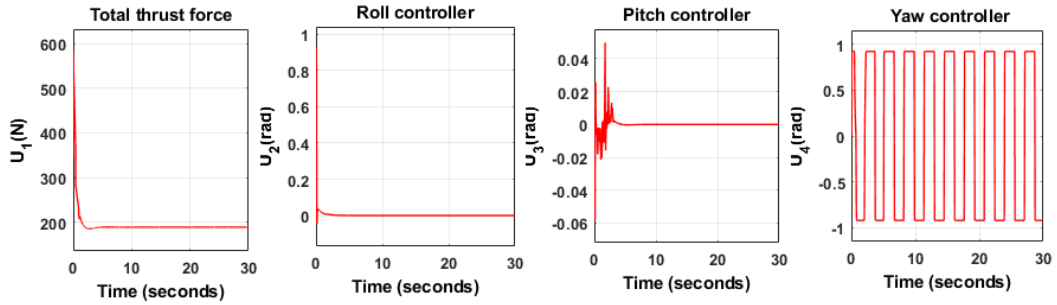

Figure 5.9: Control input signal of FSMC for pure scenario

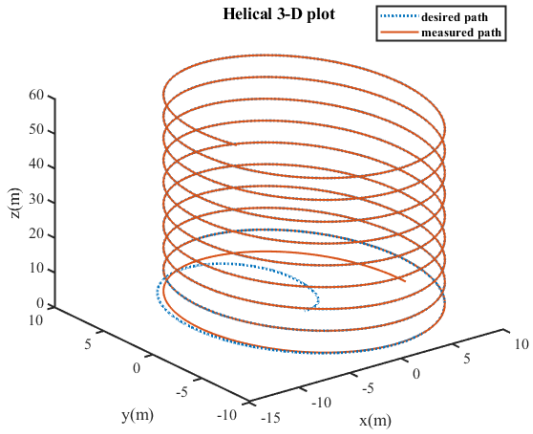

Figure 5.10: 3D helical trajectory tracking performance for FSMC

5.2.2.2 Helical trajectory tracking performance of FSMC with uncertainty

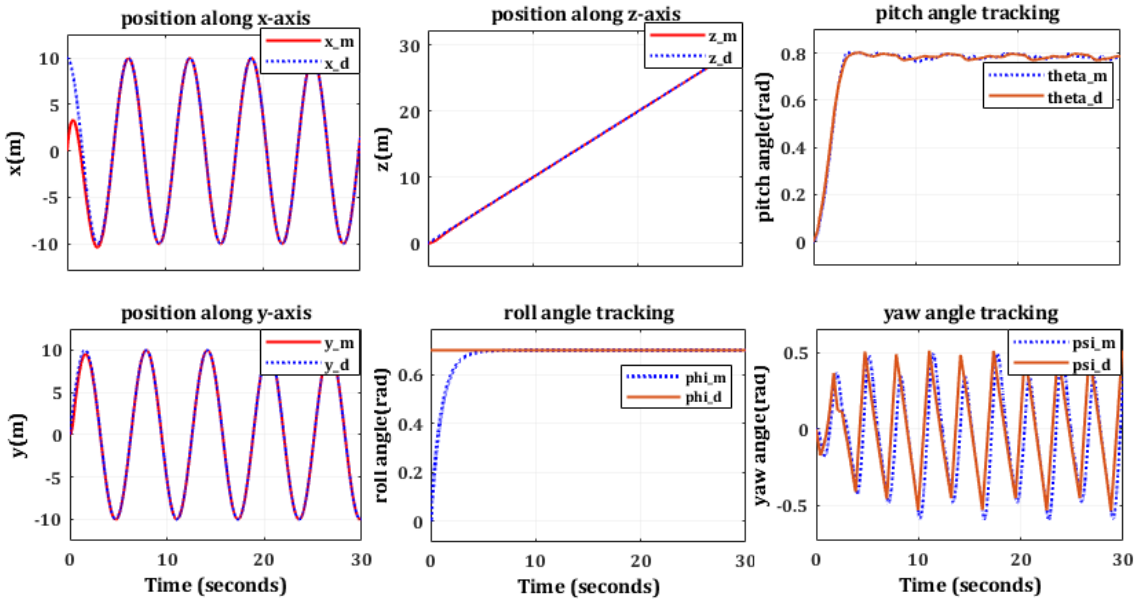

Figure 5.11: Helical trajectory position and attitude controller tracking performance of FSMC for case two

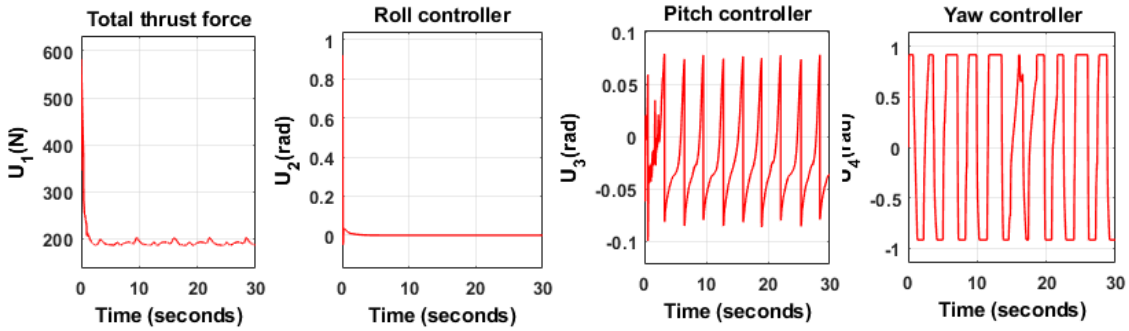

Figure 5.12: Control effort of FSMC with uncertainty

5.3 Takeoff, Navigation, and Landing Trajectory Planning

In this section, the desired trajectory of each phase for the FWUAV is designed based on different constraints, like slop continuity constraints and path continuity constraints called flight constraints [48]. The path must be smooth during banking schemes. The aircraft's takeoff, navigation, and landing trajectory is the desired aircraft path, which the aircraft follows over a given period of time$[t_0, t_f]$.

5.3.1 Takeoff Phase

The action of takeoff with a FWUAV is significantly less difficult than the landing phase. There are many ways to perform takeoff like launching from a hand throw, catapult, or runway and climbing to a specified altitude [43]. But for this thesis, launching from a catapult is chosen as takeoff because the launcher accelerates the aircraft smoothly by designing the launching speed correctly [49]. From the parameters of the fixed-wing UAV, it is taken that the take-off speed is 15 m/sec, the launcher height is 1.45 m, and the flight path angle(γ) be (15°) [6]. Then a third-order smooth trajectory is applied as a reference input after the catapult operation(lift-off climb phase) by taking initial and final way-points with the speed profile of the aircraft, and at the final point, a constant altitude is maintained and navigation is started. i.e

$$x_d = a_0 + a_1 t + a_2 t^2 + a_3 t^3 \tag{5.1}$$

And the altitude linearly depend on x_d with a slope of $\tan(\gamma)$

$$z_d = \tan(\gamma) x_d + 1.45 \tag{5.2}$$

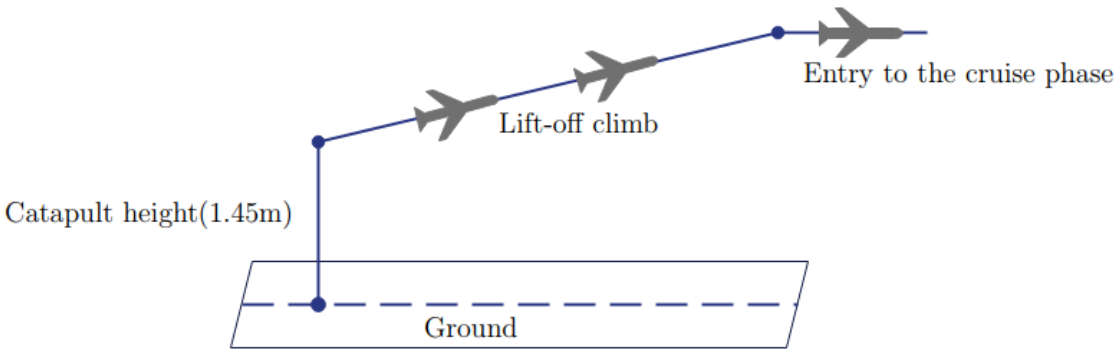

Figure 5.13: Take-off Trajectory [50]

5.3.2 Navigation Phase

The cruise, or navigation, is the phase of aircraft flight that starts when the aircraft levels off after a climb until it begins to descend for landing. After the aircraft performs takeoff operations, the navigation (cruise) scheme is a very important phase in which the normal mission of the aircraft is started. From the literature, the speed (cruising speed) of the FWUAV during this phase is constant and takes a value of 20m/sec [6] for this thesis work.

The speed in this scheme is constant until the operation is done. The flight path in this phase is taken as a third-order smooth trajectory based on the slope continuity and the path continuity constraints, as well as the banking scheme. The equation of the trajectory for navigation and banking schemes is given as follows:

$$x_d = a_0 + a_1 t + a_2 t^2 + a_3 t^3$$
$$y_d = b_0 + b_1 t + b_2 t^2 + b_3 t^3$$
$$z_d = constant$$

During the banking scheme, both the forward (x_d) and the lateral (y_d) paths are used for a certain amount of time (4 seconds for this work) in order to create a suitable turn of the aircraft (to avoid a sharp turn).

5.3.3 Landing Phase

The landing trajectory must be secure, free from the risk of harm, and provide a comfortable landing. There are two main phases during landing. These are the glide slope phase and the flare-out phase [48] [51]. The glide phase is the first phase of landing, and it is modeled as a straight line whose slope is determined in terms of the flight path angle(γ). In Figure 5.14 the desired landing trajectory is depicted in the forward path (x)-altitude (z) plane. The

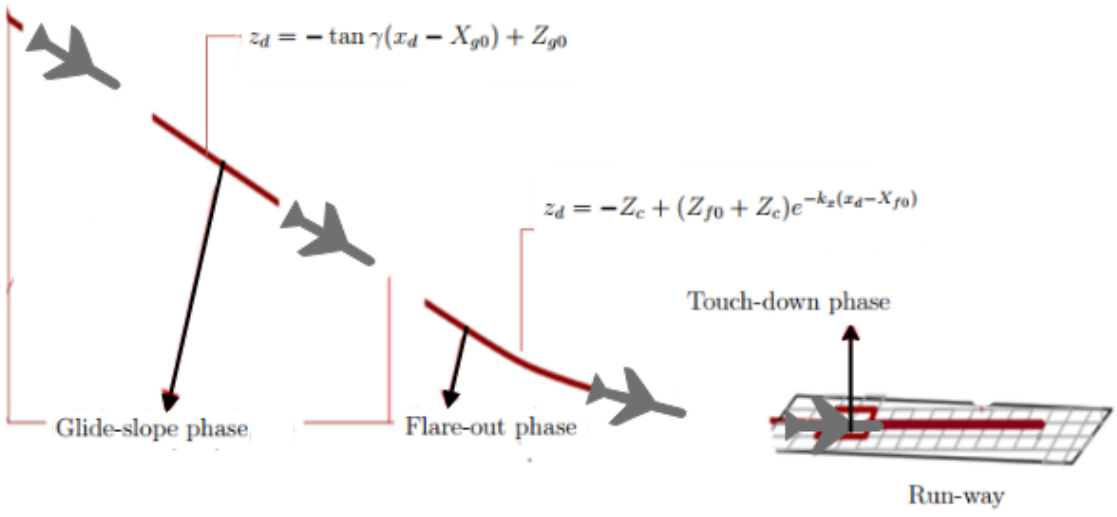

Figure 5.14: Aircraft's landing path [48]

other part is the flare-out path, which begins when the aircraft reaches a certain height(Z_{f0}) which is the final point of the glide slope phase and the initial point of the flare-out phase. It is an exponential path with a given path angle at touchdown [51]. In 5.14 (k_x, Z_c, X_{f0}) are unknown, and the procedure to calculate these coefficients is explained in **Appendix B**.

And then, in both phases, the forward trajectory is given by:

$$x_d = a_0 + a_1 t + a_2 t^2 + a_3 t^3 \tag{5.3}$$

5.4 Simulation Results: Takeoff, Navigation, and Landing

This section shows the simulation results of the three phases of the flight path for both SMC tracking performance and FSMC tracking performance with the considered uncertainty during the decoupling procedure.

5.4.1 SMC Trajectory Tracking Performance

The tracking performance of the classical SMC and the control signal are depicted in figures 5.15 and 5.16, respectively. As a result, the aircraft's translational and rotational motions track the required input trajectory and orientation with good performance. However, the control signal in figure 5.16 varies at a high frequency, which is known as chattering.

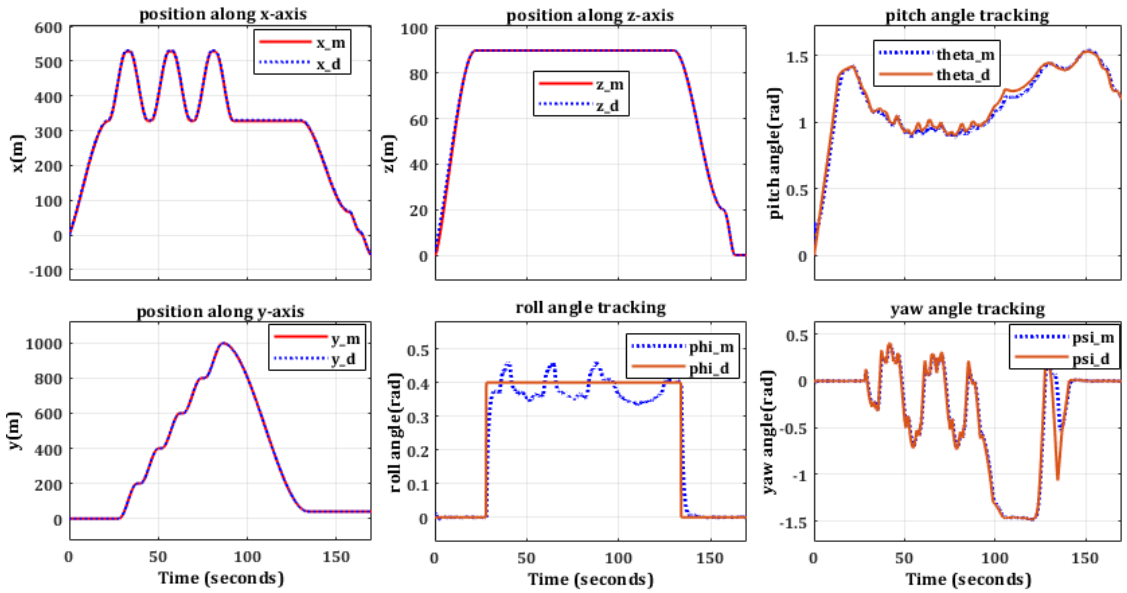

Figure 5.15: Flight path tracking performance of SMC

5.4.2 FSMC Trajectory Tracking Performance

From the results shown below, the chattering effect is reduced with the fuzzy-based sliding mode controller compared with the conventional SMC. And we can observe from the result

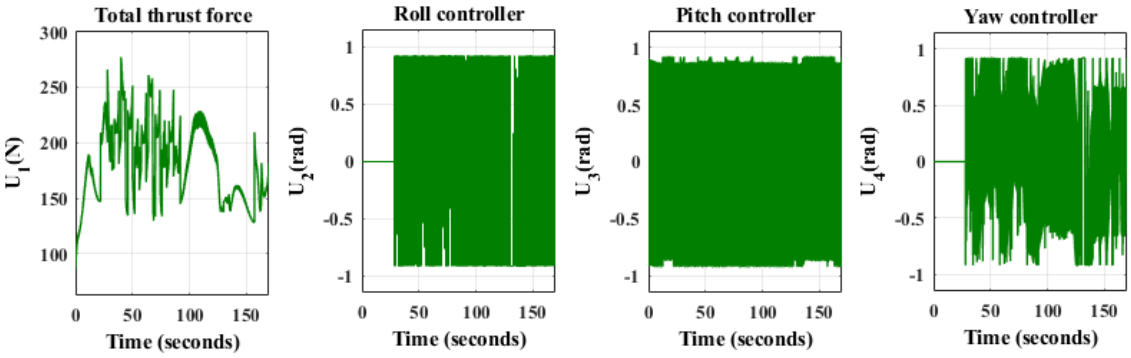

Figure 5.16: Control effort for conventional SMC

that the translational and rotational trajectory of the aircraft tracks the desired reference path, and the 3D trajectory tracking in figure 5.19 also proves the designed controller guarantees accurate desired reference path tracking by stabilizing the aircraft to perform the required task. The control effort here is also in between the boundaries explained in Chapter 4 at Table 4.2. A comparison between the tracking performance of the controller can

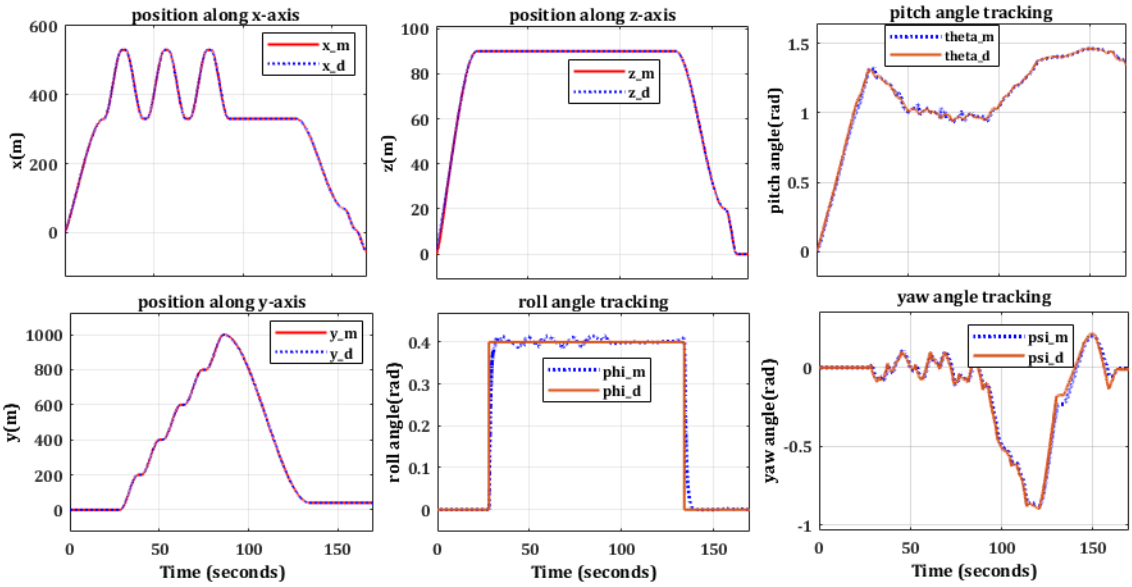

Figure 5.17: Flight path tracking performance of FSMC

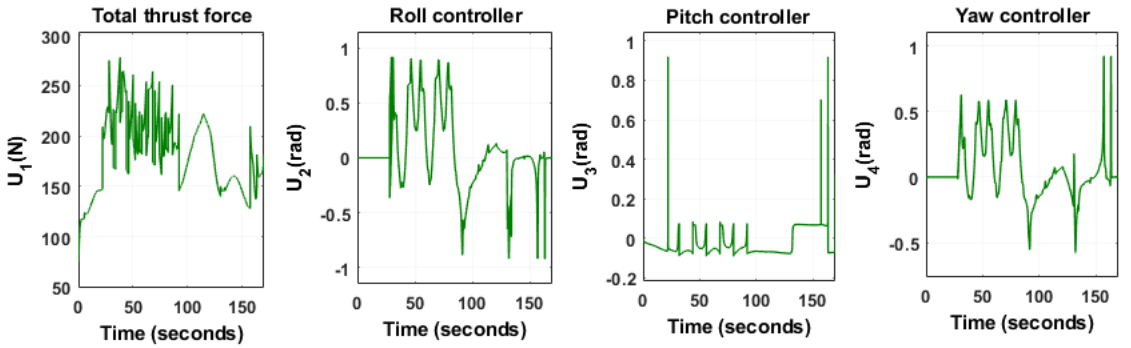

Figure 5.18: Control effort for fuzzy SMC

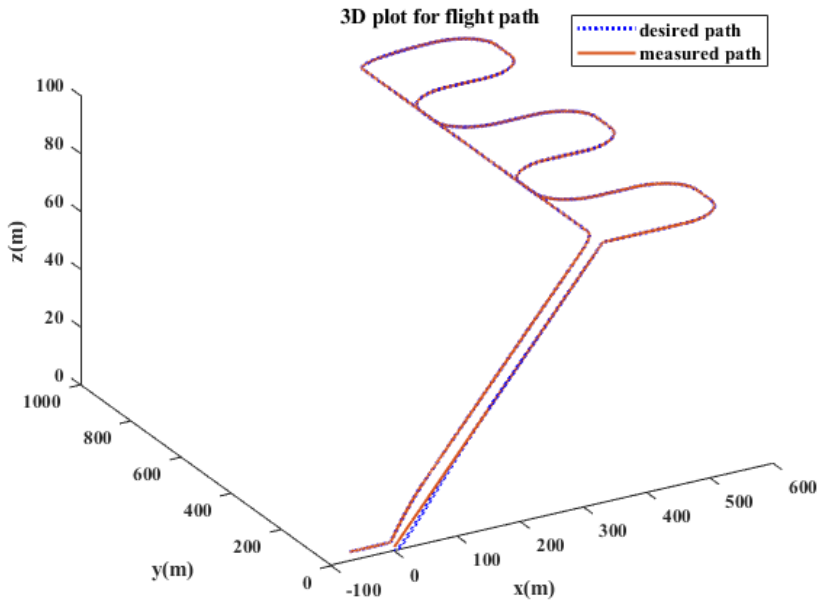

Figure 5.19: Trajectory tracking of flight path 3D plot

be achieved by calculating the trajectory error based on the following equation [52].

$$e_{tr} = \sqrt{e_x^2 + e_y^2 + e_z^2} = \sqrt{(x_m - x_d)^2 + (y_m - y_d)^2 + (z_m - z_d)^2} \tag{5.4}$$

The equivalent trajectory errors for the SMC and FSMC are 0.6143 and 0.2797, respectively. As can be observed from the results, the FSMC's trajectory error is lower than that of the SMC, with the amount of control effort indicated in the figures 5.16 and 5.18. And to assess the capacity of the FSMC compared with conventional SMC, the mean square of the trajectory error (MSTE) is taken based on the following formula [52].

$$MSTE = \frac{1}{N_s} \Sigma_{i=1}^{N_s} e_{tr}^2 \tag{5.5}$$

Based on this equation, the MSTE will be 0.3774 for the SMC and 0.07825 for the proposed controller (FSMC), which indicates the tracking capacity of the FWUAV is highly enhanced with the proposed controller. The tracking improvement percentage (TIP) can be calculated by using the formula:

$$TIP = \frac{MSTE_{SMC} - MSTE_{FSMC}}{MSTE_{SMC}} \times 100 \tag{5.6}$$

Then, based on this equation, the tracking performance of the FSMC is improved by 79.266% which means that the trajectory error is decreased by this percentage during the FSMC.

5.5 The Effect of External Disturbance on FSMC

Use an unknown disturbance for a step reference input along the x, y, and z axes to demonstrate the capability and robustness of the FSMC scheme in tracking problems. The system response of the suggested controllers to an external disturbance is shown in figure 5.21. The simulation shows that the controller performs well under the applied disturbance rejection. According to the diagram below, the external disturbance modeled in this thesis is a random signal with varying axes of acceleration, as shown in figure 5.20.

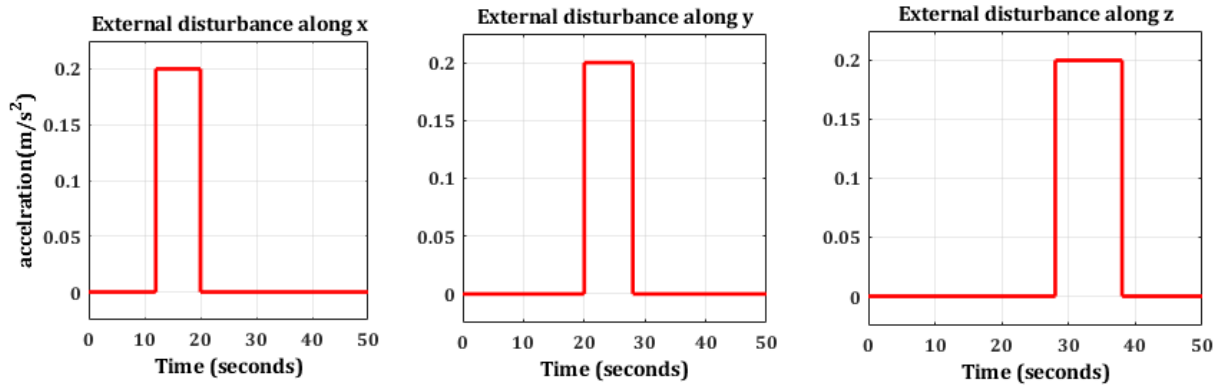

Figure 5.20: Injected external disturbance along x,y,z axis

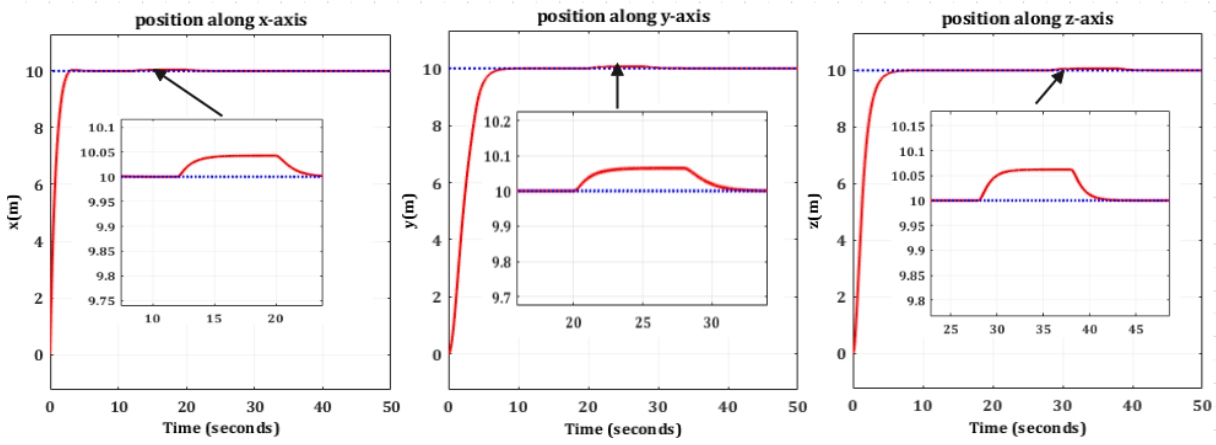

Figure 5.21: Effect of injected disturbance for the position of the UAV

Figure 5.21 depicts the effect of disturbance and the range of the controller's capabilities for disturbance rejection along the fixed-wing UAV position. It shows how the suggested controller (FSMC) enables system stabilization and convergence of position to target position.

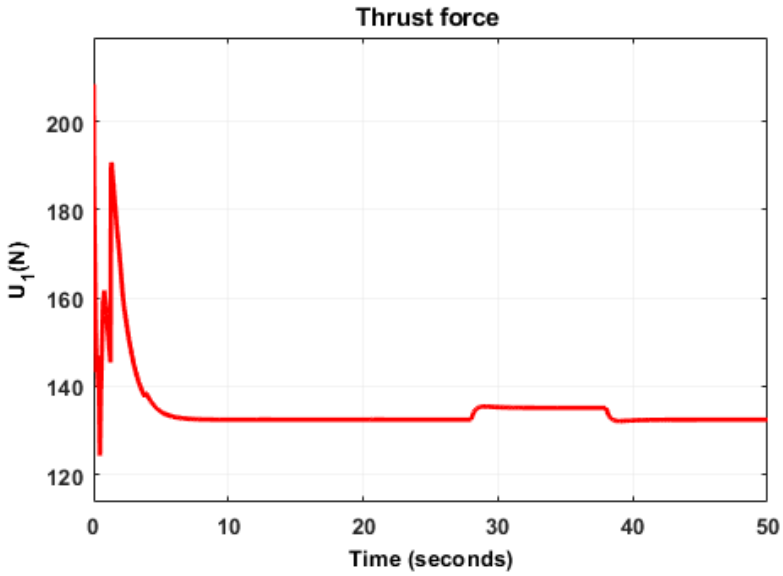

Figure 5.22: Total thrust force of the system with disturbance

5.6 Comparison Between FSMC and SMC in Terms of Steady State Error and Settling Time

From the result, we can say that the proposed controller (FSMC) provides a promising result and gives a fast response (with respect to the classical SMC) of settling time around 2.802 seconds with minimum steady state error compared to the conventional sliding mode controller of settling time around 5.065 seconds, as shown in figure 5.23.

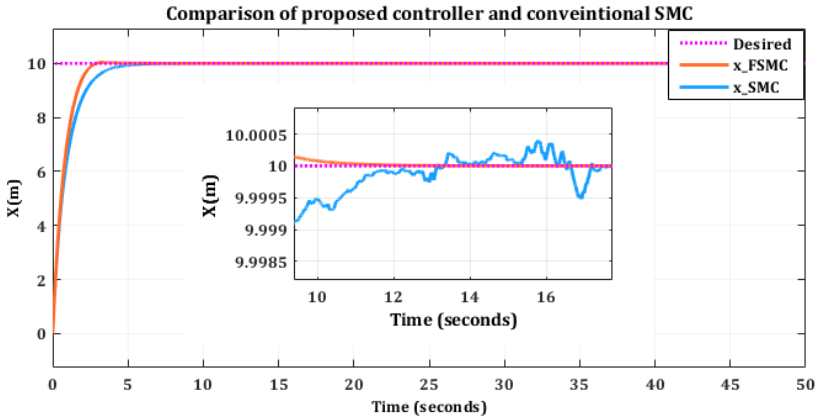

Figure 5.23: Comparison between tracking performance of the proposed controller and conventional SMC

Chapter 6

Conclusion and Recommendation

6.1 Conclusion

A fixed-wing unmanned aerial vehicle (UAV) is a nonlinear, multivariable, and tightly coupled system. As a result, many unmodeled dynamics and external disturbances might easily disrupt the control process. The work in this thesis includes modeling the FWUAV dynamics established using Newton-Euler approaches, verifying the developed model using different scenarios, input decoupling, designing the conventional SMC and fuzzy-based SMC to compensate for the traditional SMC's drawbacks, and stabilizing the aircraft's full 6 DoF around the referenced target trajectory. And the finite-time convergence of the designed controller is performed based on Lyapunov's theory of stability analysis. To simulate the model and the designed controller, the MATLAB®/Simulink® platform is used.

On various flight paths, the performance of the developed controllers' path tracking is evaluated while taking into account both normal and disrupted flight conditions. The result shows the proposed controller has good performance in terms of disturbance rejection, tracking capability, chattering reduction, which is the main drawback of the existing SMC, and steady-state error reduction.

Additionally, the comparison of the FSMC and the traditional SMC reveals that the suggested controller significantly enhances the tracking performance of the aircraft by 79.266% in accordance with the flight route of the aircraft.

6.2 Recommendation for Future Work

The following points discuss this thesis's potential future extensions and recommendations:

- As it is clear, the sliding mode controller is robust against matched uncertainty, but its robustness fails when unmatched uncertainty is applied to the plant. Then the interested researcher in this area can design the Neuro-fuzzy SMC or Fuzzy SMC based on adaptation law to make the controller robust in front of both matched and unmatched uncertainties for the same dynamic model of this thesis.

- In addition, interested researchers can improve the work of this thesis by including the drone's target identification mechanism and at least a basic implementation of the system.

Bibliography

[1] Amber Israr, Eman H Alkhammash, and Myriam Hadjouni. Guidance, navigation, and control for fixed-wing uav. *Mathematical Problems in Engineering*, 2021:1–18, 2021.

[2] Shi Zhou and Masoud Gheisari. Unmanned aerial system applications in construction: a systematic review. *Construction Innovation*, 2018.

[3] Javier Irizarry and Dayana Bastos Costa. Exploratory study of potential applications of unmanned aerial systems for construction management tasks. *Journal of Management in Engineering*, 32(3):05016001, 2016.

[4] Darryl Jenkins and Bijan Vasigh. *The economic impact of unmanned aircraft systems integration in the United States*. Association for Unmanned Vehicle Systems International (AUVSI), 2013.

[5] Yogesh Beeharry and Vandana Bassoo. Performance of ann and alexnet for weed detection using uav-based images. In *2020 3rd International Conference on Emerging Trends in Electrical, Electronic and Communications Engineering (ELECOM)*, pages 163–167. IEEE, 2020.

[6] Randal W Beard and Timothy W McLain. *Small unmanned aircraft: Theory and practice*. Princeton university press, 2012.

[7] Xin Yu, Jun Yang, and Shihua Li. Finite-time path following control for small-scale fixed-wing uavs under wind disturbances. *Journal of the Franklin Institute*, 357(12):7879–7903, 2020.

[8] Kaan Taha Öner, Ertuğrul Çetinsoy, EFE Sirimoğlu, Cevdet Hançer, Mustafa Ünel, Mahmut Faruk Akşit, Kayhan Gülez, and Ilyas Kandemir. Mathematical modeling and vertical flight control of a tilt-wing uav. *Turkish Journal of Electrical Engineering and Computer Sciences*, 20(1):149–157, 2012.

[9] TS No, BM Min, RH Stone, and KC Wong. Control and simulation of arbitrary flight trajectory-tracking. *Control Engineering Practice*, 13(5):601–612, 2005.

[10] Yufei Guo, Leru Luo, and Changchun Bao. Design of a fixed-wing uav controller combined fuzzy adaptive method and sliding mode control. *Mathematical Problems in Engineering*, 2022, 2022.

[11] Yang Han, Peng Li, and Zhiqiang Zheng. A non-decoupled backstepping control for fixed-wing uavs with multivariable fixed-time sliding mode disturbance observer. *Transactions of the Institute of Measurement and Control*, 41(4):963–974, 2019.

[12] Wenlong Yang, Jintao Chen, Zonggang Zhang, Zongying Shi, and Yisheng Zhong. Robust cascaded horizontal-plane trajectory tracking for fixed-wing unmanned aerial vehicles. *Journal of the Franklin Institute*, 359(3):1083–1112, 2022.

[13] Alexandru Brezoescu, Tadeo Espinoza, Pedro Castillo, and Rogelio Lozano. Adaptive trajectory following for a fixed-wing uav in presence of crosswind. *Journal of Intelligent & Robotic Systems*, 69:257–271, 2013.

[14] Ony Arifianto and Mazen Farhood. Optimal control of a small fixed-wing uav about concatenated trajectories. *Control Engineering Practice*, 40:113–132, 2015.

[15] Dong-Ho Shin and Youdan Kim. Reconfigurable flight control system design using adaptive neural networks. *IEEE Transactions on control systems technology*, 12(1):87–100, 2004.

[16] J-M Kai, Tarek Hamel, and Claude Samson. A unified approach to fixed-wing aircraft path following guidance and control. *Automatica*, 108:108491, 2019.

[17] Ramesh P S and Dr Jeyan. Comparative analysis of fixed-wing, rotary-wing and hybrid mini unmanned aircraft systems (uas) from the applications perspective. *INCAS BULLETIN*, 14:137–151, 03 2022.

[18] BM Albaker and NA Rahim. Flight path pid controller for propeller-driven fixed-wing unmanned aerial vehicles. *International Journal of the Physical Sciences*, 6(8):1947–1964, 2011.

[19] Amr Sarhan and Shiyin Qin. Adaptive pid control of uav altitude dynamics based on parameter optimization with fuzzy inference. *International Journal of Modeling and Optimization*, 6(4):246, 2016.

[20] Jiaming Zhang, Qing Li, Nong Cheng, and Bin Liang. Non-linear flight control for unmanned aerial vehicles using adaptive backstepping based on invariant manifolds. *Proceedings of the Institution of Mechanical Engineers, Part G: Journal of Aerospace Engineering*, 227(1):33–44, 2013.

[21] Herman Castañeda, Oscar S Salas-Peña, and Jesús de León-Morales. Extended observer based on adaptive second order sliding mode control for a fixed-wing uav. *ISA transactions*, 66:226–232, 2017.

[22] Tadeo Espinoza, AE Dzul, Rogelio Lozano, and Pavel Parada. Backstepping-sliding mode controllers applied to a fixed-wing uav. *Journal of Intelligent & Robotic Systems*, 73:67–79, 2014.

[23] Syed Ussama Ali, Raza Samar, M Zamurad Shah, Aamer I Bhatti, and Khalid Munawar. Higher-order sliding mode based lateral guidance for unmanned aerial vehicles. *Transactions of the Institute of Measurement and Control*, 39(5):715–727, 2017.

[24] BJ Parvat and SD Ratnaparkhi. A second order sliding mode controller applications in industrial process. *International Journal of Engineering Trends and Technology (IJETT)*, 19(4), 2015.

[25] Yufei Guo, Leru Luo, Changchun Bao, et al. Design of a fixed-wing uav controller combined fuzzy adaptive method and sliding mode control. *Mathematical Problems in Engineering*, 2022, 2022.

[26] Tadeo Espinoza, AE Dzul, Rogelio Lozano, and Pavel Parada. Backstepping-sliding mode controllers applied to a fixed-wing uav. *Journal of Intelligent & Robotic Systems*, 73:67–79, 2014.

[27] Chaofan Zhang, Guoshan Zhang, and Qi Dong. Multi-variable finite-time observer-based adaptive-gain sliding mode control for fixed-wing uav. *IET control theory & applications*, 15(2):223–247, 2021.

[28] STEFANO FARI. Guidance and control for a fixed-wing uav. 2017.

[29] Donald T Greenwood. *Principles of dynamics*. Prentice-Hall Englewood Cliffs, NJ, 1988.

[30] MV Cook. Dynamics of flight, 1997.

[31] Zaid Tahir, Waleed Tahir, and Saad Ali Liaqat. State space system modelling of a quad copter uav. *arXiv preprint arXiv:1908.07401*, 2019.

[32] S Sieberling, QP Chu, and JA Mulder. Robust flight control using incremental nonlinear dynamic inversion and angular acceleration prediction. *Journal of guidance, control, and dynamics*, 33(6):1732–1742, 2010.

[33] Christopher Edwards and Sarah Spurgeon. *Sliding mode control: theory and applications*. Crc Press, 1998.

[34] Dereje Shiferaw and R Mitra. Neuro-fuzzy sliding mode controller: design and stability analysis. *International Journal of Computational Intelligence Studies*, 1(3):242–255, 2010.

[35] KS Holkar and LM Waghmare. Sliding mode control with predictive pid sliding surface for improved performance. *International Journal of Computer Applications*, 78(4), 2013.

[36] Sezai Tokat, Ibrahim Eksin, and M Guzelkaya. Sliding mode control using a nonlinear time-varying sliding surface. *Proceedings of the 10th IEEE International Mediterranian Conference on Control and Automation (MED'2002)*, 01 2013.

[37] Hassan K Khalil. Lyapunov stability. *Control systems, robotics and automation*, 12:115, 2009.

[38] PD Armi. A quick introduction to sliding mode control and its applications. *Universita'Degli Studi Di Cagliari*, pages 1–22, 2016.

[39] Jose Gomez and Mo Jamshidi. Fuzzy logic control of a fixed-wing unmanned aerial vehicle. *World Automation Congress (WAC), 2010*, pages 1 – 8, 01 2010.

[40] Guanrong Chen, Trung Tat Pham, and NM Boustany. Introduction to fuzzy sets, fuzzy logic, and fuzzy control systems. *Applied Mechanics Reviews*, 54(6):B102–B103, 2001.

[41] Trung-Kien Dao and Chih-Keng Chen. Tuning fuzzy-logic controllers. In *Fuzzy Logic-Controls, Concepts, Theories and Applications*, pages 351–372. InTech, 2012.

[42] K Baghaei, Hosein Ghaffarzadeh, A Hadigheh, and Daniel Dias-da Costa. Chattering-free sliding mode control with a fuzzy model for structural applications. 2019.

[43] Vestergren Magnus. Automatic takeoff and landing of unmanned fixed wing aircrafts: A systems engineering approach, 2016.

[44] Zuhtu Hakan Akpolat. *Application of fuzzy-sliding mode control and electronic load emulation to the robust control of motor drives*. PhD thesis, University of Nottingham, 1999.

[45] Jacob S Glower and Jeffrey Munighan. Designing fuzzy controllers from a variable structures standpoint. *IEEE Transactions on Fuzzy Systems*, 5(1):138–144, 1997.

[46] Ahcene Boubakir, Fares Boudjema, and Salim Labiod. A neuro-fuzzy-sliding mode controller using nonlinear sliding surface applied to the coupled tanks system. *International Journal of Automation and Computing*, 6:72–80, 2009.

[47] Abdul Sattar, Liuping Wang, Shahzeb Ansari, Ayaz Ahmed Hoshu, and Shah Khalid Khan. Disturbance rejection enhancement using predictive control for the fixed-wing uav with multiple ailerons. *International Journal of Adaptive Control and Signal Processing*, 2023.

[48] Solomon Gudeta and Ali Karimoddini. Design of a smooth landing trajectory tracking system for a fixed-wing aircraft. In *2019 American Control Conference (ACC)*, pages 5674–5679. IEEE, 2019.

[49] J Muliadi. An empirical method for the catapult performance assessment of the bppt-developed uavs. In *Journal of Physics: Conference Series*, volume 1130, page 012033. IOP Publishing, 2018.

[50] Israel Lugo Cardenas. *Autonomous take-off and landing for a fixed wing UAV*. PhD thesis, Université de Technologie de Compiègne, 2017.

[51] DMKK Venkateswara Rao and Tiauw Hiong Go. Automatic landing system design using sliding mode control. *Aerospace Science and Technology*, 32(1):180–187, 2014.

[52] Omid Mohareri. *Mobile robot trajectory tracking using neural networks*. PhD thesis, 2009.

Appendix A

Simulink Function Code

A.1 Fixed Wing UAV dynamic model

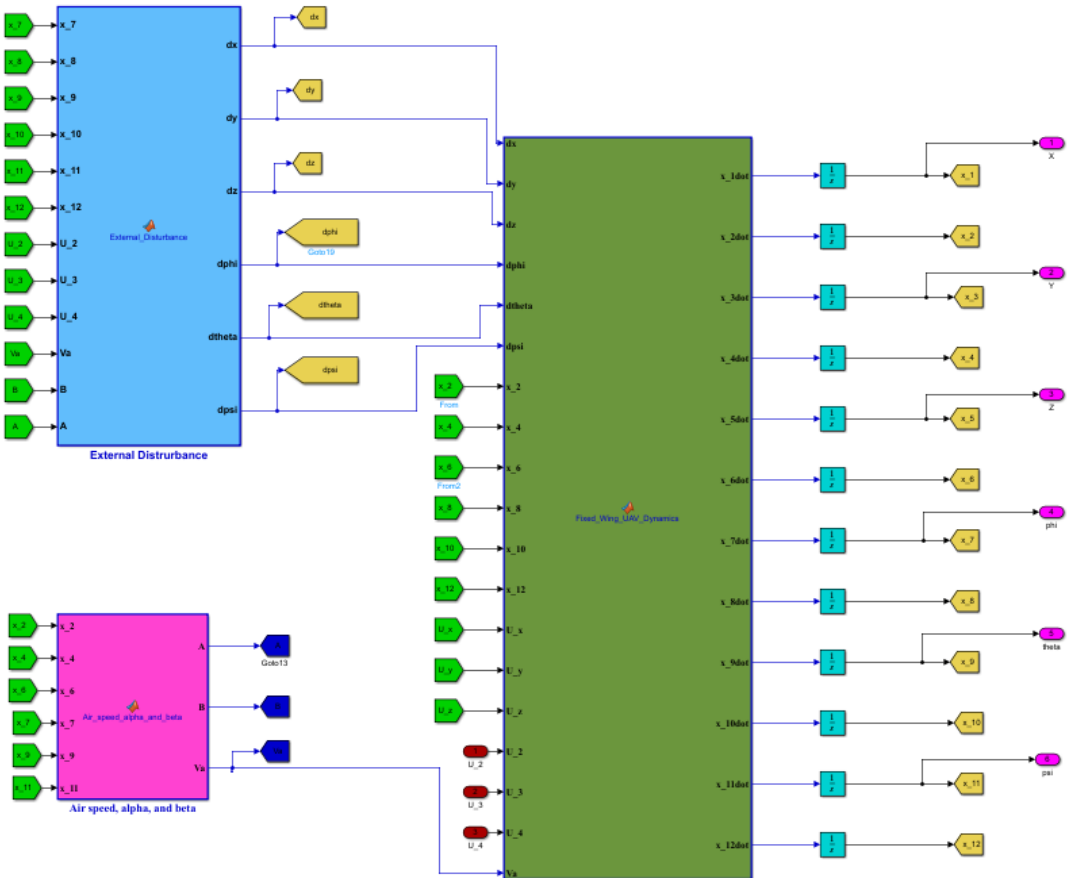

Figure A.1: Fixed wing UAV non linear mathematical model built in simulink

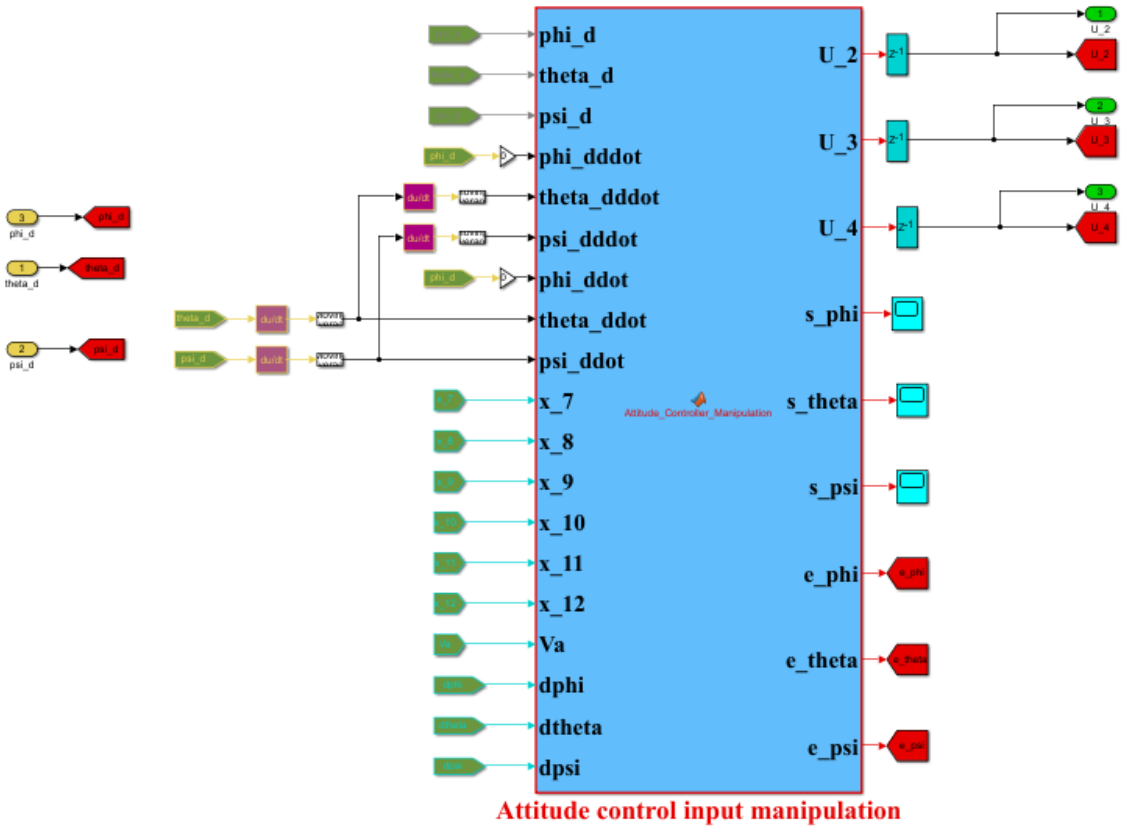

Figure A.2: Attitude controller block built in simulink

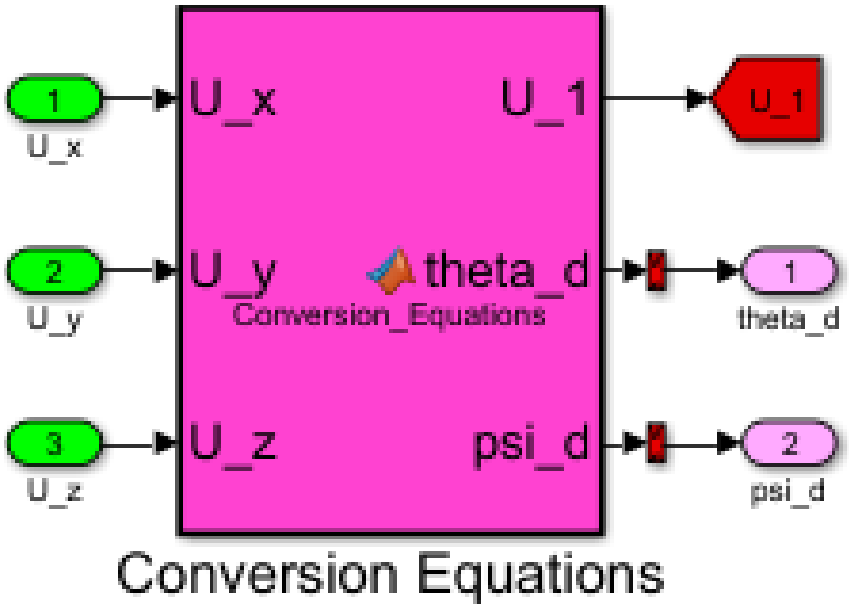

Figure A.3: Conversion block

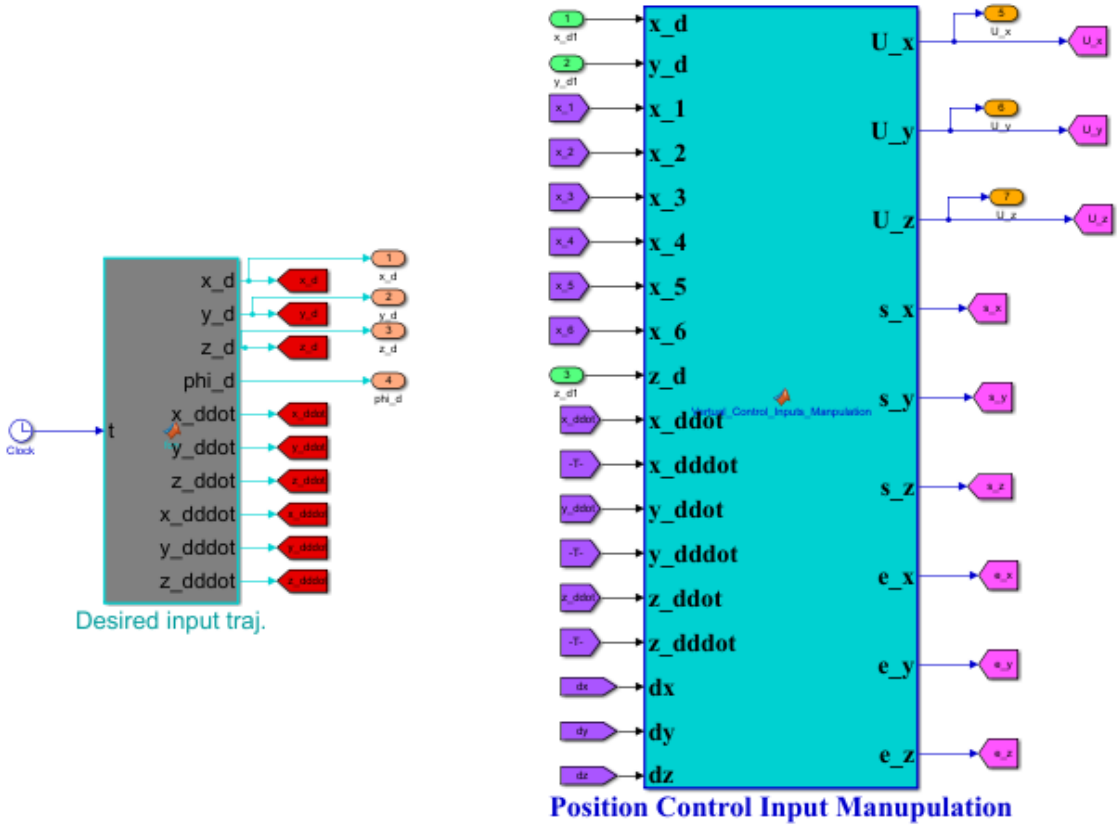

Figure A.4: Desired trajectory and position controller

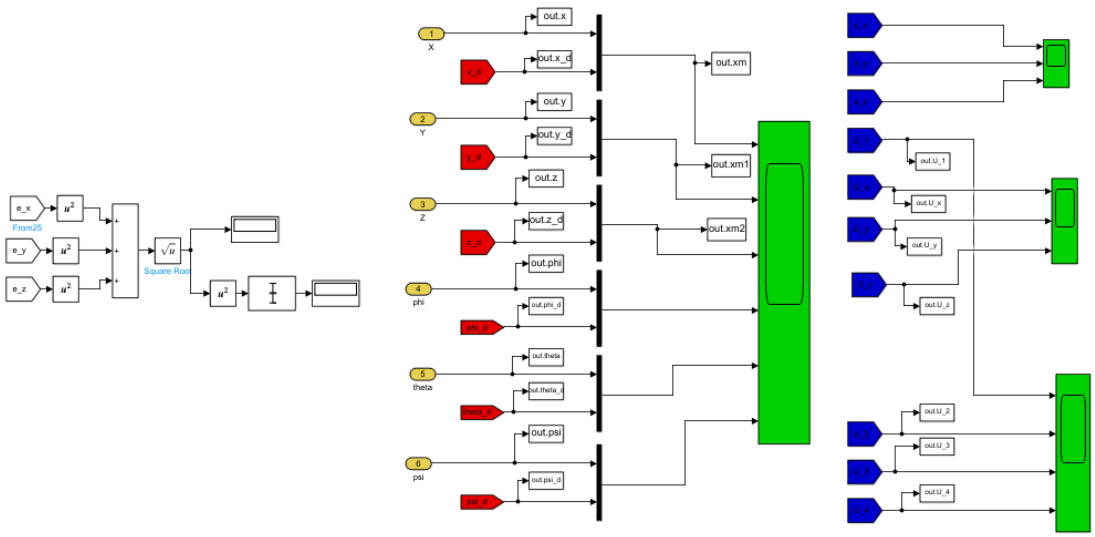

Figure A.5: Output demonstration block

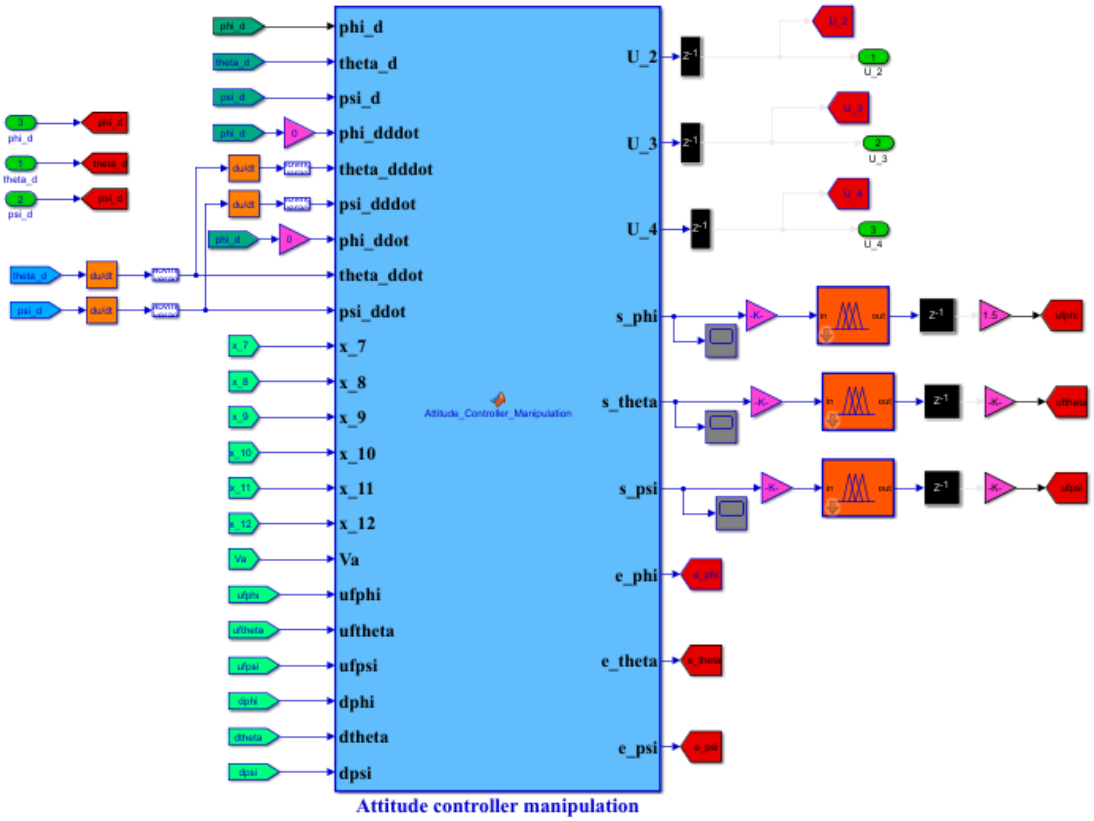

Figure A.6: Attitude controller for fuzzy based SMC simulink block.

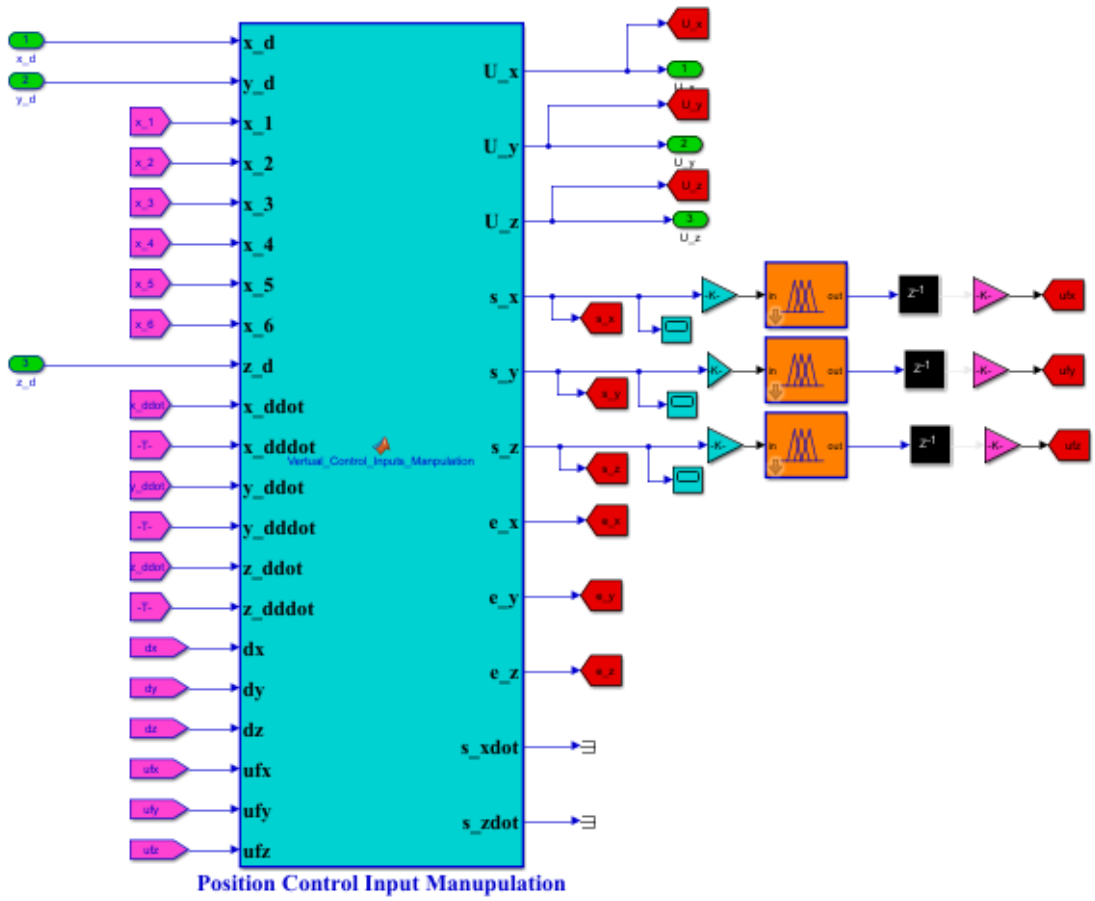

Figure A.7: Position controller for fuzzy based SMC simulink block.

Appendix B

Landing trajectory Coefficient Calculation

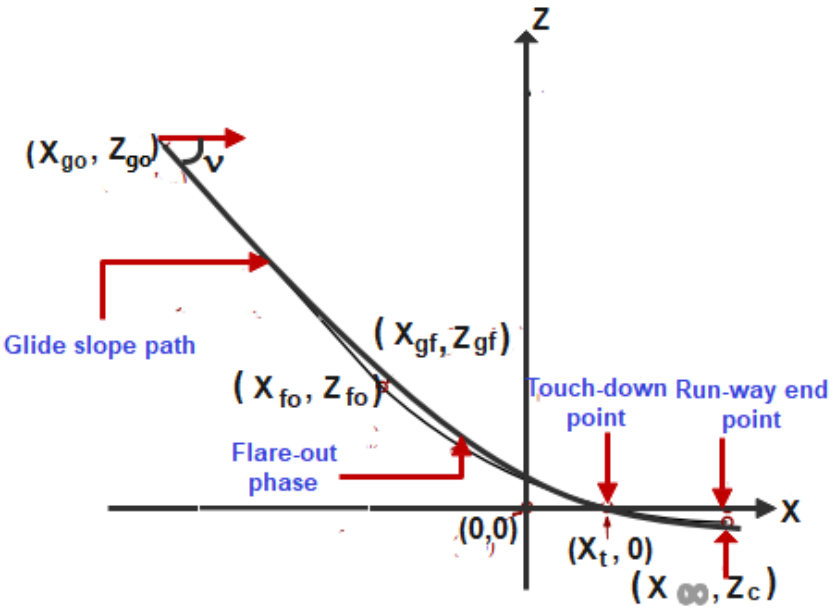

Figure B.1: Aircraft's landing path [48] [51]

During the glide slope phase, the aircraft follows a straight-line route towards the runway's start. The target altitude, z_d, is calculated using a specified flight path angle γ^d [48] [51]:

$$z_d = -\tan\gamma^d(x_d - X_{g0}) + Z_{go} \tag{B.1}$$

When the desired altitude is reached as soon as the flare-out phase begins, z_d can be calcu-

lated as:

$$z_d = -Z_c + (Z_{f0} + Z_c)e^{-K_x(x_d - X_{f0})} \tag{B.2}$$

When K_x is a constant that defines the curvature of the flare-out maneuver route based on the distance between the X-Z plane's origin and the touch-down position. For the landing trajectory shown in 5.14, X_{f0}, Z_c, K_x are unknowns that can be solved using $\tan\gamma$, Z_{f0}, and X_t given the following constraints [48] [51]:

- **Slope continuity constraint:** The slope at the beginning of the flare-out path should be equal to the slope of the glide slope path for a smooth phase change. As a result, the slope of the glide slope path can be calculated as [48] [51]:

$$\dot{z}_d = -\tan\gamma^d \tag{B.3}$$

  Similarly, the slope at the beginning of the flare-out path is:

$$\dot{z}_d = -K_x(Z_{f0} + Z_c)e^{-K_x(x_d - X_{f0})}|x_d = X_{f0} \tag{B.4}$$

  From (B.3) and (B.4) K_x can be calculated as:

$$K_x = \frac{\tan\gamma^d}{Z_{f0} + Z_c} \tag{B.5}$$

- **Path continuity constraint:** This constraint ensures that the path remains continuous when transitioning from the glide slope phase to the flare-out phase. We have done so on purpose $X_{f0} = X_{gf}$. Then it is need to ensure that Z^d at X_{gf} given in (B.1) is the same as Z^d at X_{f0} given in (B.2) resulting in [48] [51]:

$$X_{f0} = \frac{Z_{g0} - Z_{f0}}{\tan\gamma^d} + X_{go} \tag{B.6}$$

- **Touchdown constraint:** At the touchdown point X_t, the landing path intersects the ground. As a result, at the touchdown point, we have [48] [51]:

$$-Z_c + (Z_{f0} + Z_c)e^{-K_x(X_t - X_{f0})} = 0 \tag{B.7}$$

Thus from from (B.5), (B.6), and (B.7) we can determine the value of K_x and Z_c.